Espen Hauge

Automatic Kick Detection and Handling in Managed Pressure Drilling Systems

Thesis for the degree of Philosophiae Doctor

Trondheim, March 2013

Norwegian University of Science and Technology
Faculty of Information Technology, Mathematics and Electrical Engineering
Department of Engineering Cybernetics

NTNU – Trondheim
Norwegian University of
Science and Technology

NTNU
Norwegian University of Science and Technology

Thesis for the degree of Philosophiae Doctor

Faculty of Information Technology, Mathematics and Electrical Engineering
Department of Engineering Cybernetics

ISBN 978-82-471-4276-9 (printed ver.)
ISBN 978-82-471-4277-6 (electronic ver.)
ISSN 1503-8181

ITK-rapport: 2013-3-W

Doctoral theses at NTNU, 2013:88

1st edition, March 2013

Printed by NTNU-trykk

To Martine

Summary

Drilling of oil and gas wells is associated with a risk which is considered to be manageable. As the drilling campaigns extend into remote areas with inhospitable conditions, and wells and water depths grow deeper, the risk of a possible failure is increasing. To cope with this, the probability of failure must be reduced. An unwanted flux to or from the wellbore is an event which can lead to a catastrophe if not dealt with properly. Automatic detection and handling of an in-/out-flux have the possibility to reduce the magnitude, and thus the extent, of an in-/out-flux by operating on a faster time-scale than human operators and with greater precision. This thesis addresses prevention, detection, quantification, localization, handling and modelling of an in-/out-flux and is divided into the following three parts:

Part I addresses modelling of percolating gas in both a sealed annulus and for dual-gradient drilling with an evacuated riser. The model for the evacuated riser is also valid for conventional drilling. The two-phase dynamics of gas percolating up a vertical well filled with water is described by two ordinary differential equations and algebraic relations. The gas is modelled as bubbles with a distribution which can be encapsulated by a distribution function shaped like a triangle. The model is based on first principles and accommodates tracking of the front of the gas. Unmeasured states and unknown parameters are estimated with the use of an unscented Kalman filter and wired drillpipe measurements.

Part II addresses model-based in-/out-flux detection, quantification, localization and mitigation. Two approaches are described. The first is based on an ODE model while the second on a PDE model. Using an ODE model of the wellbore hydraulics, a globally exponentially stable adaptive observer which estimates the unknown states and parameters of the hydraulic system and in particular quantifies the magnitude of the in-/out-flux and its location in the well, is presented. The observer can be used purely as an in-/out-flux detection system and with a simple controller that automatically and effectively stops an in-/out-flux. Experimental results and realistic simulations with a state-of-the-art simulator are provided to show the effectiveness of the method. The PDE model is used with an infinite-dimensional observer which is capable of detecting and quantifying an in- or out-flux. The PDE model of the hydraulic system can be expressed as a 2×2 linear hyperbolic system of PDEs with spatially varying coefficients coupled with an ODE at the inlet boundary that models the in- or out-flux. Using the method of backstepping, an observer which is exponentially stable at the origin in the $\mathcal{L}^2$-

norm is designed. The observer only relies on measurements taken at the outlet boundary. Simulation results verify the validity of the observer.

Part III addresses prevention of in-/out-flux by controlling the pressure upstream the choke at the drilling rig, which effectively regulates the downhole pressure. Two types of tracking controllers are designed for a hydraulic model of a managed pressure drilling system. Both controllers are designed using backstepping. The first controller is based on a simplified model of the drilling process and considers the disturbance as measured. For the second controller, we regard the disturbance as unmeasured and slowly varying. This allows us to introduce its estimate and design an adaptive controller. The first controller gives exponential stability and tunable convergence rate, while the latter gives asymptotic stability. The performance of the tracking controllers is compared.

Preface

This thesis is submitted in partial fulfillment of the requirements for the degree of philosophiae doctor (PhD) at the Norwegian University of Science and Technology (NTNU). The research has been conducted at the Department of Engineering Cybernetics during the period between November 2009 and December 2012. The work has been carried out under the guidance of Ole Morten Aamo and John-Morten Godhavn. Funding for the work was provided by the Research Council of Norway and Statoil ASA. During the first half of 2012 I had the privilege of visiting Associate Professor Erik Weyer at the University of Melbourne. I am very grateful for his hospitality, and the help he provided during the stay.

The main part of the thesis is composed as a collection of five selected articles, which each make up a chapter. The articles have only been slightly modified, so each chapter can be read independently.

Acknowledgments

After finishing my MSc, which also was carried out under the guidance of Ole Morten Aamo and John-Morten Godhavn, I worked for two years with a company in Oslo. When the offer to pursue a PhD with the same supervisors that I had during my MSc came up, the choice was easy. I am very grateful for getting this opportunity. I would like to thank Ole Morten Aamo for his helpful and encouraging support. He has not only given excellent technical guidance, but also motivated and inspired. I am also very thankful to John-Morten Godhavn for his constructive comments and practical advice.

I have appreciated the stay at the department and the help provided by the administrative and technical staff. I have also enjoyed the (more or less) meaningful discussions with the fellow temporary employees and the inclusive social atmosphere.

Finally I would like to express my gratitude towards my loving and supporting family. Your encouraging words have made this possible. Last, but not least, I hope I somehow can repay my dear Martine's heartwarming devotedness.

Espen Hauge
Trondheim, December 2012

Contents

Abbreviations

BHA	Bottomhole assembly
BHP	Bottomhole pressure
BOP	Blowout preventer
DGD	Dual gradient drilling
ECD	Equivalent circulation density
GES	Globally exponentially stable
HPHT	High pressure, high temperature
LOT	Leak off test
LRRS	Low riser return system
MAASP	Maximum allowable annular surface pressure
MD	Measured depth
MPD	Managed pressure drilling
MWD	Measurement while drilling
OBM	Oil-based drilling mud
ODE	Ordinary differential equation
PDE	Partial differential equation
RCD	Rotating control device
ROP	Rate of penetration
SCR	Slow circulation rate
TVD	True vertical depth
UKF	Unscented Kalman filter
WBM	Water-based drilling mud
WDP	Wired drillpipe
WOB	Weight on bit

Introduction

Chapter 1

Introduction

The scope of this work is to look into new and automatic ways to detect and handle in-fluxes, or kicks, whether it is in gas or in liquid form. Out-fluxes, or losses, are equally important to handle since it may reduce the hydrostatic head in the well, which in turn may lead to a kick. Conceptually, a kick and a loss are two sides of the same issue. However, a *gas* kick changes the flow from being single-phase to two-phase which complicates modelling, estimation and control matters.

In this chapter, a short introduction to drilling, available drilling technology, well control, and modelling of in-/out-flux will be given.

1.1 Managed pressure drilling

The Macondo incident brought awareness to the challenges in drilling, and the possible fatal and environmental consequences. It also made expressions like blow-out preventer (BOP) and deepwater known to the public. Although some of the drilling vocabulary might be known to the reader, this section will cover the most important aspects of drilling, especially managed pressure drilling (MPD), which are necessary to understand the contribution of the thesis.

Drilling of oil wells was already carried out in China in year 347 AD with the help of bamboo poles (Totten, 2004). The wells were up to 240 m deep and the oil was used to produce salt from brine. Today's deepwater wells are highly sophisticated structures and compete with skyscrapers both in terms of magnitude and complexity. The motivation for drilling such expensive wells is given by the world's energy needs combined with the high price of oil. For the drilling contractor, the task amounts to accessing the reservoir in a cost effective manner, and at the same time facilitate for maximum production. The way this is done depends on the water-depth, if it is offshore, the formation above the reservoir, and the reservoir itself. To reach the reservoir, a hole must be drilled through the formation above the reservoir and further into the reservoir. This may sound like a straightforward task, but doing so in rough sea with water-depths spanning kilometers is challenging. Depending on the water depth, a platform, also called rig, carrying the drilling equipment and personnel is either floating or placed on the seabed. The actual drilling is carried out by rotating the drillstring and applying force at the top.

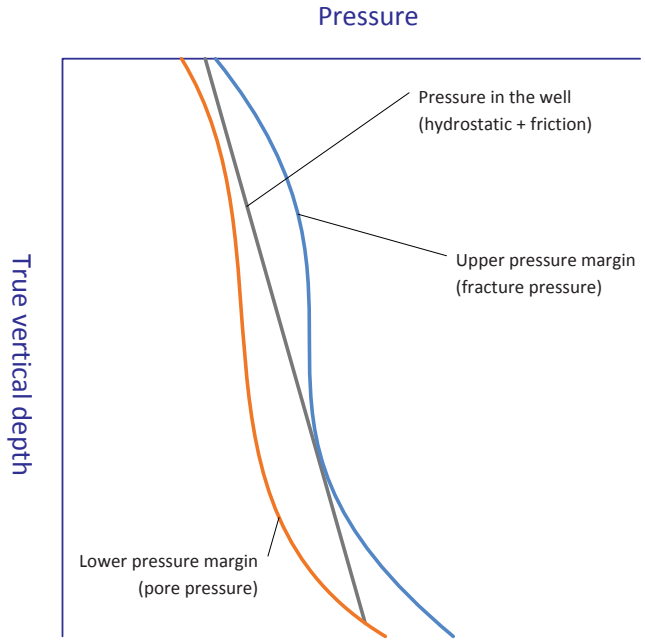

Figure 1.1: Pore pressure, fracture pressure and the pressure in the well.

The drillstring is assembled by a column of hollow drill-pipes with a length of approximately 9 m. Three drill-pipes mounted together make up a stand, which is the way the drill-pipes are stored on the deck of the rig. At the bottom, the bit crushes the rock and the drilling fluid carries the rock chips, called cuttings, back to the platform. Mud, which the drilling fluid commonly is called, is pumped through the inside of the drill-string, jetted through nozzles in the bit and circulated through the annulus back up to the rig. In addition to carrying cuttings, the drilling fluid also cools the bit and acts as the primary safety barrier by keeping the well overbalanced. The term overbalance can be described by looking at the pressure margins in the well in Figure 1.1. Overbalance simply means that the hydrostatic head of the mud is greater than the pore pressure of the formation. So if circulation is stopped, the pressure exerted by the mud throughout the well is greater than any pressure in the formation. If the well is underbalanced, the hydrostatic pressure of the mud is lower than the pore pressure. If, in addition, the formation is permeable and the pore fluid has sufficiently low viscosity, in-flux to the well is possible (Nas, 2011). An in-flux is called a kick in the drilling terminology. If the pressure in the well is higher than the fracture pressure, the mud will start flowing into the formation, which is called a loss. A loss can actually trigger a kick since the pressure in the well is reduced. In Figure 1.1, the grey, straight line represents the pressure in the well due to hydrostatic head and friction. In the annulus, the frictional pressure drop is added to the hydrostatic head. In the depicted case, increasing the frictional pressure drop by increasing the flow rate would cause a loss, which in turn could trigger a kick. Drilling further with the same mud density, also called mud weight,

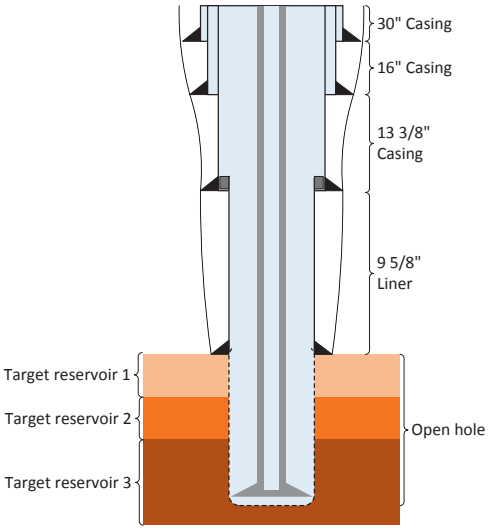

Figure 1.2: Example of a casing program.

would also cause a kick. To be able to drill further, a casing must be set. A casing is a steel cylinder which is hammered into the open hole to safeguard the formation from the pressure exerted by the mud. Figure 1.2 depicts a casing program with a liner hanging from the bottom of the 13 3/8" casing. The so-called open hole is the region of the well which is being drilled. This part is exposed to the formation and is prone to kicks and losses. With newer fields, the pressure margin depicted in Figure 1.1 is getting narrower than what is safe to drill conventionally. MPD is meant as an enabling technology by providing better control of the pressure in the well. It is suggested in Godhavn (2009) that an MPD equipped rig should be able to maintain the pressure in the well within $\pm$ 2.5 bar of the reference pressure.

In addition to the safety barrier provided by the hydrostatic head of the mud, there is a secondary safety barrier which is the BOP stack, sketched in Figure 1.3. It can either be placed on the rig or on the seabed. It is a stack of different type of blowout preventers acting as a redundant system, and its main functions are to contain unwanted reservoir inflow in the well and facilitate well control through the choke and kill lines. The redundant set of rams can either clasp around the drillstring, as with the pipe ram, or cut it, as with the shear ram. If there is no drillstring, a blind ram can be used. The annular preventers can be used to shut in the well while still allowing the drillstring to move vertically, but they are not as effective at containing the pressure in the well as the rams. Failing to seal the well will lead to an uncontrolled flow of reservoir fluids to the surface. If the fluids ignite, the blowout can cause fatalities as with the Deepwater Horizon accident (Graham et al., 2011) and the West Vanguard accident (Holand, 1997).

A simplified drawing of the hydraulic system of a MPD rig with a sealed annulus is shown in Figure 1.4. It highlights the main components that circulate the drilling fluid through the system and pressurize the well. The circulated drilling fluid is

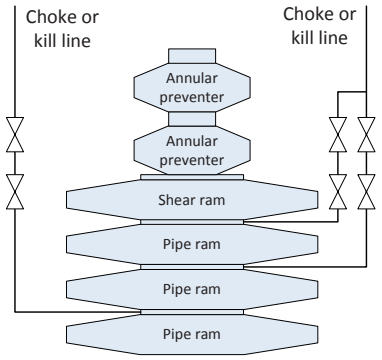

Figure 1.3: Example of a blowout preventer stack.

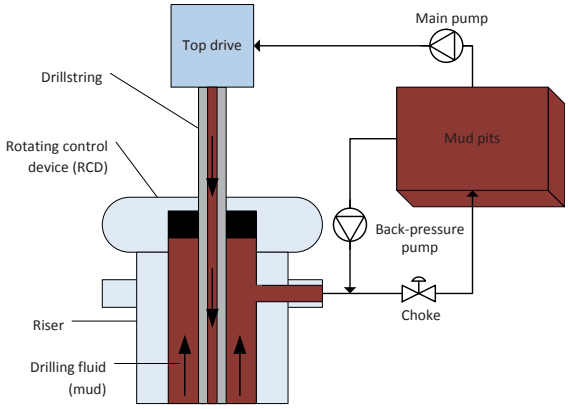

Figure 1.4: The topside part of the hydraulic system at an MPD rig.

stored in the so-called mud pits which are an array of coupled tanks where the mud is treated and mixed before being pumped into the well. The main pump transports the drilling fluid through a hose to the top drive which is connected to the drillstring. The drilling fluid then flows through the inside of the drillstring, through the bit, and back up to the rig through the annulus. At the rig, the rotating control device (RCD) seals the annulus by clasping around the drillstring. The flow is directed into the mud pits through the choke manifold. The pressure in the well can quickly be controlled by manipulating the opening of the choke. Since the choke alone might not apply enough pressure at low flow rates, an additional back-pressure pump is available. Increasing the flow rate from this pump helps maintain the desired pressure in the well.

Another form of MPD is dual gradient drilling (DGD). This method is based on using two fluids with different density in the annulus and separating these spatially, which yields a piecewise linear hydrostatic pressure profile. There is a range of different DGD methods, but only the low riser return system (LRRS) described by Fossli and Sangesland (2004) and Falk et al. (2011) will be presented here. The

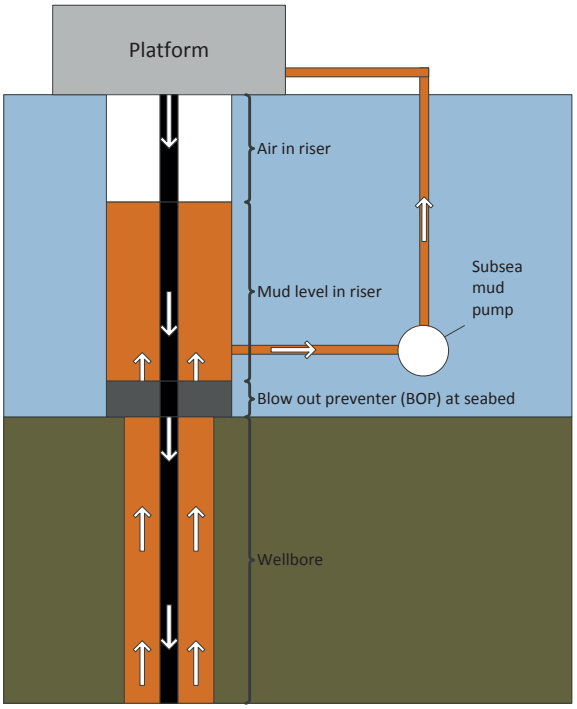

Figure 1.5: A sketch of the low riser return system.

LRRS uses an evacuated riser, as illustrated in Figure 1.5, and typically heavier mud than for conventional drilling. The mud is pumped through the drillstring as with conventional drilling, but does not have to be returned to the rig through the riser. Instead, a parasitic line in the lower part of the riser is coupled to a subsea mud pump which elevates the drilling fluid back to the rig. The mud-air interface level in the riser is typically adjusted by automatic control of the subsea pump and manual control of the main pump. This effectively controls the pressure in the well. Tighter control of the pressure in the well results in less chance of kick or loss incidents. And if a kick is taken, the driller can decide, based on the magnitude of the kick, whether to shut in the well or let the hydrocarbons flow past the BOP.

The two MPD methods previously described emphasize on controlling the pressure at a certain point in the well. Usually this is at the bit, but it could also be at the so-called shoe, which is at the start of the open-hole, or at any other anticipated weak spot in the wellbore. The pressure at a point in the annulus of a well is the sum of the hydrostatic pressure and frictional pressure drop exerted from above. Maintaining the desired pressure in the well requires proper mixing of the drilling fluid to get the desired density, but also knowledge of the frictional pressure drop. The expression equivalent circulation density (ECD) is often used when mentioning friction in the well. It refers to the sum of the hydrostatic pressure and frictional pressure drop converted to density by dividing by the gravitational acceleration and true vertical depth (TVD) of the well. Due to the complex behavior of drilling

fluids combined with varying diameter of the well, rotation of the drillstring, and curved well geometries, among others, predicting the friction in the well can be difficult. It is better to estimate it, as suggested by Stamnes (2011). In his work, a model based on ordinary differential equations (ODE) provided by Kaasa et al. (2012) is used. The drift-flux model, which is a set of partial differential equations (PDE), is also commonly used, as by Rommetveit et al. (2005) and Bjørkevoll et al. (2010). The former approach benefits from a simpler one-fluid model which is relatively easy to configure, while the latter captures spatial effects, supports two-fluid flow, and has a wide range of parameters which can be tuned. However, while a PDE model may sound tempting to use due to the flexibility of the model, the complexity, numerical and robustness issues, and also the expertize needed, must be considered. For some applications, like the pressure control in Godhavn et al. (2011) and pressure estimation in Grip et al. (2010), an ODE model can be good enough.

1.2 Well control

Maintaining the pressure in the wellbore within the limits dictated by the formation is the key to successful well control. However, accidents do happen. Schubert et al. (2006) lists the most common warning signs of unwanted in-flux to the wellbore. They include:

- Drilling break, i.e. increased rate of penetration (ROP).
- Flow increase.
- Pit gain.
- Decrease in circulating pressure and an increase in pump speed of the main pump.
- Well flows with the rig pumps off.
- Increase in rotary torque.

An in-/out-flux is actually very likely to happen when not drilling, such as when tripping, running liner or casing, and during connections. In case of an undesirable event such as a gas kick, the primary safety barrier is lost and well control must be regained. There are procedures for this which briefly can be summed up as closing the BOP, the second safety barrier, and pumping heavier drilling fluid into the well to balance the formation pressure while circulating the gas out of the well. The various well control methods will be described in more detail later in this section.

The annual report from the Petroleum Safety Authority Norway (PSA, 2012) deals with the risk in the Norwegian petroleum sector. A survey relating loss of well control to incidents, shows that 22% of the triggering causes are related to primary barrier failure and 19% to external causes such as geology and reservoir. The mentioned causes cannot be anticipated, which advocate for early detection of in-/out-flux to the wellbore to minimize its extent. In conventional drilling, an in-/out-flux is commonly detected by monitoring the level of drilling fluid in the pit or trip tank. Due to the volume of these tanks, the sensitivity to an in-/out-flux is small. An increase, which is referred to as pit-gain, can be in the range 0.5–1.0 m^3 before the drilling crew responds (Anfinsen and Rommetveit, 1992). Sonic

measurements of the annular fluid, described by Hage and ter Avest (1994), have also been used to determine the phase shift with induced by gas in the wellbore. A benefit of drilling a well with a sealed annuls, is that the closed flow loop makes it easier to detect changes in net flow rate and pressure anomalies which can signal a kick. Grayson and Gans (2012) point out this advantage and Jablonowski and Podio (2011) find consistent statistical evidence that onshore rigs in Texas, USA, with RCD have less blowouts than rigs without. A precise way to measure the net flow through the well is documented by Speers and Gehrig (1987) for conventional drilling, and Santos et al. (2007) for MPD. When drilling with oil-based drilling mud (OBM), in contrast to water-based drilling mud (WBM), the in-flux from the reservoir can dissolve in the mud under high enough pressure and temperature. This makes detection of the kick harder, which in turn emphasize that accuracy of the detection equipment is necessary. By monitoring the time-trends of the stand pipe pressure and annular discharge pressure, Reitsma (2010) is able to diagnose unwanted events such as losses, kick, plugged drillstring, pipe wash-out, among others. The smallest kick magnitude the method is able to detect is not documented. In this thesis, in-/out-flux detection is carried out using an adaptive observer which combines the use of a mathematical model of the process and the available flow and pressure measurements.

Two other triggering causes of loss of well control are listed in the annual report from the Petroleum Safety Authority Norway (PSA, 2012). 13% of the causes are due to "technical failure, or imperfect kick detection", and another 13% are grouped as "misconception/cognitive error". These numbers can be reduced with automatic control. While most wells still are drilled conventionally with manual control, more sophisticated drilling technology and automation are gaining momentum within the drilling community (Downton, 2012, Godhavn, 2009, Nikolaou, 2012, Pink et al., 2012). While fully automated drilling is a goal, today's drilling is, at best, carried out with supervised automation as pointed out by Saeed et al. (2012).

Misconceptions of kicks are often due to an effect called ballooning or breathing. If the reservoir is naturally fractured, it can act as a buffertank which gradually fills with drilling fluid and empties once the pressure is reduced, e.g. when slowing down the pump. The flow rate and pressure signature can be misconceived as an in-/out-flux, and subsequently, time consuming well control procedures will be initiated. As pointed out by Nas (2011), accurate flow meters help distinguish in-flux from ballooning. If a declining flow rate from the well is observed after shutting down the pump, and the flow rate out of the well lags behind the flow rate into the well when starting up the pump again, then ballooning is indicated. There exists different models of naturally fractured reservoirs (Helstrup et al., 2004, Lavrov and Tronvoll, 2004, Mehrabi et al., 2012) which can be used to characterize reservoir parameters and verify the ballooning effect. Another effect, which can be confused with both in-/out-flux and ballooning, is due to the change in pressure and temperature of the mud in high pressure, high temperature (HPHT) wells when stopping or starting circulation. This effect is argued for by Babu (1998), where a mud loss during circulation and pit gain after stopping the pump is explained quantitatively with calculations using the pressure-density-temperature behavior of the mud and temperature changes in the static mud column.

Well control events can occur when tripping, i.e. moving the drillstring, in or out of the bore hole too fast due to the piston effect down-hole. This effect is dubbed surge and swab among drillers, where surge is an increase in pressure and swab is a decrease in pressure. A similar problem occurs on floating rigs when a stand has to be added or removed from the drillstring. During this operation, the drillstring is suspended by the so-called slips through the drill floor. The vertical motion of the rig due to waves, also called heave, is now translated to the bottom of the well through the drillstring. The bottomhole assembly (BHA), which has a greater diameter than the drillstring, and the bit act as a piston in the wellbore, causing unwanted pressure fluctuations in the open-hole. Efforts have been made by Landet et al. (2012), Mahdianfar et al. (2012), among others, to mitigate this effect for MPD rigs. They use model-based control and manipulate the choke opening and flow rate from the backpressure pump to keep the bottomhole pressure constant during a connection.

It is appropriate to end this section by quoting an investigation report concerning the Deepwater Horizon accident (Graham et al., 2011, pp. 121) which clearly states the need for automation of the drilling process.

> In the future, the instrumentation and displays used for well monitoring must be improved. There is no apparent reason why more sophisticated, automated alarms and algorithms cannot be built into the display system to alert the driller and mudlogger when anomalies arise. These individuals sit for 12 hours at a time in front of these displays. In light of the potential consequences, it is no longer acceptable to rely on a system that requires the right person to be looking at the right data at the right time, and then to understand its significance in spite of simultaneous activities and other monitoring responsibilities.

1.2.1 Circulation procedures

When a kick has been taken and the driller has decided to shut-in the well, it can be done as either a soft or hard shut-in. A soft shut-in refers to closing the BOP while keeping the choke line open, while during a hard shut-in this is kept closed. The former method gives a gentler pressure increase in the well while the latter method stops the in-flux faster. Before shutting in, the drillstring must be hoisted from the bottom of the well to prevent clogging of cuttings and weighting material in the bit nozzles. This is important since circulation of mud through the drillstring and annulus is vital for the most common well control procedures. A non-return valve is sometimes installed upstream the bit to avoid the u-tubing effect when changing mud weight. When the flow through the bit is stopped, this valve will close, isolating the formation pressure from the stand pipe pressure (i.e. pump pressure). This is undesirable for a well control situation since the formation pressure is an important parameter for successful well control. However, it can be possible to pump at such a low flow rate that the non-return valve remains open and the stand pipe pressure can be recorded. The shut-in casing pressure, i.e. the pressure in the annulus, must also be recorded before starting the well control procedure. With proper measurements of the flow rate in and out of the well, the volume of the kick can be estimated. Pit gain also gives an indication of

the volume of the in-flux. Combining the knowledge of the mentioned pressures, volume of in-flux, density and type of mud, open-hole diameter, diameter of BHA and drillstring, the density of the in-flux can be determined. If the formation fluid is determined to be a liquid, it is considerably easier to circulate out of the well than if it is a gas. This is due to the effect that gas will carry the formation pressure while percolating if not allowed to expand. Also, the gas can be flammable and poisonous, requiring proper handling when reaching the rig. Before drilling the open-hole, and subsequently risking taking a kick, two limiting values have to be determined. These are the maximum allowable annular surface pressure (MAASP) and kick tolerance, also called kick margin (Redmann Jr., 1991). The MAASP can be limited by the pressure rating of equipment such as casings and wellhead, but it is often limited by the fracture pressure in the open-hole, just below the shoe. This pressure is determined by performing a leak off test (LOT) which is carried out after the most recent casing has been cemented and drilling is resumed. After drilling a few meters into the formation, pressure is applied by closing the annular preventer or pipe rams and steadily pumping mud into the well. The increasing pressures in the annulus and drillstring are recorded, and when the derivatives of the pressures suddenly decrease, an indication that the formation is starting to fracture is given. When the pressures have stabilized, the injection is stopped and the pressure is bled off. The recorded MAASP is used when calculating the kick tolerance, which is a term with multiple definitions (Santos et al., 2011). We define it as the largest volume of in-flux in the lowermost region of the well that can be safely circulated out without fracturing the open-hole. Chirinos et al. (2011) present a method to estimate the peak pressure when circulating out a kick which incorporates the same triangular distribution of gas as in this thesis. If the volume of the kick is within the kick tolerance, an appropriate circulation procedure must be decided upon. If not, an alternative way of killing the well, such as bullheading, must be sought. There is a range of circulation procedures, but the most common are the so-called Driller's method, Engineer's method (a.k.a. Wait and Weight), and the volumetric method. These methods are briefly described in the following subsections and are based on the notes from Skalle (2010). A sketch of ideal pressure trends with the Driller's and Engineer's method are displayed in Figure 1.6.

Driller's method

With the Driller's method, the fluid from the reservoir is circulated out of the well before the mud weight is increased to overbalance the formation pressure. This means that the volume of mud in the well has to be displaced two times before the well is properly killed. However, since the drilling fluid can be weighed up in the mixing tanks concurrently with the first circulation, the circulation can be initiated earlier than with the Engineer's method, which requires that heavy kill mud is available before circulation is started. After shutting in the well and determining the kick parameters, the pumps are set to a predetermined slow circulation rate (SCR) for which the frictional pressure drop is known. The pressure at the bit is now given by the sum of the pump pressure and hydrostatic pressure in the drillstring, minus the frictional pressure drop. The pump pressure, and bit pressure, are effectively controlled by adjusting the casing pressure. During circulation with reservoir fluid

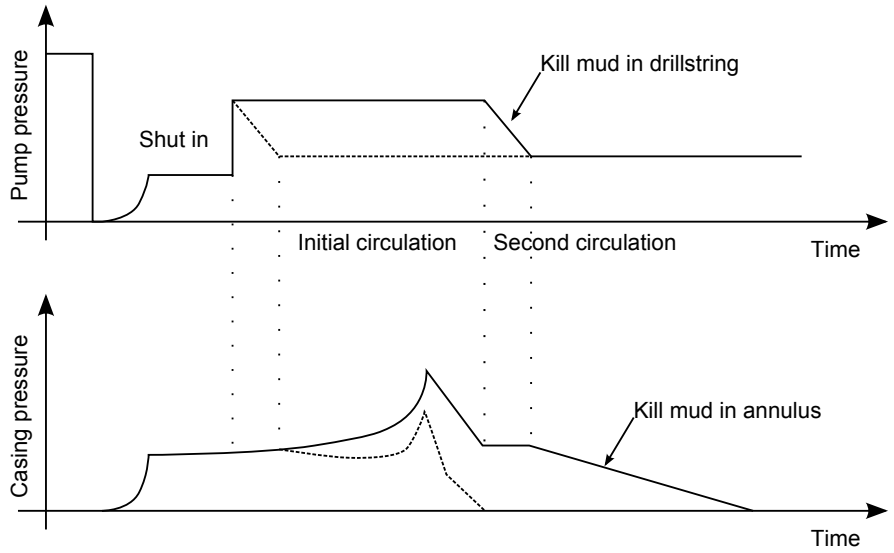

Figure 1.6: Pressure trends during Driller's (solid) and Engineer's (dashed) method.

in the annulus, the pump pressure is kept constant by manipulating the casing pressure, which in turn means that the formation pressure is constant. When the kick is circulated out of the well, the mud weight is increased to overbalance the formation pressure and the second circulation cycle is commenced. As the new heavy mud displaces the old mud, the pump pressure decreases steadily before it flattens out when the new mud reaches the bit. Once the heavy mud starts flowing into the annulus, the casing pressure starts to drop slowly as the mud gradually alleviates the formation pressure. When the mud is at the top of the annulus, the casing pressure should reflect that the formation pressure is balanced by the hydrostatic pressure exerted by the mud, plus a safety margin.

Engineer's method

The Engineer's method differs from the Driller's method by immediately starting circulation with a heavy kill mud after the well has been shut in. This shortens the duration of circulating out the reservoir fluid and killing the well. Ideally, the time consumption should be half of that of the Driller's method, but this is without taking into account the time it takes to mix the kill mud. In fact valuable time is lost while mixing since the buoyant gas will start percolating. And if the well is shut in while the gas is travelling upwards in the open-hole, the integrity of the well can be in danger. Since the mud weight is increased while circulating out the in-flux, the choke opening must be adjusted such that the pump pressure follows a predetermined trajectory, rather than keeping it constant as with the Driller's method. When the heavy mud reaches the bit, a benefit of the method becomes

evident. As heavy mud displaces the old mud in the annulus and the in-flux is on its way upwards, the heavy mud helps lighten the pressure in the annulus. However, the added value of this effect depends on the geometry and casing program of the well since these determine whether the kill mud reaches the annulus before the in-flux passes the casing shoe.

Volumetric method

An in-flux can occur while the bit is not at the bottom of the well, for instance during tripping out of the well. Not being able to circulate heavy mud through the entire stretch of the well, complicates the killing procedure. The Volumetric method is a method which lets the gas expand while travelling up the wellbore by controlling the flow of mud out of the well. The idea is that by letting out a fixed volume of mud, V_{m}, which corresponds to a loss of hydrostatic pressure, p_{m}, in the well, the gas is allowed to expand by V_{m}. So every time the pressure upstream the choke increases with p_{m}, V_{m} of mud is bled off through the choke. When the gas reaches the choke, mud is pumped through the drillstring or kill-line. The casing pressure is now reduced stepwise with p_{m} for each V_{m} which is pumped into the well. When the gas has been displaced by mud, the drillstring must be lowered to the bottom, and the well can be brought to overbalance by circulating heavy kill mud.

1.3 Modelling of in-/out-flux

An MPD rig will typically be equipped with measurements of flow-rate from the pump, q_{p}, and through the choke, q_{c}, and the pressure downstream the pump, p_{p}, and upstream the choke p_{c}. Additional measurements of the ROP, weight on bit (WOB) and level in the mud pit are also available to the driller. For some operations there are pressure and temperature transducers in the BHA and a mud pulse telemetry unit which transmits the recorded values to the rig. These measurements cannot be relied upon in a real-time system as they are intermittent and sometimes erroneous. However, they can serve as a supplement when calibrating models. A technology which is gaining momentum is the so-called wired drillpipe (WDP) where data can be transmitted at a moderate bandwidth, 57.6 kbit/s (Veeningen, 2012), both up and down the drillstring through wires running on the inside of each of the drillpipes. A major benefit with the WDP is the possibility to add pressure and temperature measurements, among others, with regular spatial intervals, producing physical data from multiple locations along the well in real-time. Measurements from the WDP are typically updated every 5 seconds. This technology and other emerging technologies are mentioned by Florence and Burks (2012), which also advocate for automation of the drilling process.

A loss has many similarities with a leak in a pipeline. However, the harsh environment downhole and the fact that it is unavailable for visual inspection, make it more complicated to detect and locate a loss than a leak in a one-phase pipeline. When loosing drilling mud to the formation, it is a risk that it will fracture, which in turn will make the loss more severe. The subsequent pressure reduction in the annulus can result in a kick higher up in the well and a very delicate well

control situation. Failing to regain control of the well can lead to a catastrophic underground blowout. Early detection of a loss can reduce the time span until a countermeasure is taken, which in turn reduces the magnitude of lost drilling fluid.

A liquid in-flux is the converse of a loss, but while the density of the drilling fluid flowing to the formation is known, the exact density of the liquid flowing into the wellbore is not. It can be water or hydrocarbons, which generally has a lower density than the drilling fluid. Depending on the extent of the in-flux, there will be a change in hydrostatic pressure in the annulus which calls for proper well control. Common practice is to circulate out the formation liquid using one of the previously mentioned circulation methods. However, with the annulus sealed by an RCD it is theoretically possible to circulate the kick fluid out of the well without closing the BOP.

While detection of a loss during drilling is possible by monitoring the net flow-rate, localization of the loss is only possible by model-based estimation. The change in frictional pressure drop induced by a loss combined with the change of net flow-rate, gives away the position of the loss. However, un-biased measurements and exact knowledge of the friction along the well is necessary to correctly point out the position of the loss. This can be exemplified using sensitivity analysis, as in Karnavas et al. (1993), by comparing the effect of different parameters on the frictional pressure drop. Using similar notation as in Karnavas et al. (1993) we have the absolute sensitivity function

$$S_\alpha^{\mathcal{F}} = \left.\frac{\partial \mathcal{F}}{\partial \alpha}\right]_{\text{NOP}} \tag{1.1}$$

where $\mathcal{F}$ is the function and α is the parameter to be varied. NOP means the nominal operating point. The relative sensitivity function is used to compare the effect of different parameters and is given by

$$\bar{S}_\alpha^{\mathcal{F}} = \frac{\%\text{ change in } \mathcal{F}}{\%\text{ change in } \alpha} = \frac{\partial \mathcal{F}/\mathcal{F}}{\partial \alpha/\alpha} = \left.\frac{\partial \mathcal{F}}{\partial \alpha}\right]_{\text{NOP}} \frac{\alpha_0}{\mathcal{F}_0} \tag{1.2}$$

where the subscripts 0 means that the parameters assume their nominal operating point values.

Assuming that the frictional pressure drop through the drillstring and the annulus is given by

$$p_{\text{f}}(F, L, q) = F(q) L |q| q, \tag{1.3}$$

where F is a friction coefficient, L is length, and q is flow-rate, we can write the frictional pressure drop from pump to choke as

$$\Delta p = p_{\text{f}}(F_{\text{d}}, L_{\text{d}}, q_{\text{p}}) + p_{\text{f}}(F_{\text{a}}, x, q_{\text{p}}) + p_{\text{f}}(F_{\text{a}}, L_{\text{a}} - x, q_{\text{p}} + q_{\text{x}}). \tag{1.4}$$

The subscripts d, a, and p denote drillstring, annulus, and pump respectively. The location of the in-/out-flux is denoted by x and q_{x} is the rate of the in-/out-flux. The parameters used in the calculations are given in Table 1.1 and the results from computing the relative sensitivity in (1.2) are shown in Table 1.2. A significant portion of the frictional pressure drop from main pump to the choke is due to the turbulent flow in the narrow diameter drillstring. For high flow rates the frictional

Table 1.1: NOP parameters used in the model.

Parameter	Value	Unit
Δp_0	$1.0980{\cdot}10^{2}$	bar
$\Delta p_{\mathrm{ds},0}$	$6.8188{\cdot}10^{1}$	bar
$\Delta p_{\mathrm{ann},0}$	$4.1607{\cdot}10^{1}$	bar
$F_{\mathrm{a},0}$	$1.3630{\cdot}10^{6}$	kg/m^8
$F_{\mathrm{d},0}$	$2.1918{\cdot}10^{6}$	kg/m^8
$q_{\mathrm{p},0}$	$2.0000{\cdot}10^{3}$	l/min
$q_{\mathrm{x},0}$	$-2.0000{\cdot}10^{1}$	l/min
$L_{\mathrm{d},0}$	$2.8000{\cdot}10^{3}$	m
$L_{\mathrm{a},0}$	$2.8000{\cdot}10^{3}$	m
x_0	$1.5000{\cdot}10^{2}$	m

Table 1.2: Values of relative sensitivity functions.

Parameter	Value	Unit
$\bar{S}^{\Delta p}_{F_{\mathrm{a}}}$	$3.7895{\cdot}10^{-1}$	-
$\bar{S}^{\Delta p}_{F_{\mathrm{d}}}$	$6.2105{\cdot}10^{-1}$	-
$\bar{S}^{\Delta p}_{q_{\mathrm{x}}}$	$-7.237{\cdot}10^{-1}$	-
$\bar{S}^{\Delta p}_{q_{\mathrm{p}}}$	2.0072	-
$\bar{S}^{\Delta p}_{x}$	$4.1174{\cdot}10^{-4}$	-

pressure drop through the annulus accounts for 38 percent of the total frictional pressure loss. Since the localization method used in this thesis relies upon the change in annular frictional pressure drop due to a loss, we need a precise model of the friction in both drillstring and annulus. This is pointed out by sensitivities with respect to F_{d} and F_{a} in Table 1.2. If a continuous measurement of the bottomhole pressure is provided, the estimated location of the loss could be more accurate since the footprint of the leak, i.e. the change in annular friction drop, would account for a greater amount of the measured pressure drop. If the wellbore is instrumented with WDP, it is possible to estimate the location quite accurately since a pressure profile would be available.

From Table 1.2 we see that given the simple model of the frictional pressure drop in (1.3), the measurement of q_{p} must be exact to locate the position of the loss since the sensitivity to this parameter is about 5000 times higher than it is for x.

A gas kick is more difficult to localize than a loss or a liquid kick due to the change of frictional pressure drop due to the transition from one-phase to two-phase flow. The rate of the gas kick, the composition of the gas, the interfacial friction between gas and mud, the distribution and the pressure of the gas, are all unknowns which complicate the modelling of a gas kick. Although, efforts have been made through the years to capture the behavior of a gas kick to a detailed level. A model of the volumetric behavior of a gas kick being transported from reservoir to surface was presented in LeBlanc and Lewis (1968). The model takes into account

non-ideal gas deviation and varying temperature along the wellbore and is used to simulate a range of well control operations with different gas in-flux volumes and positions, and mud densities. In Hoberock and Stanbery (1981a,b) the authors present a model based on the combined PDEs from a mass and a momentum balance for liquid flow. The PDEs are simplified into a hydraulic transmission line with approximated time-delays and the gas is superimposed as a function of fluid velocity. Simulation result with the resulting model is compared against published data from Rader and Ward (1975) which shows reasonable correspondence. The pit gain is over predicted by the model since it is adiabatic. Nickens (1987) presents a drift-flux model for WBM which is used for gas kick simulation. The model is, among other, used to compare the effect of letting an automatic controller govern the choke opening while circulating out a kick versus manual manipulation of the choke opening. The comparison shows that a human operator is not able to respond quickly and precisely enough to a change in pressure while keeping control of the well. Another drift-flux computer model for gas kicks was introduced by White and Walton (1990) and was designated for research purposes. The models incorporate temperature effects, OBM and WBM, dissolving gas in OBM, and density depending on cuttings, among others. The articles Ekrann and Rommetveit (1985), Rommetveit and Vefring (1991), Vefring et al. (1991) iterate on the same fundamental drift-flux model. Rommetveit and Vefring (1991) calibrate the model parameters to fit the results from 24 experiments, with both WBM and OBM, carried out on a full-scale drilling rig. Correct modelling of the gas rise velocity is highlighted as a success factor for precisely estimating the pressure along the well. The rationale behind the gas kick modelling in Milner (1992) is the same as in this thesis. A model consisting of seven ODEs is combined with a Kalman filter to estimate bottomhole pressure, volume of gas, and gas migration velocity, among others, to help the driller circulate out a kick. The available measurements are pit gain, drillpipe and casing pressure. An alarm processing method based on a cumulative sum of the residuals between measured and estimated values is also presented. Initial tests show promising results, but it is reported that more tests have to be carried out to validate both the model and alarm detection method.

There are two related problems from petroleum production which are of interest since they involve modelling of concurrent flow of gas and oil. These are casing heading for gas-lift wells and riser induced slugging in production pipelines. Casing heading is treated in Eikrem (2006) and is an instability in producing wells where the oil is lightened with the help of gas injected in the bottom of the well. The instability which occurs is called slugging and leads to a cyclic production of gas and oil which impedes productivity. Slugging is also a problem in pipelines where liquid is allowed to accumulate at the base of the riser. This phenomenon is described and modelled in Storkaas (2005). Due to the spatial variation of pressure, flow-rates, and hold-up, in a slugging well or pipeline, it is natural to model them as distributed parameter systems. There exist many such models, two of which are especially interesting from a control engineer's point of view. They are described in Jahanshahi et al. (2009), which models a gas-lift well, and Di Meglio et al. (2011, 2012), which deal with riser induced slugging. The former model is used with the small-gain theorem to predict stable and unstable regions of operation. The latter articles refer to a model which lends itself to a control design based on spatial back-

stepping. The proposed controller only actuates at the outlet boundary, but the feedback law requires full-state measurement. The mentioned model formulations do not easily lend themselves to observer- and control-design, which is why simplified ODE models have been developed for control purposes. Simplified models, such as the one used in Aamo et al. (2005) for nonlinear observer design and control, are typically derived by partitioning the region where gas and liquid flow concurrently with only one control volume. Only using one control volume precludes tracking of the position of the gas, which is of great interest in the case of gas kick modelling.

1.4 Outline and contributions

This thesis is divided into three main parts, each consisting of a separate selection of papers.

Part I considers modeling of gas kick in an MPD system with both sealed annulus and for LRRS. Estimation of states and parameters is also treated. The main contributions in this part are:

1. A compact ODE model of a gas kick for both sealed wells with either an RCD or BOP, or open wells, such as with LRRS. The model facilitates state and parameter estimation.
2. Comparison of the model for a closed annulus with state-of-the-art simulations.
3. Application of an unscented Kalman filter (UKF) to estimate states and parameters with the use of WDP measurements.

The part consists of the articles Hauge et al. (2012c,e). The latter has been slightly shortened to avoid repetition. The work in Hauge et al. (2012e) is also presented as a condensed version in Hauge et al. (2012d).

Part II covers detection, localization, and mitigation of in-/out-flux. The main contributions in this part are:

1. An ODE model of a in-/out-flux based on the model in Kaasa et al. (2012).
2. Application of a globally exponentially stable (GES) adaptive observer, with the ODE model, which estimates the states, and loss rate and position.
3. Design of a control law which quickly mitigates the in-/out-flux and a demonstration of the controller with use of a state-of-the-art simulator.
4. Verification of the observer's capability to estimate loss rate and position through experimental validation with small scale experiments.
5. Application of an infinite-dimensional observer which estimates the rate of an in-/out-flux.

The part consists of the articles Hauge et al. (2013a,b). The work in Hauge et al. (2013b) is based on results from Hauge et al. (2012a).

Part III is motivated by the need for tight pressure control when drilling with MPD systems. The main contribution in this part is:

1. A comparison of two control designs, based on adaptive backstepping, for tracking of a time-varying reference for the choke pressure.

The part consists of the article Hauge et al. (2012b).

1.5 Publications

The following is a list of publications that form the basis for the thesis.

- **E. Hauge**, Ø.N. Stamnes, J.-M. Godhavn and O.M. Aamo, A Dynamic Model of Percolating Gas in a Wellbore, *SPE Drilling & Completion*, 2012e.
- **E. Hauge**, J.-M. Godhavn, Ø.N. Stamnes and O.M. Aamo, A Dynamic Model of Percolating Gas in an Open Well-Bore, *7th Vienna Conference on Mathematical Modelling (MATHMOD), Proceedings*, 2012c.
- **E. Hauge**, J.-M. Godhavn, Ø.N. Stamnes and O.M. Aamo, Dynamic Modelling of Gas Rising in a Wellbore, *Modelling, Identification and Control / 770: Advances in Computer Science and Engineering, Proceedings*, 2012d.
- **E. Hauge**, O.M. Aamo and J.-M. Godhavn, Model-Based Estimation and Control of In/Out-Flux During Drilling, *American Control Conference (ACC) 2012, Proceedings*, 2012a.
- **E. Hauge**, O.M. Aamo and J.-M. Godhavn, Tracking of Choke Pressure during Managed Pressure Drilling, *Modelling, Identification and Control / 770: Advances in Computer Science and Engineering, Proceedings*, 2012b.
- **E. Hauge**, O.M. Aamo and J.-M. Godhavn, Application of an infinite-dimensional observer for drilling systems incorporating kick and loss detection, *European Control Conference (ECC2013), Proceedings*, 2013a, *Accepted for publication.*
- **E. Hauge**, O.M. Aamo, J.-M. Godhavn and G. Nygaard, A novel model-based scheme for kick and loss mitigation during drilling, *Journal of Process Control*, 2013b, *Accepted for publication.*

The following is an additional contribution made during my PhD studies. The article is not included in the thesis.

- U.J.F. Aarsnes, O.M. Aamo, **E. Hauge** and A. Pavlov, Limits of Controller Performance in the Heave Disturbance Attenuation Problem, *European Control Conference (ECC2013), Proceedings*, 2013, *Accepted for publication.*

My contribution consists of helping with simulations, general discussion, and review of the written presentation.

Part I

Gas kick modelling

Chapter 2

A dynamic model of percolating gas in a wellbore

Summary

The two-phase dynamics of gas percolating up a vertical well filled with water is described by two ordinary differential equations and algebraic relations. We model the gas as bubbles distributed with a distribution function along the well. The model is based on first principles and accommodates tracking of the front of the gas. An unscented Kalman filter is used together with the model and wired drillpipe pressure measurements to estimate the liquid holdup profile as the gas is circulated out of the well. The performance of the model and the method of estimation are compared with results from a state-of-the-art simulator.

2.1 Introduction

After the Macondo incident, the report to the President of the USA (Graham et al., 2011, pp. 121) highlighted the need for automatic systems aiding the drilling crew in making the right decisions during critical events before possible blowouts. In this paper we address the modeling of a gas-kick in a vertical well and estimation of the liquid holdup profile during circulation. A gas-kick is an unwanted influx of gas from the reservoir, or the formation above the reservoir, into the wellbore. The influx is driven by a pressure difference between the wellbore and formation containing the gas. If no measure is taken to mitigate and handle the influx, the gas will expand as it rises upwards, thereby reducing the hydrostatic head in the well, which in turn will cause more gas to enter the wellbore. Such a situation can evolve into a blowout with disastrous consequences. The objective of this paper is to model gas percolating up a wellbore in a simple manner without resorting to the use of partial differential equations. We are motivated by the simplified models for managed pressure drilling (MPD) Kaasa et al. (2011), gas-lift Eikrem et al. (2008) and slugging Di Meglio et al. (2009) which have proven to be instrumental in the design of controllers and adaptive observers.

Research on gas-kicks in the drilling community has an extensive record span-

ning several decades. The authors of Rommetveit and Olsen (1989) carried out 24 experiments with gas-kicks in a full-scale, inclined research well. The data from the experiments reveal dynamic behavior of gas-kicks and help to understand the kick process. Based on full-scale experiments with a conventional drilling rig, Anfinsen and Rommetveit (1992) demonstrates that the reduction in pit gain due to gas solubility is significant when drilling with oil-based mud (OBM) compared to water-based mud (WBM). As a result, kicks in OBM are difficult to detect. Experiments with WBM showed that pit gain and standpipe pressure are valuable kick detectors. In Hovland and Rommetveit (1992) the same test rig is used to analyze gas-rise velocities with both OBM and WBM. Dependencies on density, void fraction, pipe inclination, rheology and surface tension are covered. The main result from the study is that high concentration gas-kicks rise faster than low and medium concentration gas-kicks. The authors of Tarvin et al. (1994) verify this result and add that when the gas fraction is less than 2 % the gas will move slowly. Their experiments also indicate that gas rises faster than expected from the previous research available at that time. By using micro flux control Santos et al. (2007) states that small kicks can be detected earlier than with conventional methods. The results are based on both experiments and actual drilling and kicks smaller than 0.5 bbl were detected. A simulation study comparing initial responses to a kick during MPD is presented in Das et al. (2008). They investigate the effect of either shutting in, increasing pump speed or choking. No single best response is found since it may depend on well geometry, kick zone productivity and likelihood of lost returns. In Gravdal et al. (2008) it is stated that a real time model is beneficial even with wired drillpipe (WDP), and an algorithm for detecting and locating kicks and losses with the additional measurements down-hole provided by the wired drillpipe is presented. It is pointed out why WDP is beneficial for kick detection and the issue of calibrating a hydraulic model with a WDP is addressed. In Gravdal et al. (2009) the methodology for kick evaluation is refined. The algorithm evaluates the time derivative of certain pressures along the drillstring together with time derivatives of both the choke opening and the flow rates. A novel approach to pore pressure estimation at an MPD rig with WDP is demonstrated in Gravdal (2009). The estimation of the pore pressure is carried out after a soft shut-in and the annulus pump is shut down until the time derivative of the pressure upstream the choke is constant. The set point for bottomhole pressure (BHP) is adjusted to be higher than before the kick and circulation is restarted. The results from a thorough simulation study of well control procedures for MPD are presented in Davoudi et al. (2010). The procedures are equivalent to the industry standard procedures used in conventional drilling. Three different wells combined with four different well control procedures are considered. Many factors impose limitations on which response will be most successful, and the most important were identified to be whether a kick is conclusively detected and whether accurate flow out metering is available. No single best procedure is decided upon. The concept of switched control for pressure regulation is introduced in Zhou et al. (2011). An MPD system is considered; by adjusting the choke flow rate, the bottomhole pressure is kept constant when drilling and kicks are handled automatically. The controller switches between a combination of pressure and flow control when there is no kick and pure flow control when a kick is detected. In Godhavn (2009) it is argued in favor of

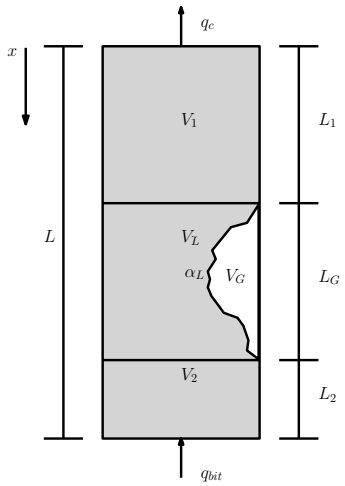

Figure 2.1: Sketch of the modeled bubble structure.

the use of more automatic control during drilling to reduce the non-productive time and to increase the number of wells which can be drilled. Requirements for the control system, hydraulic model, sensors and data logging are presented, with a drilling window for MPD specified to be ± 2.5 bar. Control performance during normal drilling operations is also discussed.

The outline of this paper is as follows. In the next section, we present a general model for the percolating gas without any assumption on its distribution. We continue by deriving a model with a triangular shaped gas distribution which is used for model validation and estimation of the liquid holdup profile. The simulation results are presented in separate sections. The two last sections sum up the conclusions and suggest further work.

2.2 Mathematical model

We intend to model a gas kick in a vertical well of length L initially filled with liquid which is circulated through the drillstring and up the annulus. The model is valid from the kick is taken until the influx is stopped, and captures the dynamics of the percolating gas. We assume that the annulus is sealed by either a rotating control device or the blowout preventer. For simplicity we consider a pipe instead of an annulus, which has only minor effects on the results.

Figure 2.1 shows a sketch of the two-phase model with the physics we are trying to capture. We assume that the distribution of gas is given by a function which we will denote f_α. The derivation of the model is done without any specific assumption regarding the distribution function.

The well is divided into four control volumes: the volume above the bubble structure, V_1; the gas in the bubble structure, V_G; the liquid in the bubble structure, V_L; and the volume underneath the bubble structure, V_2. The control volumes have the associated lengths L_1, L_G, L_L and L_2, respectively, with $L_\mathrm{G} = L_\mathrm{L}$.

Since the model is designed for the time span from the gas-kick is detected until the gas is at the choke, we consider only the liquid volumetric flow rates in, q_{bit}, and out, q_{c}, of the well. Since the well is sealed, we can write the sum of the derivatives with respect to time of the control volumes as

$$\dot{V}_1 + \dot{V}_2 + \dot{V}_{\text{L}} + \dot{V}_{\text{G}} = 0. \tag{2.1}$$

For simplicity we assume that the liquid is incompressible. This enables us to write the expansion of gas as the difference in volumetric flow rate in and out of the well, i.e.

$$\dot{V}_{\text{G}} = q_{\text{c}} - q_{\text{bit}}. \tag{2.2}$$

The time-derivative of the lower control volume V_2 is governed by the rise speed k_{r} of the tail of the bubble structure. We use the expression from Orell and Rembrand (1986) for this rise speed.

$$k_{\text{r}} = C_0 \frac{q_{\text{bit}}}{A_{\text{p}}} + 1.53 \left[\frac{\sigma(\rho_{\text{L}} - \rho_{\text{G}})g}{\rho_{\text{L}}^2} \right]^{\frac{1}{4}} \alpha_{\text{SL}}^n \tag{2.3}$$

where A_{p} is the cross-sectional area of the pipe, ρ_{L} the density of the liquid, ρ_{G} the density of the gas, σ the surface tension between the liquid and the gas, α_{SL} the average liquid holdup, and n is a number that reflects the hindering effect surrounding bubbles has on the terminal velocity. C_0 is a constant that relates how the flow rate in the well impacts the rise velocity of the bubbles. We write the time-derivative for the lower control volume as

$$\dot{V}_2 = k_{\text{r}} A_{\text{p}}. \tag{2.4}$$

Inserting (2.4) into (2.1) gives

$$\dot{V}_1 = -k_{\text{r}} A_{\text{p}} - \dot{V}_{\text{L}} - \dot{V}_{\text{G}}. \tag{2.5}$$

The term $\dot{V}_{\text{L}}$ is dependent on the choice of liquid holdup distribution function. For further derivation of the model we will use the average of the liquid holdup which is given by either

$$\alpha_{\text{SL}} = 1 - \frac{V_{\text{G}}}{L_{\text{G}} A_{\text{p}}} = 1 - \alpha_{\text{SG}} \tag{2.6}$$

where α_{SG} is the average gas fraction, or by solving the integral

$$\alpha_{\text{SL}} = \frac{1}{L_{\text{G}}} \int_{L_1}^{L_1 + L_{\text{G}}} \hat{f}_\alpha(x, \cdot)\, \mathrm{d}x. \tag{2.7}$$

where $\hat{f}_\alpha(x, \cdot) \in (0, 1]$ with $x \in [0, L]$ is some distribution function depending on the spatial variable x, and possibly other variables. The distribution function also gives the volume of gas in the well

$$V_{\text{G}} = A_{\text{p}} \int_{L_1}^{L_1 + L_{\text{G}}} \left(1 - \hat{f}_\alpha(x, \cdot)\right)\, \mathrm{d}x. \tag{2.8}$$

For later use we define the function f_α which is more general as

$$f_\alpha(x,\cdot) = \begin{cases} \hat{f}_\alpha(x,\cdot), & L_1 < x < L_1 + L_\mathrm{G} \quad (2.9a) \\ 1, & \text{else} \quad (2.9b) \end{cases}$$

where $f_\alpha(x,\,\cdot) \in (0,\,1]$.

The average liquid holdup relates the cross-sectional area of liquid in the pipe to the total cross-sectional area of the pipe and also the cross-sectional area of the pipe occupied by gas,

$$A_\mathrm{L} = \alpha_\mathrm{SL} A_\mathrm{p} \quad (2.10)$$
$$A_\mathrm{G} = (1-\alpha_\mathrm{SL}) A_\mathrm{p} \quad (2.11)$$

where A is cross-sectional area and the subscripts L, G and p denotes liquid, gas and pipe, respectively.

Since the rate at which V_L and V_G change length is equal, we can write

$$\dot{L}_\mathrm{G} = \dot{L}_\mathrm{L} \quad (2.12)$$

or equally

$$\frac{\dot{V}_\mathrm{L}}{A_\mathrm{L}} = \frac{\dot{V}_\mathrm{G}}{A_\mathrm{G}}. \quad (2.13)$$

Inserting (2.10) and (2.11) into (2.13) and rearranging we get

$$\dot{V}_\mathrm{L} = \frac{\alpha_\mathrm{SL}}{1-\alpha_\mathrm{SL}} \dot{V}_\mathrm{G} \quad (2.14)$$

which we can insert into (2.5) to get

$$\dot{V}_1 = -k_\mathrm{r} A_\mathrm{p} - \frac{\dot{V}_\mathrm{G}}{1-\alpha_\mathrm{SL}}. \quad (2.15)$$

Since we are interested in the length of this control volume we divide by A_p and insert (2.2)

$$\dot{L}_1 = -k_\mathrm{r} - \frac{(q_\mathrm{c} - q_\mathrm{bit})}{A_\mathrm{p}(1-\alpha_\mathrm{SL})}. \quad (2.16)$$

The length of the lower control volume is given by

$$L_2 = L - L_1 - L_\mathrm{G}. \quad (2.17)$$

We assume that the pressure in the bubble structure has a single value which is the pressure at the point with the greatest gas fraction. The pressure is assumed given by the equation of state

$$p_\mathrm{G} = \frac{Z m_\mathrm{G} R T}{M_\mathrm{G} V_\mathrm{G}} \quad (2.18)$$

where Z is the compressibility factor, m_G is the mass of gas, R the gas constant, T the temperature at the middle of the bubble structure, and M_G is the molar mass of the gas.

We are interested in the pressure upstream the choke and at the bottom of the well. With the front of the gas located at depth L_1, and the maximum gas fraction at

$$x_{\mathrm{G}} = L_1 + \lambda L_{\mathrm{G}}, \tag{2.19}$$

where $\lambda \in (0, 1)$, we can write the momentum balance for the choke pressure as

$$p_{\mathrm{c}} = p_{\mathrm{G}} - \rho_{\mathrm{L}} g L_1 - \rho_{\mathrm{L}} g \int_{L_1}^{x_{\mathrm{G}}} f_\alpha(x, \cdot)\, \mathrm{d}x - \rho_{\mathrm{G}} g \int_{L_1}^{x_{\mathrm{G}}} (1 - f_\alpha(x, \cdot))\, \mathrm{d}x \\ - \lambda p_{\mathrm{fric,G}} - p_{\mathrm{fric},1} \tag{2.20}$$

where p_{c} is the pressure upstream the choke, and p_{G} the pressure in the middle of the bubble structure. We assume that the density of the gas is given as

$$\rho_{\mathrm{G}} = \frac{m_{\mathrm{G}}}{V_{\mathrm{G}}} \tag{2.21}$$

while the density of the liquid is constant. $p_{\mathrm{fric,G}}$ and $p_{\mathrm{fric},1}$ are the frictional pressure drop along the bubble structure and upper control volume, respectively. Similarly, using the bubble pressure as the starting point we express the pressure at the bit, assuming it is at the bottom of the well, as

$$p_{\mathrm{bit}} = p_{\mathrm{G}} + \rho_{\mathrm{L}} g L_2 + \rho_{\mathrm{L}} g \int_{x_{\mathrm{G}}}^{L_1 + L_{\mathrm{G}}} f_\alpha(x, \cdot)\, \mathrm{d}x + \rho_{\mathrm{G}} g \int_{x_{\mathrm{G}}}^{L_1 + L_{\mathrm{G}}} (1 - f_\alpha(x, \cdot))\, \mathrm{d}x \\ + (1 - \lambda) p_{\mathrm{fric,G}} + p_{\mathrm{fric},2} \tag{2.22}$$

where $p_{\mathrm{fric},2}$ is the frictional pressure drop along the lower control volume. Having the pressure upstream the choke and assuming a known pressure, p_0, downstream the choke we can write the volumetric flow rate through the choke using the valve equation from Merritt (1967) with linear valve characteristic

$$q_{\mathrm{c}} = k_{\mathrm{c}} u_{\mathrm{c}} \sqrt{\frac{1}{\rho_{\mathrm{L}}} (p_{\mathrm{c}} - p_0)} \tag{2.23}$$

where k_{c} is a constant related to the cross-sectional area of the orifice and $u_{\mathrm{c}} \in [0, 1]$ is the opening of the choke.

2.2.1 Wired drillpipe.

If the well is instrumented with wired drillpipe (WDP), there will be pressure readings along the drillpipe which are available in real time. When the gas passes by a pressure sensor, the hydrostatic head above the sensor is reduced, giving a footprint of the front of the gas. The pressure at such a sensor, located at depth x_{s}, is given by

$$p_{\mathrm{s}}(x_{\mathrm{s}}) = p_{\mathrm{G}} - \int_{x_{\mathrm{s}}}^{x_{\mathrm{G}}} f_{\mathrm{fric}}(x, \cdot)\, \mathrm{d}x - \rho_{\mathrm{L}} g \int_{x_{\mathrm{s}}}^{x_{\mathrm{G}}} f_\alpha(x, \cdot)\, \mathrm{d}x \\ - \rho_{\mathrm{G}} g \int_{x_{\mathrm{s}}}^{x_{\mathrm{G}}} (1 - f_\alpha(x, \cdot))\, \mathrm{d}x, \tag{2.24}$$

where $f_{\mathrm{fric}}(x, \cdot)$ is some function that accounts for the frictional pressure drop.

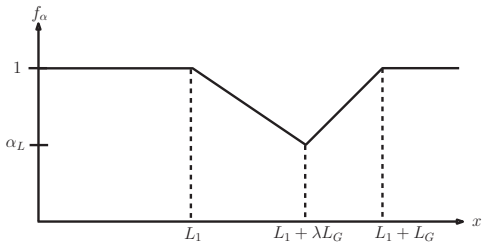

Figure 2.2: The distribution function (2.9) using $\hat{f}_\alpha$ from (2.25).

2.2.2 Triangular holdup distribution.

The distribution profile of the gas fraction, $1-f_\alpha$, will take on a shape resembling a bell curve, possibly skewed. Our goal in this paper is to make a simple model of the percolating gas, and this is achieved by choosing the distribution function for the gas as a simple triangle. The idea of using a bubble structure with a triangular shape originates from Ohara et al. (2004) and has proven to be a sufficiently accurate approximation to the shape which the distribution of gas bubbles will usually form.

We write the function $\hat{f}_\alpha$ for the holdup used in (2.9) as

$$\hat{f}_\alpha = \begin{cases} \alpha_{\mathrm{L}} + \dfrac{(1-\alpha_{\mathrm{L}})(x-L_1)}{\lambda L_{\mathrm{G}}}, & L_1 < x \leq L_1 + \lambda L_{\mathrm{G}} \quad (2.25a) \\ \alpha_{\mathrm{L}} - \dfrac{(1-\alpha_{\mathrm{L}})(x-L_1-\lambda L_{\mathrm{G}})}{(1-\lambda)L_{\mathrm{G}}}, & L_1 + \lambda L_{\mathrm{G}} < x < L_1 + L_{\mathrm{G}} \quad (2.25b) \end{cases}$$

where α_{L} is the minimum liquid holdup of the distribution. The function is sketched in Figure 2.2. The parameter λ decides the shift of the maximum gas-fraction towards the endpoints of the bubble structure. λ close to 0 corresponds to a maximum gas-fraction at the top of the bubble structure, while λ close to 1 corresponds to a maximum gas-fraction at the bottom of the bubble structure. The average holdup is found by solving (2.7) with (2.25) which gives

$$\alpha_{\mathrm{SL}} = \frac{1+\alpha_{\mathrm{L}}}{2}. \tag{2.26}$$

Inserting (2.26) into (2.16), (2.25) into (2.9), and (2.9) into (2.20), (2.22) and (2.24), we get a simple model for the percolating gas. The dynamic equations are

$$\dot{L}_1 = -\frac{2(q_{\mathrm{c}} - q_{\mathrm{bit}})}{A_{\mathrm{p}}(1-\alpha_{\mathrm{L}})} - k_{\mathrm{r}} \tag{2.27}$$

$$\dot{V}_{\mathrm{G}} = q_{\mathrm{c}} - q_{\mathrm{bit}} \tag{2.28}$$

while the algebraic equations are the equation of state, (2.18), the volumetric flow rate through the choke, (2.23), and

$$L_{\mathrm{G}} = \frac{2V_{\mathrm{G}}}{A_{\mathrm{p}}(1-\alpha_{\mathrm{L}})} \tag{2.29}$$

where we have found (2.29) by solving (2.8) and dividing by A_{p}. Pressures upstream the choke and at the bit are given by

$$p_{\mathrm{c}} = p_{\mathrm{G}} - \rho_{\mathrm{L}} g L_1 - \lambda p_{\mathrm{fric,G}} - p_{\mathrm{fric},1} - \lambda g \left(\frac{1+\alpha_{\mathrm{L}}}{1-\alpha_{\mathrm{L}}} \frac{\rho_{\mathrm{L}} V_{\mathrm{G}}}{A_{\mathrm{p}}} + \frac{m_{\mathrm{G}}}{A_{\mathrm{p}}} \right) \tag{2.30}$$

$$p_{\mathrm{bit}} = p_{\mathrm{G}} + \rho_{\mathrm{L}} g L_2 + (1-\lambda) p_{\mathrm{fric,G}} + p_{\mathrm{fric},2} + (1-\lambda) g \left(\frac{1+\alpha_{\mathrm{L}}}{1-\alpha_{\mathrm{L}}} \frac{\rho_{\mathrm{L}} V_{\mathrm{G}}}{A_{\mathrm{p}}} + \frac{m_{\mathrm{G}}}{A_{\mathrm{p}}} \right). \tag{2.31}$$

The expression for the pressure at a sensor in the WDP located at position x_{s} is given by

$$p_{\mathrm{s}}(x_{\mathrm{s}}) = \begin{cases} p_{\mathrm{G}} - \displaystyle\int_{x_{\mathrm{s}}}^{x_{\mathrm{G}}} f_{\mathrm{fric}} \, \mathrm{d}x - \rho_{\mathrm{L}} g (x_{\mathrm{G}} - x_{\mathrm{s}}) & \\ \quad + (\rho_{\mathrm{L}} - \rho_{\mathrm{G}}) g \dfrac{\lambda L_{\mathrm{G}} (\alpha_{\mathrm{L}} - 1)}{2}, & 0 \le x_{\mathrm{s}} \le L_1 \quad (2.32\mathrm{a}) \\ p_{\mathrm{G}} - \displaystyle\int_{x_{\mathrm{s}}}^{x_{\mathrm{G}}} f_{\mathrm{fric}} \, \mathrm{d}x - \rho_{\mathrm{L}} g (x_{\mathrm{s}} - x_{\mathrm{G}}) & \\ \quad + (\rho_{\mathrm{L}} - \rho_{\mathrm{G}}) g \dfrac{(x_{\mathrm{s}} - x_{\mathrm{G}})(\alpha_{\mathrm{L}} - 1)}{2\lambda L_{\mathrm{G}}} & L_1 < x_{\mathrm{s}} \le x_{\mathrm{G}} (2.32\mathrm{b}) \\ \quad \times (x_{\mathrm{s}} - 2L_1 + x_{\mathrm{G}}), & \\ p_{\mathrm{G}} - \displaystyle\int_{x_{\mathrm{s}}}^{x_{\mathrm{G}}} f_{\mathrm{fric}} \, \mathrm{d}x & \\ \quad - \rho_{\mathrm{L}} g \dfrac{(x_{\mathrm{s}} - x_{\mathrm{G}})(\alpha_{\mathrm{L}} - \lambda)}{\lambda - 1} & \\ \quad + \dfrac{(x_{\mathrm{s}} - x_{\mathrm{G}})(\alpha_{\mathrm{L}} - 1) g}{2 L_{\mathrm{g}} (\lambda - 1)} & x_{\mathrm{G}} < x_{\mathrm{s}} < L_{\mathrm{i}} \, (2.32\mathrm{c}) \\ \quad \times \Big(\rho_{\mathrm{L}} (x_{\mathrm{s}} - 2L_1 + x_{\mathrm{G}}) & \\ \quad + \rho_{\mathrm{G}} (2L_1 + 2L_{\mathrm{g}} - x_{\mathrm{s}} - x_{\mathrm{G}}) \Big), & \\ p_{\mathrm{G}} - \displaystyle\int_{x_{\mathrm{s}}}^{x_{\mathrm{G}}} f_{\mathrm{fric}} \, \mathrm{d}x + \rho_{\mathrm{L}} g (\alpha_{\mathrm{L}} - \lambda) L_{\mathrm{g}} & \\ \quad - \rho_{\mathrm{G}} g (\alpha_{\mathrm{L}} - 1) L_{\mathrm{g}} - \rho_{\mathrm{L}} g (L_1 + L_{\mathrm{G}} - x_{\mathrm{s}}), & L_{\mathrm{i}} \le x_{\mathrm{s}} \le L, (2.32\mathrm{d}) \end{cases}$$

where $L_{\mathrm{i}} = L_1 + L_{\mathrm{G}}$.

We have chosen α_{L} as a constant throughout the simulations. However, it is desirable to express this parameter as a function of the slip between the two phases. Unfortunately, this is difficult with the proposed model due to the lack of distinction between superficial and in-situ velocity of the phases.

2.2.3 Friction modeling.

The frictional pressure drop is accounted for by using the expression from Orell and Rembrand (1986)

$$p_{\mathrm{fric,CV}} = \frac{2 f L_{\mathrm{CV}} q_{\mathrm{CV}}^2 \rho_{\mathrm{CV}}}{D A_p^2} \tag{2.33}$$

where the subscript CV can be replaced with 1, 2, and m which denotes mixture. For the mixture flow in the bubble structure, the friction factor f is found by the relationship in Chen (1979)

$$f = \frac{1}{\left[4\log\left(\frac{\varepsilon/D}{3.7065} - \frac{5.0452}{\mathrm{Re_m}}\log\Lambda\right)^2\right]} \tag{2.34}$$

$$\Lambda = \frac{(\varepsilon/D)^{1.1098}}{2.8257} + \left(\frac{7.149}{\mathrm{Re_m}}\right)^{0.8981}, \tag{2.35}$$

where ε is the roughness of the pipe, D its diameter, and $\mathrm{Re_m}$ is the mixture Reynolds number which can be found by evaluating

$$\mathrm{Re_m} = \frac{u_\mathrm{m} D \rho_\mathrm{m}}{\mu_\mathrm{m}}, \tag{2.36}$$

where u_m is the mixture velocity, μ_m is the mixture viscosity and ρ_m the density of the mixture. We use the following expressions for the three aforementioned variables

$$u_\mathrm{m} = \frac{q_\mathrm{bit}}{A_\mathrm{p}} + k_\mathrm{r} \tag{2.37}$$

$$\mu_\mathrm{m} = \alpha_\mathrm{SL}\mu_\mathrm{L} + (1-\alpha_\mathrm{SL})\mu_\mathrm{G} \tag{2.38}$$

$$\rho_\mathrm{m} = \alpha_\mathrm{SL}\rho_\mathrm{L} + (1-\alpha_\mathrm{SL})\rho_\mathrm{G} \tag{2.39}$$

where μ_L and μ_G is the viscosity of the liquid and gas, respectively. For the one-phase control volumes, we use (2.34), (2.35) and (2.36) with the in-situ parameters and velocities.

2.3 Comparison with high-fidelity simulator

The proposed model is brief and compact but is still able to replicate the most important dynamics of percolating gas in a well. To benchmark the model we compare our results with simulations from the multiphase flow simulator OLGA[1]. We simulate a large methane gas-kick in a vertical pipe carrying water. In the OLGA simulations, the gas is injected over a 1 minute interval with a constant flow rate. Our model is started with the same mass of gas distributed with the triangular function at the bottom of the pipe at the time $t = 0$. During the simulation there is a constant flow rate of water, q_bit, entering at the bottom of the pipe. The parameters used in our model and the OLGA simulator are listed in Table 2.1. The values denoted PVT in this table are found by OLGA using a look-up table for pressure, volume and temperature.

Since the model is not valid after the gas front has reached the choke, only the results from OLGA are plotted for this period. Figure 2.3 displays the pressure upstream the choke, and the volumetric flow rate is seen in Figure 2.4. Figure 2.5 shows the pressure at the bottom of the well which is accurately captured in our model. The volume of the gas is plotted in Figure 2.6. Fixing the gas fraction,

[1]OLGA is a commercial multiphase flow simulator provided by SPT Group.

Table 2.1: Parameters used in the compared models.

Parameter	Matlab	OLGA	Unit
ρ_{L}	1000	1000	$\mathrm{kg/m^3}$
σ	$75.640{\cdot}10^{-3}$	PVT	N/m
L	2200	2200	m
D	0.330	0.330	m
q_{bit}	400	400	l/min
Z	0.800	PVT	-
m_{G}	605.890	605.890	kg
M_{G}	$16.042{\cdot}10^{-3}$	$16.042{\cdot}10^{-3}$	kg/mol
T	288	288	K
α_{L}	0.790	·	$\mathrm{m^2/m^2}$
λ	0.770	·	-
k_{c}	0.304	·	$\mathrm{m^2}$
ε	10^{-5}	10^{-5}	m
μ_{L}	10^{-3}	PVT	$\mathrm{Ns/m^2}$
μ_{G}	10^{-5}	PVT	$\mathrm{Ns/m^2}$
C_0	0.750	·	-
n	4	·	-
p_{amb}	3	3	atm

presented in Figure 2.7, inhibits the gas to expand in the radial direction, and an increase in volume is accounted for only in the vertical direction. This is clearly seen in Figure 2.8 which presents the position of the front and tail of the bubble structure. In OLGA the gas occupies a fraction of the pipe cross-sectional area which is time varying, meaning that when the gas is expanding, it may expand both vertically and radially. The pressure in the bubble structure at the point with maximum gas-fraction is presented in Figure 2.9. This pressure is about 7 bar lower in our model due to the location of the bubble structure, as seen in Figure 2.8. Figure 2.10 highlights an interesting feature of WDP pressure sensors. The plot displays how the pressure decreases from 20 min and onwards for our model. At 45 min, the signature of the maximum gas-fraction can be seen. The presented model has a sharper signature than OLGA due to the triangular shape of the distribution function, whereas OLGA has a smoother bell-shaped distribution.

From Figure 2.3 – Figure 2.5, which are the measurements that usually are available for the driller, we see that the presented model gives a good match although the position and gas-fraction are not correctly captured. This highlights the difficulty with determining how the gas is distributed in the well while percolating. To draw conclusions about the distribution profile, additional pressure readings along the well is necessary. In the next section we use WDP with an established method of estimation to determine the holdup profile.

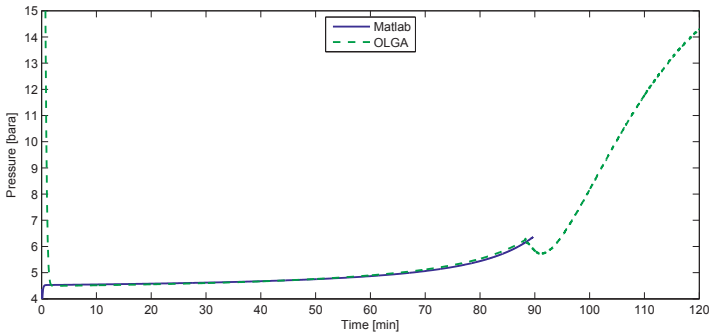

Figure 2.3: *Model tuning.* Pressure upstream the choke.

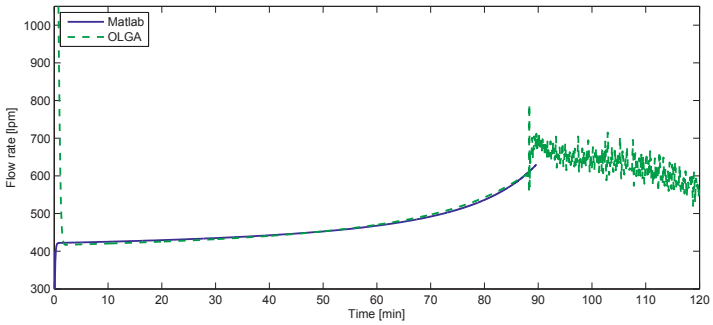

Figure 2.4: *Model tuning.* Volumetric flow rate of water.

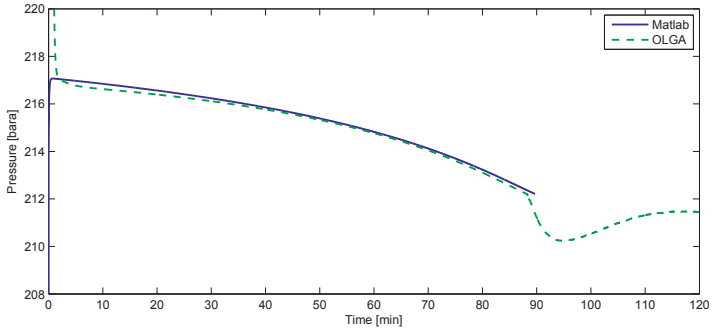

Figure 2.5: *Model tuning.* Pressure at the bottom of the well.

2.4 Application

To demonstrate possible use of the model, we present a gas-kick case where WDP pressure and temperature readings are used with a model-based estimation scheme to determine how the gas is distributed while percolating. We have simulated the same large methane-kick as in the previous section using OLGA. Parameters are

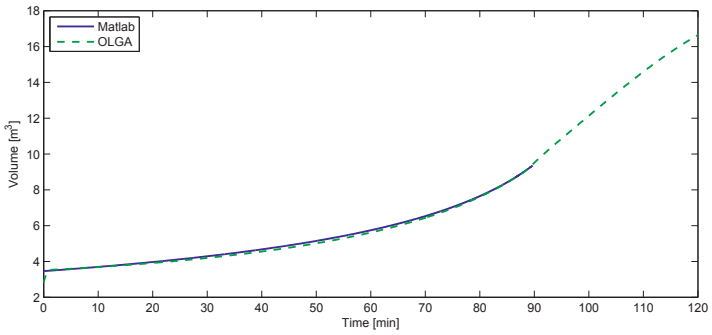

Figure 2.6: *Model tuning.* Gas content in the well.

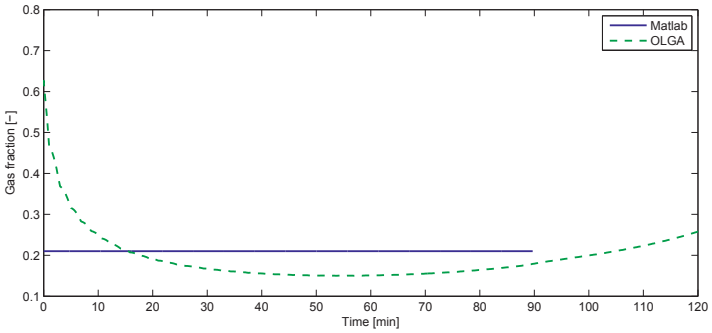

Figure 2.7: *Model tuning.* The maximal gas fraction in the pipe (1-α_{L}).

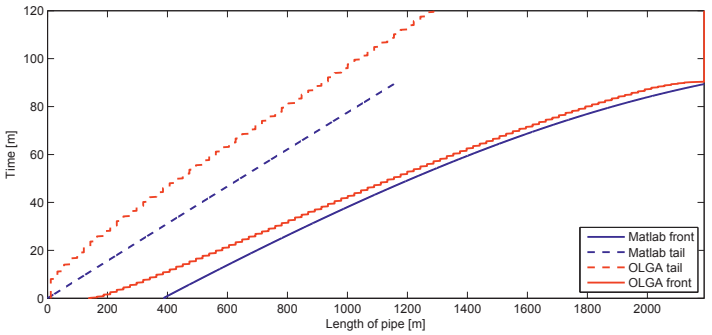

Figure 2.8: *Model tuning.* Position of the front and tail of the bubble structure.

specified in Table 2.1. In contrast to the model tuning case, we now enable the temperature dynamics in the simulations and use the Unscented Kalman filter (UKF) to estimate the dynamic states, L_1 and V_{G}, and slowly-varying parameters, α_{L}, k_{r}, m_{G} and λ. An introduction to the UKF can be found in Julier and Uhlmann (2004). In the simulated case, the initial flow rate is 1000 lpm prior to the kick.

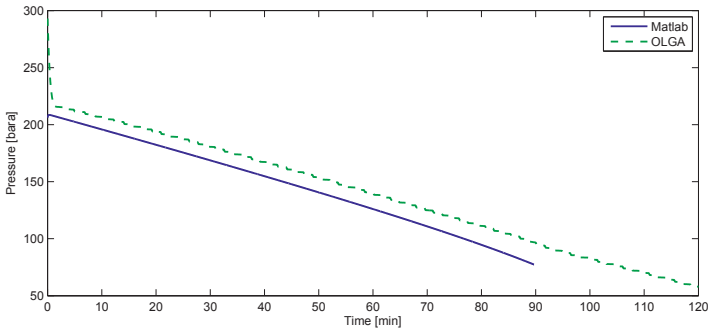

Figure 2.9: *Model tuning.* Pressure in the bubble structure.

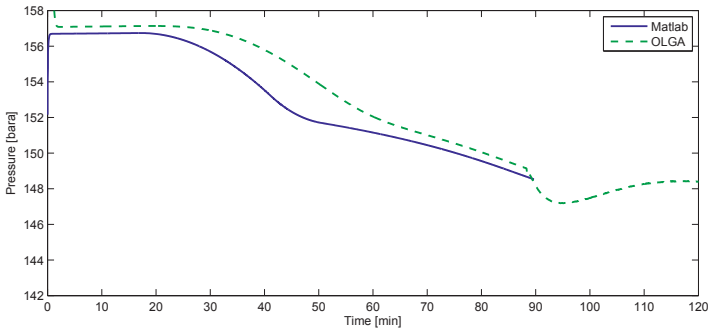

Figure 2.10: *Model tuning.* Pressure reading from a pressure sensor at 1551 m TVD.

After the kick is taken, the flow rate is reduced to 400 lpm and the choke opening is governed by a PI-controller maintaining constant BHP. I.e., we use the Driller's method to circulate out the kick.

Since the temperature is no longer assumed constant, we have to measure it with the WDP. From the temperature readings we can determine the temperature profile in the well. The temperature at the bit is 51° C, and at the choke it is 33° C. The sensors in the WDP are located 220 m apart, starting at 231 m and ending at 1991 m. There are 9 sensors in the well. The standard deviation of the measurement noise is 0.1 bar for the pressure sensors, and 0.1° C for the temperature sensors. When starting the UKF, we use the initial values $\hat{L}_1(t=0) = 2059.70$ m, $\hat{V}_{\mathrm{G}}(t=0) = 3.00$ m^3, $\alpha_{\mathrm{L}}(t=0) = 0.50$, $\hat{k}_r(t=0) = 0.25$ m/s^2, $\hat{m}_{\mathrm{G}}(t=0) = 600.00$ kg and $\hat{\lambda}(t=0) = 0.50$, where the hat $(\hat{\cdot})$ indicates that the values are estimated. When tuning the UKF, we use the following values for standard deviation for the states and parameters: $\hat{L}_1$, 10^{-1} m; $\hat{V}_{\mathrm{G}}$, 10^{-2} m^3; α_{L}, 10^{-3}; $\hat{k}_r$, 10^{-5} m/s^2; $\hat{m}_{\mathrm{G}}$, 10^{-1} kg; and $\hat{\lambda}$, 10^{-4}. These values reflect the anticipated change of the estimated value for each time step. The water and gas are immiscible, and we assume that we know that the influx is methane so we can determine M_{G}.

Figure 2.11 through Figure 2.14 show that the estimated lengths of the control volumes and the estimated volume of the gas in the well are converging towards

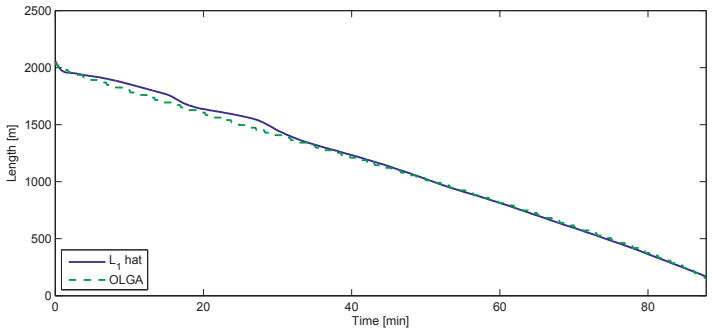

Figure 2.11: *Estimation – Onshore well.* Length of upper control volume.

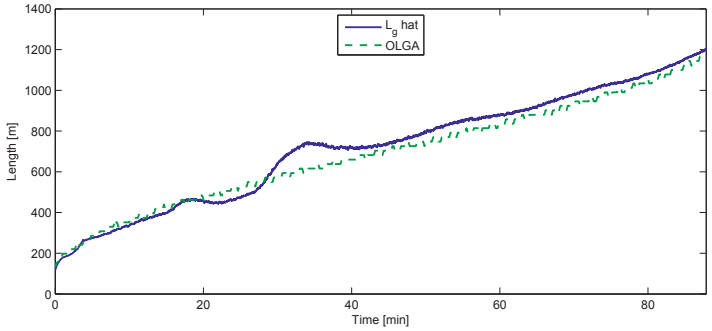

Figure 2.12: *Estimation – Onshore well.* Length bubble structure.

the actual values. We also see that the minimum liquid holdup in Figure 2.15 is properly estimated. The skewness parameter λ in Figure 2.16 is correctly estimated after 60 minutes, indicating that much of the gas is portioned towards the tail of the bubble structure. In Figure 2.17 the estimated mass of the gas is diverging from the actual value. This is expected, due to the low weight of the gas which only accounts for 0.7 bar of the hydrostatic pressure in the well. The rise velocity of the tail of the gas bubble is displayed in Figure 2.18. After about 60 min the estimated value is diverging, but this does not affect the more important estimates such as lengths and volume. Figure 2.19 presents the pressure reading from a sensor in the WDP. Since the UKF is correctly estimating the most important states and parameters, the estimated pressure is close to the actual pressure.

2.5 Discussion

Using first principles modeling, we obtain a simplified model of a gas-kick percolating up a well. The simplifications made during the modeling process, are done with estimation in mind. Using the model by itself will produce erroneous results since the relation between slip and holdup is not considered, and time-varying parameters such as α_{L} and λ are considered constant. However, the model is well suited for

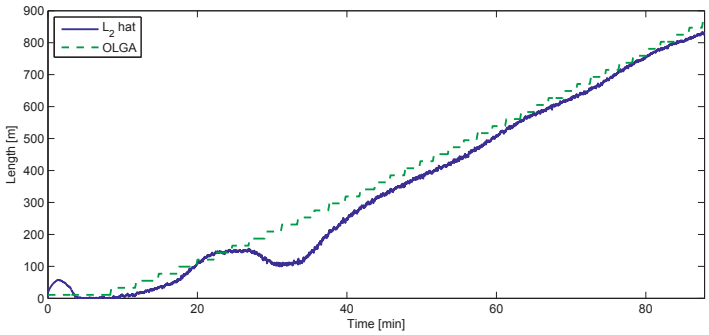

Figure 2.13: *Estimation – Onshore well.* Length of lower control volume.

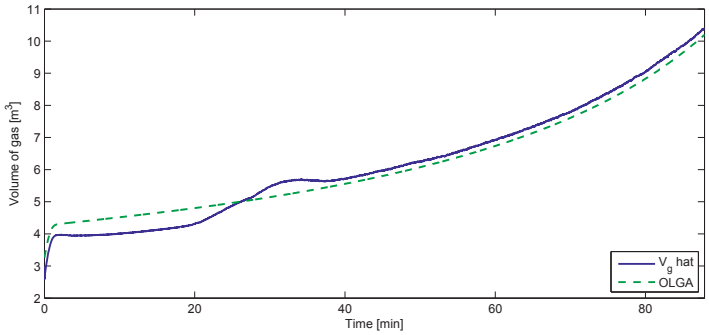

Figure 2.14: *Estimation – Onshore well.* Volume of gas in the well.

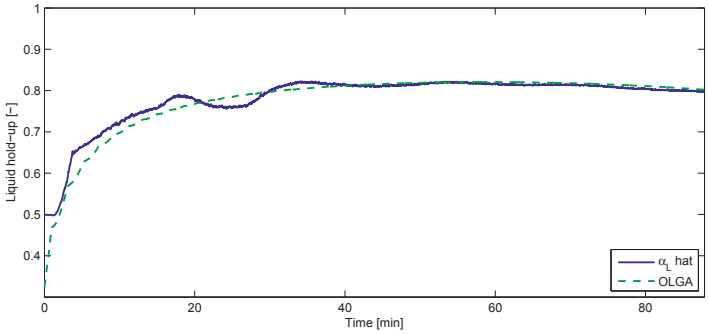

Figure 2.15: *Estimation – Onshore well.* Minimum liquid holdup.

estimation since both important dynamics and parameters are incorporated. The particularly simple triangular holdup profile provides an explicit expression for the pressure at any point in the well during circulation. Note that this expression also provides the correct BHP, $p_{\mathrm{s}}(L) = p_{\mathrm{bit}}$, and the correct choke pressure, $p_{\mathrm{s}}(0) = p_{\mathrm{c}}$. The triangular profile is able to encapsulate a realistic gas distribution due to the

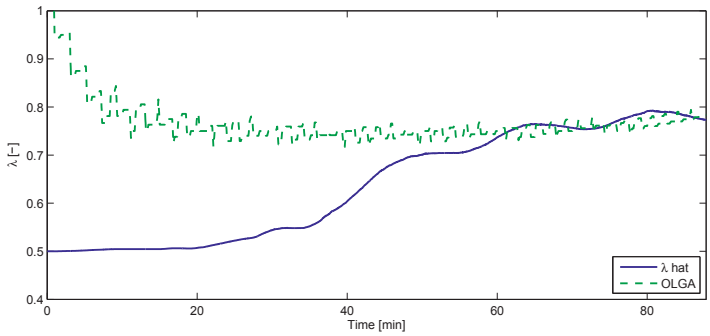

Figure 2.16: *Estimation – Onshore well.* Skewness parameter.

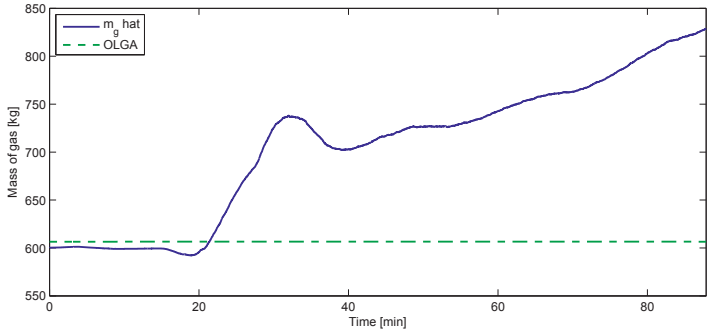

Figure 2.17: *Estimation – Onshore well.* Mass of gas in the well.

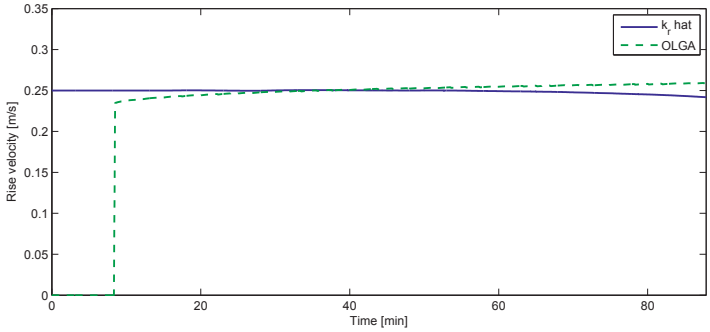

Figure 2.18: *Estimation – Onshore well.* Rise velocity of the tail of the bubble structure.

skewness parameter λ and the minimum liquid holdup α_{L}. It is possible to use a smoother profile, but this will result in a more complex model. For immiscible fluids, the gas bubbles will usually gather towards the tail of the bubble structure. If flashing occurs, this would happen in the front of the bubble structure and increase

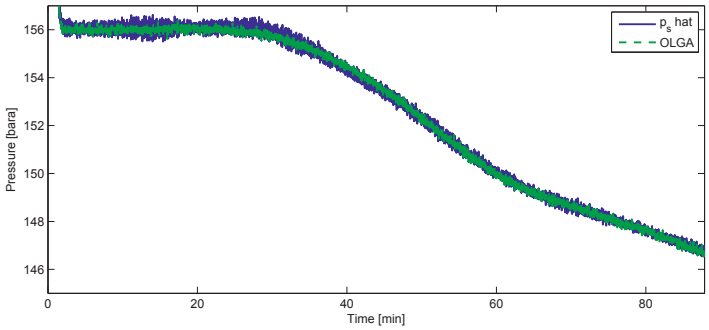

Figure 2.19: *Estimation – Onshore well.* Pressure reading from a sensor at 1551 m TVD.

the gas fraction in this region. As for the equation of state, (2.18), we have chosen the modified ideal gas law including the compressibility factor Z. This expression could be replaced with e.g. a Virial equation of state, as in Duan et al. (1992), which works for an extensive range of pressure and temperature. It is also possible to consider p_{G} as a slow-varying constant and use the UKF to estimate it. This is necessary for high-pressure, high-temperature wells since it is difficult to correctly capture the behavior of the gas under such conditions. An unwanted side-effect is that it will be harder for the UKF to estimate the mass of gas. This is due to the reduction in sensitivity of (2.32) with respect to m_{G} when p_{G} is considered constant.

The simulation results from the comparison with OLGA show that a wrong initial state caused by incorrect $L_1(t = 0)$, λ and α_{L} produce pressure trends at the choke and at the bit which are almost indistinguishable from the trends produced by the OLGA simulation. However, the difference is clearly visible from the WDP pressure readings. By incorporating the WDP measurements in a UKF, which uses the dynamic model and the measurement equation (2.32), we are able to determine the time-varying holdup profile. The UKF effectively translates the complex information in the WDP measurements to a format that is clear and understandable for the driller, namely volume of gas, location of gas and minimum liquid holdup. The information can also be presented as an approximated holdup-profile for the well. The accuracies of the estimated values depend on the number of available pressure readings. It also improves as the gas expands and passes more pressure transducers on its way towards the choke.

2.6 Conclusion

The presented model is a simplification of the complex two-phase dynamics which occur during a gas-kick. Since we focus on capturing the dominant effects using important parameters, we obtain a simple and compact model. The model lacks the relation between slip velocity and holdup, and the skewness of the bubble distribution is assumed constant while actually being time-varying. However, the

model successfully facilitates parameter and state estimation. By using a UKF, we extract information from multiple WDP pressure transducers, as the gas is percolating, and build a time-varying liquid holdup profile. Simulation of a gas-kick circulated out of the well using the driller's method, shows that it is possible to use noisy WDP pressure readings to successfully estimate the liquid holdup profile. WDP measurements are necessary to produce timely estimates. Using only BHP and choke pressure does not provide enough information about the percolating gas.

2.7 Further work

Possible further work is to augment the model to capture the compressibility in the liquid. This will result in a more realistic propagation of a pressure change. Most wells have varying casing diameter which should be taken into account and the friction model should be updated for non-Newtonian fluids such as drilling mud. Inclined wells should also be modeled.

Chapter 3

A dynamic model of percolating gas in an open well-bore

Summary

The two-phase dynamics of a gas-kick percolating up a vertical well, drilled using a partly evacuated riser, is described by two ordinary differential equations and algebraic relations. We model the gas as bubbles distributed with a distribution function along the well. The simplicity of the model makes it well suited for estimation purposes and controller design. We present simulation results where an unscented Kalman filter is used to estimate the current location of the gas, distribution of the gas, and rise-velocity. These estimates can be used to predict when the gas will pass the blowout preventer and reach the drilling rig.

3.1 Introduction

Drilling for gas and oil at deep and ultra-deep water depths, 300–1500 m and 1500 m and beyond, respectively, is now a reality. These wells require special care when being drilled, and can be problematic to drill using conventional methods due to narrow pressure margins and borehole stability issues (Rocha et al., 2003). In Sangesland (1998) it is argued for a mud lift pump which can be mounted along the riser at a water depth of 200–300 m. The method allows for drilling with a partly evacuated riser and is considered as a solution to the many problem faced in deep-water drilling. Well control when drilling with a partly evacuated riser is discussed in Fossli and Sangesland (2004) and Schubert et al. (2006), where the ability to quickly add a tripping margin, compensating for ECD, and the presence of a riser margin are mentioned as important benefits. Well control for a partly evacuated riser is also considered in Falk et al. (2011). Two applications of well control with the dual-gradient method low riser return system (LRRS) are explained. For a small kick it is argued that the blowout preventer (BOP) need not to be closed since the kick can be stopped by increasing the hydrostatic head in the well by shutting down the subsea mud return pump for a short period and keeping the rig pump going. With this method the kick can be vented out in the riser. Zhou

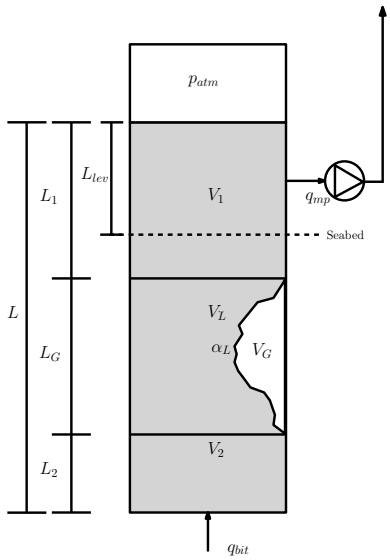

Figure 3.1: Sketch of a low riser return system with control volumes and lengths.

and Nygaard (2011) refines the concept of switched control for pressure regulation in Zhou et al. (2011) for dual-gradient drilling where the kick detection algorithm responds to an unwanted increase of the liquid level in the partly evacuated riser. A shortcoming of the proposed design is the lack of a valid model when there is gas in the annulus. The percolating gas will expand freely, and subsequently the level in the riser will increase, triggering new kick alarms. The proposed model in this article is meant to deal with this problem.

In this paper we start by presenting a general model for the percolating gas in a dual gradient drilling system. The model is developed for a triangular shaped gas distribution. Simulation results of an application of the model are shown before conclusions and suggestions for further work are given.

3.2 Mathematical model

We intend to model a gas kick in a vertical well with a partly evacuated riser where the mud level is governed by a subsea mud pump (SSMP). The LRRS is thoroughly described in Fossli and Sangesland (2004) and sketched in Figure 3.1. The SSMP helps lift the mud from the riser back to the mud pits. At the same time it affects the mud level in the riser, which makes it well suited for controlling the hydrostatic head. Depending on the diameter of the riser and the capacity of the main pump and SSMP, the driller can change the bottomhole pressure within minutes by manipulating the speed of the pumps. This is beneficial for attenuating and handling kicks. The usual procedure for circulating out the gas from the well, is to seal off the annulus by closing the BOP and use a slow circulation rate (400 lpm) from the main pump. During this operation, the pressure in the well is governed by

the driller who manually adjusts the opening of a choke located at the BOP. The driller must carefully control the pressure so that the formation is not fractured or a new kick is taken. The flow through the choke is routed to a parasite line going either to the drilling rig or back into the riser. Such an operation leaves the rig non-productive for several hours. With LRRS the driller can choose not to close in the well as the gas is percolating, based on the magnitude of the kick. When the gas burst through the mud surface in the riser, it is allowed to fully expand into the void before it is vented out. Since the well is not closed in while the gas is percolating, the driller is not running the risk of fracturing the well. After the kick has been stopped by increasing the hydrostatic head, the BHP is only varying due to further changes in hydrostatic head using the pumps, and change in frictional pressure drop.

To simplify the modeling, we ignore the dynamics of the flow rate through the bit and simply set this to the main pump flow rate. Considering the fact that time constants related to percolating gas in the well-bore and transient changes of liquid flow rate through the bit differ with minutes or even hours, justifies this simplification. We also consider a pipe instead of an annulus, which has only minor effects on the results.

Figure 3.1 shows a sketch of the two-phase model which physics we are trying to capture. We assume that the distribution of gas is given by a function which we will denote f_{a}. The gas and liquid are assumed to be two separate phases so that no gas can be dissolved in the liquid.

The well is divided into four control volumes: the volume above the bubble structure, V_1; the gas in the bubble structure, V_{G}; the liquid in the bubble structure, V_{L}; and the volume underneath the bubble structure, V_2. The control volumes have the associated lengths L_1, L_{G}, L_{L} and L_2, respectively, with $L_{\mathrm{G}} = L_{\mathrm{L}}$.

Since the model is designed for the time span from the gas-kick is detected to the gas reaches the mud surface, we consider only the liquid volumetric flow rates in, q_{bit}, and out, q_{mp}, of the well. The change in volume of mud in the well is then given by

$$\dot{V}_1 + \dot{V}_2 + \dot{V}_{\mathrm{L}} = q_{\mathrm{bit}} - q_{\mathrm{mp}} \tag{3.1}$$

where q_{mp} is the volumetric flow rate out of the SSMP.

The time-derivative of the liquid part of the bubble structure, $\dot{V}_{\mathrm{L}}$, is dependent on the choice of liquid holdup distribution function. For further derivation of the model we will use the average of the liquid holdup α_{SL} which is given by either

$$\alpha_{\mathrm{SL}} = 1 - \frac{V_{\mathrm{G}}}{L_{\mathrm{G}} A_{\mathrm{p}}} = 1 - \alpha_{\mathrm{SG}} \tag{3.2}$$

where α_{SG} is the average gas fraction, or by solving the integral

$$\alpha_{\mathrm{SL}} = \frac{1}{L_{\mathrm{G}}} \int_{-\frac{L_{\mathrm{G}}}{2}}^{\frac{L_{\mathrm{G}}}{2}} \hat{f}_{\alpha}(x, \cdot)\, \mathrm{d}x. \tag{3.3}$$

where $\hat{f}_{\alpha}(x, \cdot) \in (0, 1]$ with $x \in [-\frac{L_{\mathrm{G}}}{2}, \frac{L_{\mathrm{G}}}{2}]$ is some distribution function depending on the spatial variable x, and possibly other variables. The distribution function

also gives the volume of gas in the well

$$V_{\mathrm{G}} = A_{\mathrm{p}} \int_{-\frac{L_{\mathrm{G}}}{2}}^{\frac{L_{\mathrm{G}}}{2}} \left(1 - \hat{f}_{\alpha}(x, \cdot)\right) \, \mathrm{d}x. \tag{3.4}$$

For later use we define the function f_{a} which is more general as

$$f_{\mathrm{a}} = \begin{cases} \hat{f}_{\alpha}, & |x| \leq \frac{L_{\mathrm{G}}}{2} \quad (3.5\mathrm{a}) \\ 1, & \text{else} \quad (3.5\mathrm{b}) \end{cases}$$

where $f_{\mathrm{a}}(x, \cdot) \in (0, 1]$ with $x \in \mathbb{R}$.

The average liquid holdup relates the area of liquid in the pipe to the total area of the pipe and also the area of the pipe occupied by gas,

$$A_{\mathrm{L}} = \alpha_{\mathrm{SL}} A_{\mathrm{p}} \tag{3.6}$$

$$A_{\mathrm{G}} = (1 - \alpha_{\mathrm{SL}}) A_{\mathrm{p}} \tag{3.7}$$

where A is cross sectional area and the subscripts L, G and p denotes liquid, gas and pipe, respectively.

Since the rate at which V_{L} and V_{G} change length is equal, we can write

$$\dot{L}_{\mathrm{G}} = \dot{L}_{\mathrm{L}} \tag{3.8}$$

or equally

$$\frac{\dot{V}_{\mathrm{L}}}{A_{\mathrm{L}}} = \frac{\dot{V}_{\mathrm{G}}}{A_{\mathrm{G}}}. \tag{3.9}$$

Inserting (3.6) and (3.7) into (3.9) and rearranging we get

$$\dot{V}_{\mathrm{L}} = \frac{\alpha_{\mathrm{SL}}}{1 - \alpha_{\mathrm{SL}}} \dot{V}_{\mathrm{G}}. \tag{3.10}$$

The rise speed of the tail of the bubbles governs the dynamics of V_2, which is

$$\dot{V}_2 = k_{\mathrm{r}} A_{\mathrm{p}}. \tag{3.11}$$

The rise speed of the tail of the bubble structure, k_{r}, can be expressed similarly as in Orell and Rembrand (1986) which use a slightly modified terminal velocity given by Harmathy (1960)

$$k_{\mathrm{r}} = C_0 \frac{q_{\mathrm{bit}}}{A_{\mathrm{p}}} + 1.53 \left[\frac{\sigma(\rho_{\mathrm{L}} - \rho_{\mathrm{G}}) g}{\rho_{\mathrm{L}}^2} \right]^{\frac{1}{4}} \alpha_{\mathrm{SL}}^n \tag{3.12}$$

where σ is the surface tension between the liquid and the gas and n is a number that reflects the hindering effect surrounding bubbles has on the terminal velocity. C_0 is a constant that relates how the flow rate in the well impacts the rise velocity of the bubbles.

We assume that the pressure in the bubble structure has a single value which is the pressure at the center of mass, x_{m}, defined by

$$\int_{\tilde{x}}^{x_{\mathrm{m}}} (1 - f_{\mathrm{a}}) \, \mathrm{d}x = \int_{x_{\mathrm{m}}}^{x_{\mathrm{f}}} (1 - f_{\mathrm{a}}) \, \mathrm{d}x = \frac{V_{\mathrm{G}}}{2A_{\mathrm{p}}}. \tag{3.13}$$

where $\tilde{x}$ and x_f denote the position of the tail and front of the gas, respectively. We choose to evaluate (3.13) in the reference frame of the bubble structure. By this we mean that $x_\mathrm{m} = 0$, $\tilde{x} < 0 < x_\mathrm{f}$ and $L_\mathrm{G} = x_\mathrm{f} - \tilde{x}$. If the distribution f_a is symmetric around its mean, then $x_\mathrm{f} = \frac{L_\mathrm{G}}{2}$ and $\tilde{x} = \frac{-L_\mathrm{G}}{2}$. We can express the pressure of the gas in two ways, using either the ideal gas law or a momentum-balance. The ideal gas law states

$$p_\mathrm{G} = \frac{m_\mathrm{G} R T}{M_\mathrm{G} V_\mathrm{G}} \tag{3.14}$$

where m_G is the mass of gas, R the gas constant, T the temperature at the middle of the bubble structure and M_G is the molar mass of the gas. A momentum-balance gives

$$\begin{aligned} p_\mathrm{G} = p_\mathrm{atm} + \rho_\mathrm{L} g L_1 + \rho_\mathrm{L} g \int_{x_\mathrm{m}}^{x_\mathrm{f}} f_\mathrm{a} \, \mathrm{d}x \\ + \rho_\mathrm{G} g \int_{x_\mathrm{m}}^{x_\mathrm{f}} (1 - f_\mathrm{a}) \, \mathrm{d}x + \frac{|\tilde{x} - x_\mathrm{m}|}{L_\mathrm{G}} p_\mathrm{fric,G} + p_\mathrm{fric,1} \end{aligned} \tag{3.15}$$

where ρ_L and ρ_G are the density of the liquid and gas, respectively, and p_atm is the atmospheric pressure. $p_\mathrm{fric,G}$ and $p_\mathrm{fric,1}$ are the frictional pressure drop along the bubble structure and the upper control volume, respectively. They are given by the Hagen-Poiseuille law

$$p_\mathrm{fric,CV} = \frac{8 \pi \mu_\mathrm{CV} L_\mathrm{CV} q_\mathrm{CV}}{A_\mathrm{p}^2} \tag{3.16}$$

under the assumption of laminar flow. The subscript CV denotes the control volume and can be substituted with 1,2 and G. μ is the viscosity of the liquid/gas.

We assume that the actual distribution profile of the gas fraction, $1 - f_\mathrm{a}$, will take on a shape resembling a bell curve. Our goal in this paper is to make a simple model of the percolating gas, and this is achieved by choosing the distribution function for the gas as a simple symmetrical triangle. The idea of using a bubble structure with a triangular shape originates from Ohara et al. (2004) and has proven to be a sufficiently accurate approximation to the bell shaped curve which the distribution of gas bubbles will usually form. Under this assumption, we write the function $\hat{f}_\alpha$ for the holdup used in (3.5) as

$$\hat{f}_\alpha = \alpha_\mathrm{L} + \frac{2(1 - \alpha_\mathrm{L})}{L_\mathrm{G}} |x|, \quad |x| \leq \frac{L_\mathrm{G}}{2} \tag{3.17}$$

where α_L is the minimum liquid holdup of the distribution. Since this function is symmetric around its mean, we can conclude that $x_\mathrm{m} = 0$, $\tilde{x} = \frac{-L_\mathrm{G}}{2}$ and $x_\mathrm{f} = \frac{L_\mathrm{G}}{2}$. The function is sketched in Figure 3.2. The average holdup is found by solving (3.3) with (3.17) which gives

$$\alpha_\mathrm{SL} = \frac{1 + \alpha_\mathrm{L}}{2}. \tag{3.18}$$

We have chosen α_L as a constant throughout the simulations. However, it is desirable to express this parameter as a function of the slip between the two phases.

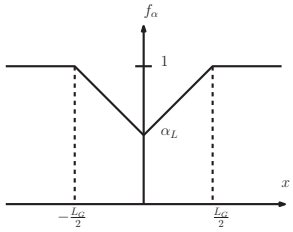

Figure 3.2: The distribution function (3.5) using $\hat{f}_\alpha$ from (3.17).

Unfortunately, this is difficult with the proposed model due to the lack of distinction between superficial and in-situ velocity of the phases.

Assuming constant temperature we have that

$$p_{\mathrm{G}} V_{\mathrm{G}} = \text{constant} \tag{3.19}$$

and thus

$$\dot{p}_{\mathrm{G}} V_{\mathrm{G}} + p_{\mathrm{G}} \dot{V}_{\mathrm{G}} = 0. \tag{3.20}$$

We proceed by inserting (3.17) into (3.5), and this expression into (3.15) which gives

$$p_{\mathrm{G}} = p_{\mathrm{atm}} + \rho_{\mathrm{L}} g L_1 + \frac{1}{2}\left(\frac{(1+\alpha_{\mathrm{L}})\rho_{\mathrm{L}} g V_{\mathrm{G}}}{(1-\alpha_{\mathrm{L}})A_{\mathrm{p}}} + \frac{m_{\mathrm{G}} g}{A_{\mathrm{p}}}\right) + \frac{1}{2}p_{\mathrm{fric,G}} + p_{\mathrm{fric},1}. \tag{3.21}$$

Taking the time-derivative of p_{G} gives

$$\dot{p}_{\mathrm{G}} = \rho_{\mathrm{L}} g \dot{L}_1 + \frac{(1+\alpha_{\mathrm{L}})\rho_{\mathrm{L}} g \dot{V}_{\mathrm{G}}}{2(1-\alpha_{\mathrm{L}})A_{\mathrm{p}}} + \frac{\mathrm{d}}{\mathrm{d}t}\left(\frac{1}{2}p_{\mathrm{fric,G}} + p_{\mathrm{fric},1}\right). \tag{3.22}$$

As the frictional pressure losses are slowly changing we can neglect the last term in (3.22). Inserting (3.22) into (3.20) and multiplying with A_{p} we get

$$\rho_{\mathrm{L}} g V_{\mathrm{G}} \dot{V}_1 + \left(\frac{(1+\alpha_{\mathrm{L}})\rho_{\mathrm{L}} g V_{\mathrm{G}}}{2(1-\alpha_{\mathrm{L}})} + p_{\mathrm{G}} A_{\mathrm{p}}\right)\dot{V}_{\mathrm{G}} = 0. \tag{3.23}$$

Inserting (3.10) and (3.11) into (3.1) and rearranging gives

$$\dot{V}_1 + \frac{1+\alpha_{\mathrm{L}}}{1-\alpha_{\mathrm{L}}}\dot{V}_{\mathrm{G}} = q_{\mathrm{bit}} - q_{\mathrm{mp}} - k_{\mathrm{r}} A_{\mathrm{p}}. \tag{3.24}$$

We now have two equations, (3.23) and (3.24), with two unknowns which we can solve to express the dynamics of V_1 and V_{G}. This results in

$$\dot{V}_1 = \frac{(u - k_{\mathrm{r}} A_{\mathrm{p}})(\frac{1+\alpha_{\mathrm{L}}}{2(1-\alpha_{\mathrm{L}})}\rho_{\mathrm{L}} g V_{\mathrm{G}} + \frac{m_{\mathrm{G}} R T A_{\mathrm{p}}}{M_{\mathrm{G}} V_{\mathrm{G}}})}{\frac{m_{\mathrm{G}} R T A_{\mathrm{p}}}{M_{\mathrm{G}} V_{\mathrm{G}}} - \frac{1+\alpha_{\mathrm{L}}}{2(1-\alpha_{\mathrm{L}})}\rho_{\mathrm{L}} g V_{\mathrm{G}}} \tag{3.25}$$

$$\dot{V}_{\mathrm{G}} = \frac{-\rho_{\mathrm{L}} g V_{\mathrm{G}}(u - k_{\mathrm{r}} A_{\mathrm{p}})}{\frac{m_{\mathrm{G}} R T A_{\mathrm{p}}}{M_{\mathrm{G}} V_{\mathrm{G}}} - \frac{1+\alpha_{\mathrm{L}}}{2(1-\alpha_{\mathrm{L}})}\rho_{\mathrm{L}} g V_{\mathrm{G}}} \tag{3.26}$$

where the input $u = q_{\text{bit}} - q_{\text{mp}}$ and p_{G} is given by the ideal gas law (3.14). The dynamics from (3.25) is actually not needed as we can find an explicit expression for V_1 by solving (3.21) for L_1. The lengths of the control volumes can be found according to

$$L_1 = \frac{V_1}{A_{\text{p}}} \tag{3.27}$$

$$L_{\text{G}} = \frac{2V_{\text{G}}}{A_{\text{p}}(1-\alpha_{\text{L}})} \tag{3.28}$$

$$L_2 = \frac{V_2}{A_{\text{p}}}. \tag{3.29}$$

The bottomhole pressure is given by

$$p_{\text{bit}} = \rho_{\text{L}} g L - \rho_{\text{L}} g \frac{V_{\text{G}}}{A_{\text{p}}} + \frac{m_{\text{G}} g}{A_{\text{p}}} + p_{\text{fric,L}} \tag{3.30}$$

where $p_{\text{fric,L}}$ is the total frictional pressure drop along the entire mud column. The pressure at other locations in the well, e.g. along the drill string, at the BOP or at the SSMP inlet, are valuable measurements when handling a gas kick. The pressure trend at such a sensor will disclose when the front and tail of the bubble structure passes by due to a reduction in hydrostatic head. The distance from the rig floor to the sensor is denoted with x_{s}. The mud level in the riser is L_{lev} and the length of the riser is L_{r}. The distance from the rig floor to the center of mass of the bubble structure is denoted x_{m}. We define

$$x_{\text{l}} = x_{\text{s}} - x_{\text{m}} + \frac{L_{\text{G}}}{2} \tag{3.31}$$

which is 0 when the front of the bubble structure reaches the sensor, and L_{G} when the tail passes by. The expression for the pressure at a sensor at position x_{s} is given by (3.32), which is derived from a momentum equation similar to (3.15). The density of the gas can be found from $\rho_{\text{G}} = \frac{m_{\text{G}}}{V_{\text{G}}}$, and the frictional pressure drop is

$$f_{\text{fric}}(q, L) = \frac{8\pi\mu L q}{A_{\text{p}}^2}. \tag{3.33}$$

The SSMP is controlled by setting the rotational speed. We assume that there is a flow controller governing the pump speed, giving the demanded volumetric flow from the SSMP (q_{mp}).

When the front of the gas reaches the mud plane, the model is not valid anymore and the simulation is terminated.

3.3 Simulation

We use the model to simulate a methane kick at the bottom of the well. The kick is considered small enough to circulate out without closing the BOP. The simulation is started with 500 kg of methane occupying 0.6 m^3 at the bottom of an 8000 m

$$
p_{\mathrm{s}} = \begin{cases}
p_{\mathrm{atm}} + \rho_{\mathrm{L}} g (L_{\mathrm{lev}} + x_{\mathrm{s}} - L_{\mathrm{r}}) & \\
\quad + f_{\mathrm{fric}}(q_{\mathrm{bit}}, L_{\mathrm{lev}} + x_{\mathrm{s}} - L_{\mathrm{r}}), & x_{\mathrm{l}} < 0 \qquad (3.32\mathrm{a}) \\
p_{\mathrm{atm}} + \rho_{\mathrm{L}} g (L_{\mathrm{lev}} + x_{\mathrm{s}} - L_{\mathrm{r}}) & \\
\quad + f_{\mathrm{fric}}(q_{\mathrm{bit}}, L_{\mathrm{lev}} + x_{\mathrm{s}} - L_{\mathrm{r}}) & \\
\quad + \rho_{\mathrm{G}} g \Big[x_{\mathrm{l}} (1 - \alpha_{\mathrm{L}}) & \\
\quad - \mathrm{sign}(x_{\mathrm{l}} - \frac{L_{\mathrm{G}}}{2}) (\frac{1 - \alpha_{\mathrm{L}}}{L_{\mathrm{G}}}) (x_{\mathrm{l}} - \frac{L_{\mathrm{G}}}{2})^2 & \\
\quad - \frac{1 - \alpha_{\mathrm{L}}}{4} L_{\mathrm{G}} \Big] + \rho_{\mathrm{L}} g \Big[x_{\mathrm{l}} \alpha_{\mathrm{L}} & 0 \le x_{\mathrm{l}} \le L_{\mathrm{G}} \qquad (3.32\mathrm{b}) \\
\quad + \mathrm{sign}(x_{\mathrm{l}} - \frac{L_{\mathrm{G}}}{2}) (\frac{1 - \alpha_{\mathrm{L}}}{L_{\mathrm{G}}}) (x_{\mathrm{l}} - \frac{L_{\mathrm{G}}}{2})^2 & \\
\quad + \frac{1 - \alpha_{\mathrm{L}}}{4} L_{\mathrm{G}} \Big], & \\
p_{\mathrm{atm}} + \rho_{\mathrm{L}} g (L_{\mathrm{lev}} + x_{\mathrm{s}} - L_{\mathrm{r}}) & \\
\quad + f_{\mathrm{fric}}(q_{\mathrm{bit}}, L_{\mathrm{lev}} + x_{\mathrm{s}} - L_{\mathrm{r}}) & \mathrm{else.} \qquad (3.32\mathrm{c}) \\
\quad - \frac{g}{A_{\mathrm{p}}} (\rho_{\mathrm{L}} V_{\mathrm{G}} - m_{\mathrm{G}}), &
\end{cases}
$$

vertical well. Simulation parameters are given in Table 3.1. We assume that the kick has been detected, possibly with the method proposed in Zhou and Nygaard (2011), and that the SSMP has been shut off, as proposed in Falk et al. (2011). After two minutes the SSMP is started up again, and from Figure 3.3 we see that the BHP increases with 8 bar due to the increase in hydrostatic head. The mud level in the riser in Figure 3.4 increases with 47 m in this period. Note that the level is rising after circulation is resumed. With the proposed kick detection algorithm in Zhou and Nygaard (2011), new kick alarms would be triggered after completion of the kick handling routine since their model does not incorporate the effect of gas expansion. When turning the SSMP back on, the flow rate is simply set to the same flow rate as from the main pump as seen in Figure 3.5.

We use an unscented Kalman filter, Julier and Uhlmann (2004), to estimate the states, V_{G} and V_2, and to estimate the parameters, α_{L} and k_{r}. An estimate for V_1 is found by solving (3.21), with the estimates of V_{G}, α_{L} and k_{r} inserted, for L_1. Measurement of the level in the riser is assumed to be available, and also pressure sensors at every 300 m starting from the bottom of the well. Note that the mass of the gas, m_{G}, and its molar mass, M_{g}, is assumed to be known. These constants can be found from knowledge about the formation being drilled and the magnitude of the influx.

Lengths, and estimates of the lengths, of the control volumes are shown in Figure 3.6 through Figure 3.8. Estimates of the parameters are presented in Figure 3.9 and Figure 3.10. The pressure at the 100 m below the BOP is plotted in Figure 3.11

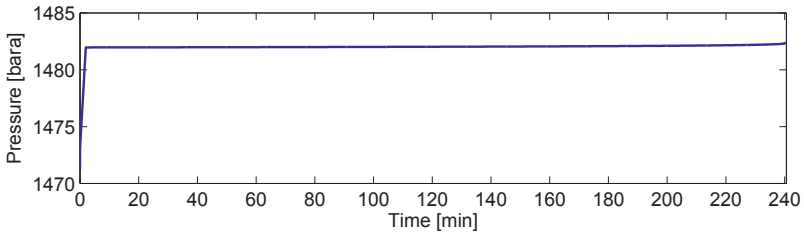

Figure 3.3: Controlled bottomhole pressure.

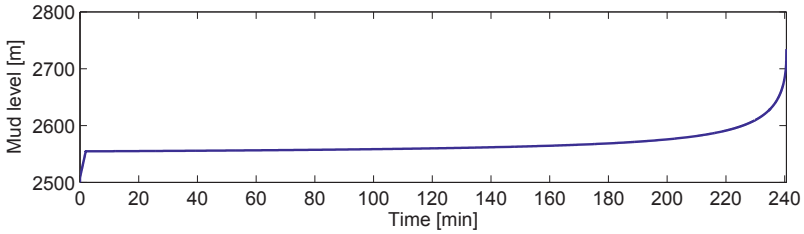

Figure 3.4: Level in riser.

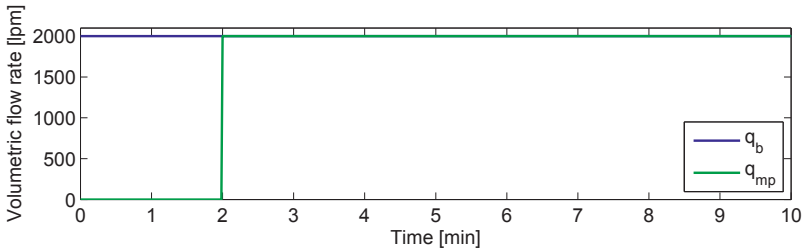

Figure 3.5: Volumetric flow rates from the pumps. Magnified, but constant for the remaining period.

which clearly show the front and tail of the bubble structure at 170 min.

3.4 Conclusion

The presented model is a simplification of the complex two-phase dynamics which occur during a gas-kick. We focus on capturing the qualitative behavior during such an event to gain insight to what is happening in the well. Using an unscented Kalman filter with the model, we estimate the dynamic states and two parameters and successfully determine the position of the bubble structure and its length. This information is useful for the driller, who must consider whether to close the BOP or vent the gas out into the riser.

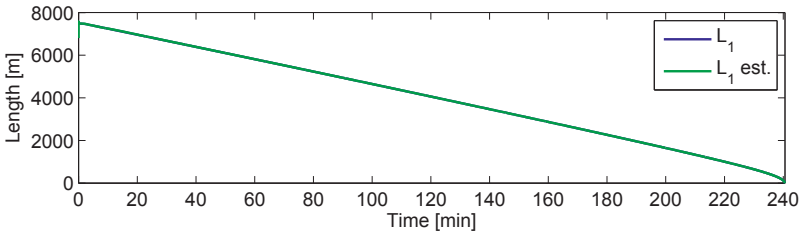

Figure 3.6: Length of the upper control volume.

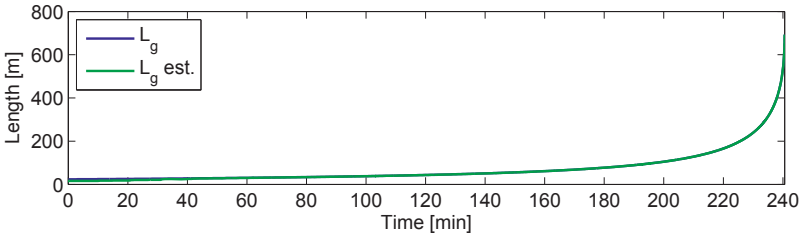

Figure 3.7: Length of the bubble structure.

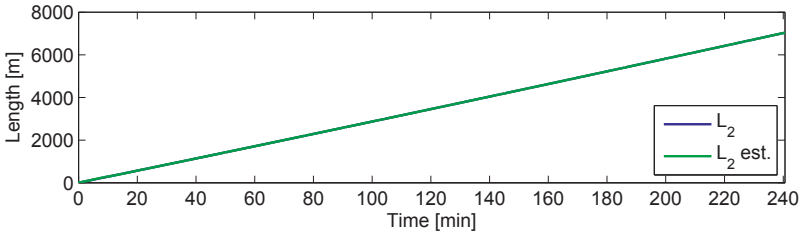

Figure 3.8: Length of the lower control volume.

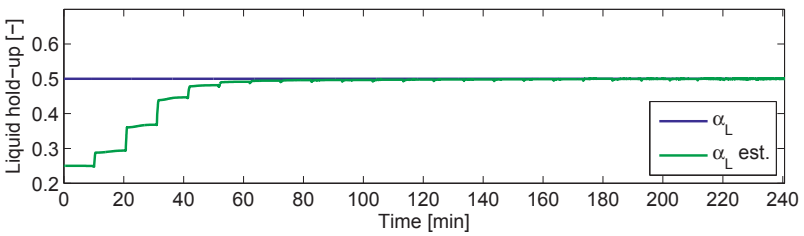

Figure 3.9: Liquid holdup.

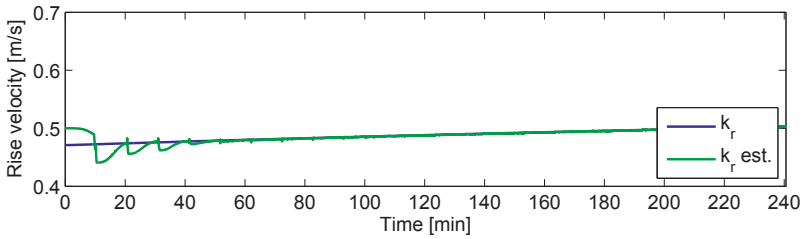

Figure 3.10: Rise velocity of the bubble structure.

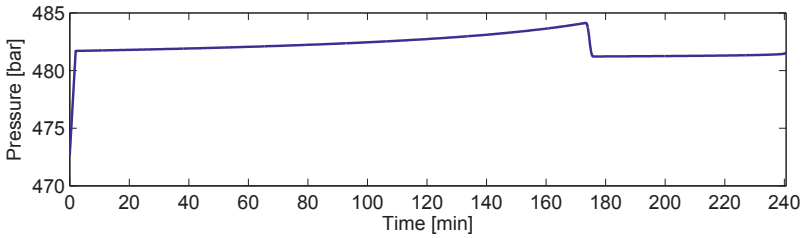

Figure 3.11: Pressure 100 m below the BOP.

Table 3.1

Parameter	Value	Unit
ρ_{L}	1700	kg/m^3
σ	$75.64{\cdot}10^{-3}$	N/m
Depth of well (TVD)	8000	m
Distance from seabed to bottomhole	5000	m
Length of riser	3000	m
D	0.33	m
q_{bit}	2000	l/min
m_{G}	500	kg
M_{G}	$16.042{\cdot}10^{-3}$	kg/mol
T	288	K
α_{L}	0.5	m^2/m^2
μ	$40{\cdot}10^{-3}$	Pa s
C_0	0.75	-
n	4	-
p_{amb}	1	atm

3.5 Further work

Possible further work is to augment the model to capture the compressibility in the liquid. Most wells have varying casing diameter which should be accounted for, and the friction model should be updated for non-Newtonian fluids such as mud. Inclined wells should also be modeled. Combining this model with the work in Zhou and Nygaard (2011) could result in a more robust kick detection algorithm. A time-varying liquid holdup, possibly dependent on the slip velocities of the different phases, would improve the model. The bursting of the gas when reaching the mud plane could also be modeled, but we consider this as less important.

Part II

In-/out-flux detection and localization

Chapter 4

A novel model-based scheme for kick and loss mitigation during drilling

Summary

A model-based in-/out-flux detection scheme for managed pressure drilling is presented. We apply a globally exponentially stable adaptive observer which estimates the unknown states and parameters of the hydraulic system and in particular quantifies the magnitude of the in-/out-flux and its location in the well. While the observer can be used purely as an in-/out-flux detection system, the paper also presents a simple controller that automatically and effectively stops an in-/out-flux. This novel control scheme departs from common practice for automatic managed pressure drilling, which is to regulate down-hole pressure to some predetermined set point. Experimental results and realistic simulations with a state-of-the-art simulator are provided to show the effectiveness of the method.

4.1 Introduction

Drilling with narrow pressure margins at greater depths increases the risk of unplanned events such as unwanted in-flux (kick) or out-flux (loss/lost circulation). In addition to posing an environmental threat and causing monetary loss, such events compromise the safety of the personnel on the rig. In some cases the integrity of the wellbore is also weakened.

The Macondo incident represents the worst-case scenario of the consequences of a blowout. In the aftermath of the accident, the report to the President of the USA Graham et al. (2011) highlighted the need for automatic systems aiding the drilling crew in making the right decisions during critical events. In both onshore and offshore transportation pipelines it is common that governments have legislated for leak detection systems. The regulations vary between countries as pointed out in Geiger and Werner (2003), but often include an internally based system. Internally based systems use field measurements combined with, for instance, some kind of line balance to infer the occurrence of a leak. Externally based systems, on the other hand, trigger an alarm based on sensors located close to the leakage point. As the

externally based systems are costly and can be complex to install, an internally based method often turns out to be the only realistic option. This is also the case for drilling. Even with wired drill pipe (WDP), there is still a need for a hydraulic model, as emphasized in Gravdal et al. (2010).

Localization of the in-/out-flux is important when drilling extended open sections. It is also important to locate an in-/out-flux caused by a perforated casing since this implies that a safety barrier is lost. The special case when there is a leak from the drillstring to the annulus, caused either by a twist-off or imperfections in the joint-sealings, is not treated in this paper. Such a leakage from the drillstring would cause a drop in the pressure downstream the main pump while the difference in flow rate in and out would be unchanged.

This paper will focus on model-based in-/out-flux quantification, localization and mitigation. Our scheme is based on an adaptive observer for a managed pressure drilling (MPD) hydraulic system. The adaptive observer reacts to the change in frictional pressure drop downstream the point of the loss and gives away the position of the leak. The adaptive observer is used with results from a small scale experimental rig for verification of the detection and localization method. We also use the adaptive observer with a controller which is able to stop an in-/out-flux. Realistic scenarios with the controller are simulated using OLGA[1].

An early example of model-based leak detection can be found in Billmann and Isermann (1987) where a correlation technique is used to detect, quantify and locate the leak. Using the water hammer equations based on a collocation method, a model-based leak detection scheme using an extended Kalman filter is implemented in Torres et al. (2008). In Torres et al. (2009), it is shown that multiple leaks in a pipeline can be detected if the system is sufficiently excited through the boundary conditions. Leaks in open water channels are covered in Bedjaoui et al. (2009) where the Saint-Venant equations are used in both an observer and in a bank of models. For both cases, the position is determined by minimizing a quadratic cost function containing measurements from the plant and observers. In Bedjaoui and Weyer (2011), three off-line leak localization methods for leaks in open water channels are compared and an on-line leak detection algorithm is proposed. Both articles include experimental data. The work of Aamo et al. (2006) covers a PDE-observer which is able to adapt to the friction of a horizontal pipeline before quantifying and locating a leak. The observer uses non-reflective boundaries for robustness to initial conditions. In Hauge et al. (2007) the observer is modified with adaption of a pressure dependent leak and tested during transients. Since the leak quantification and localization is only dependent on measurements from the boundaries, a commercial computational fluid dynamics simulator can be proven to work as an observer in Hauge et al. (2009). By inspecting the trends of annular discharge pressure and stand pipe pressure, Reitsma (2010) distinguishes between unplanned events such as kick, loss, wash-out and plugging of drillstring. The method is simple and has proven effective through experiments, but cannot point out the location of the in-/out-flux. The model used in this paper is also used in Zhou et al. (2011) for gas kick detection and mitigation. The concept of switched control of the bottomhole

[1] OLGA is a multi-phase flow simulator commercialized by SPT Group. It is frequently used for dynamic flow simulations in the oil and gas industry.

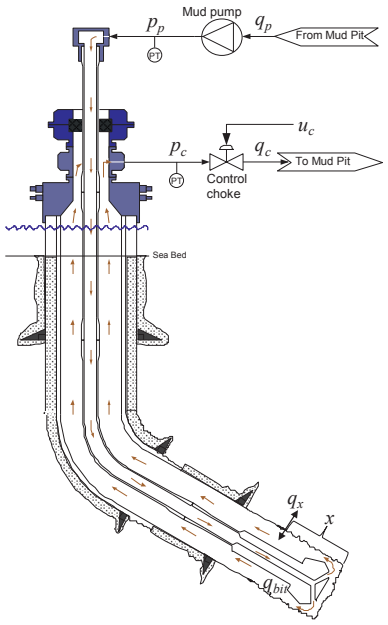

Figure 4.1: Schematic of a managed pressured drilling system.

pressure is presented. An MPD system is considered where a controller manipulating the choke and back-pressure pump switches between a combination of pressure and flow control when there is no in-flux and pure flow control when a kick is detected. The controller designed in this article is a pure flow controller and does not rely upon switching.

The rest of this paper is organized in the following manner. In Section 4.2 the mathematical model of the hydraulics of the well is presented. Section 4.3 covers the observer design and is followed by the controller design in Section 4.4. In Section 4.5 we explain how we determine physical parameters for the experimental rig and the simulations. The experimental setup and the experimental results are then presented in Section 4.6 and Section 4.7. Similarly, the simulation setup and simulation results are presented in Section 4.8 and Section 4.9. Results are discussed in Section 4.10, and finally, conclusions are given in Section 4.11.

4.2 Mathematical model

We now present the model for the hydraulics of the MPD system. A thorough derivation of the model can be found in Kaasa et al. (2011) together with results where it is used as an adaptive observer with field data as input. The model has also been used in Stamnes et al. (2008), Zhou et al. (2011) and Godhavn et al. (2011) for estimation of bottomhole pressure, kick mitigation and pressure control, respectively. Figure 4.1 shows the hydraulic system with measurements. The model

is

$$\dot{p}_{\mathrm{p}} = \frac{\beta_{\mathrm{d}}}{V_{\mathrm{d}}}(q_{\mathrm{p}} - q_{\mathrm{bit}}), \tag{4.1}$$

$$\dot{p}_{\mathrm{c}} = \frac{\beta_{\mathrm{a}}}{V_{\mathrm{a}}}(q_{\mathrm{bit}} - q_{\mathrm{c}} + q_{\mathrm{x}}), \tag{4.2}$$

$$\begin{aligned}\dot{q}_{\mathrm{bit}} = &\frac{1}{M}[p_{\mathrm{p}} - p_{\mathrm{c}} - F_{\mathrm{d}}(q_{\mathrm{p}})q_{\mathrm{p}}L_{\mathrm{d}} - F_{\mathrm{a}}(q_{\mathrm{p}})q_{\mathrm{p}}x - F_{\mathrm{a}}(q_{\mathrm{c}})q_{\mathrm{c}}(L_{\mathrm{a}} - x) \\ &- (\rho_{\mathrm{a}} - \rho_{\mathrm{d}})gh_{\mathrm{TVD}}],\end{aligned} \tag{4.3}$$

$$q_{\mathrm{c}} = k_{\mathrm{c}}u_{\mathrm{c}}\mathrm{sign}(p_{\mathrm{c}} - p_0)\sqrt{|p_{\mathrm{c}} - p_0|}, \tag{4.4}$$

$$q_{\mathrm{x}} = k_{\mathrm{PI}}(p_{\mathrm{res}} - p_{\mathrm{x}}), \tag{4.5}$$

where q_{p}, q_{c}, and q_{bit} are volumetric flow rates from the main pump, through the choke, and through the bit, respectively. p_{p} and p_{c} are the pressures downstream the pump and upstream the choke, respectively. The choke equation (4.4) is similar to that in Merritt (1967). k_{c} is a lumped constant related to the valve characteristic, $u_{\mathrm{c}} \in [0, 1]$ is the opening of the choke and p_0 is the pressure downstream of the choke. $F_{\mathrm{d}}(q)$ and $F_{\mathrm{a}}(q)$ are time-varying frictional pressure drop coefficients for the drillstring and annulus, respectively. The subscripts a and d denote the control volumes annulus and drillstring, respectively. L is the measured depth (MD), i.e. length, β the effective bulk-modulus, and V the volume. The density ρ can be different in the drillstring and annulus due to different pressure profiles and the presence of cuttings in the annulus. The gravitational constant is g, and the true vertical depth (TVD) of the bit is given by h_{TVD}[2]. M is a mass-like property given by

$$M = \frac{\rho_{\mathrm{d}}L_{\mathrm{d}}}{A_{\mathrm{d}}} + \frac{\rho_{\mathrm{a}}L_{\mathrm{a}}}{A_{\mathrm{a}}}, \tag{4.6}$$

where A_{d} and A_{a} are the cross-sectional areas of the drillstring and annulus, respectively. $x \in [0, L_{\mathrm{a}}]$ is the location of an in-/out-flux and q_{x} is the volumetric flow rate of the in-/out-flux, which we assume is a linear function of the difference between pressure in the formation and pressure in the wellbore at the point of the in-/out-flux, given by p_{res} and p_{x}, respectively. The productivity index is represented by the positive constant k_{PI}. The formation pressure, p_{res}, is assumed constant, and it is assumed that the in-/out-flux does not influence density in the well. The measured signals are

$$y = \begin{bmatrix} p_{\mathrm{p}} & p_{\mathrm{c}} \end{bmatrix}^{\top}.$$

Since p_{c} is measured, the nonlinearity introduced by the choke in (4.4) can be removed, as in Godhavn et al. (2011), by letting

$$u_{\mathrm{c}} = \frac{q_{\mathrm{c,ref}}}{k_{\mathrm{c}}\mathrm{sign}(p_{\mathrm{c}} - p_0)\sqrt{|p_{\mathrm{c}} - p_0|}}, \tag{4.7}$$

[2] TVD relates to the hydrostatic head as opposed to MD which refers to the actual length of the well.

where $q_{\mathrm{c,ref}}$ is the volumetric flow rate reference for the choke. Assuming that the choke is sufficiently fast, and $p_{\mathrm{c}} > p_0$, we achieve $q_{\mathrm{c}} = q_{\mathrm{c,ref}}$, and we may view q_{c} as an input in (4.2). Thus we define the available inputs

$$u = \begin{bmatrix} q_{\mathrm{p}} \\ q_{\mathrm{c}} \end{bmatrix} = \begin{bmatrix} q_{\mathrm{p}} \\ k_{\mathrm{c}} u_{\mathrm{c}} \mathrm{sign}(p_{\mathrm{c}} - p_0)\sqrt{|p_{\mathrm{c}} - p_0|} \end{bmatrix}.$$

We treat identification of parameters such as friction factors and bulk-moduli in Section 4.5. The notation is described in the nomenclature in Appendix 4.C.

4.3 Observer design

In this section we adopt an adaptive observer from Zhang (2002), which apply to systems in the form

$$\dot{z}(t) = Az(t) + B(u,t)u(t) + \Psi(u,t)\theta(t), \tag{4.8a}$$
$$y(t) = Cz(t). \tag{4.8b}$$

System (4.1)–(4.3) can be written in this form by defining $z = [p_{\mathrm{p}}\, p_{\mathrm{c}}\, q_{\mathrm{bit}}]^\top$, $\theta = [q_{\mathrm{x}}\, x\, w]^\top$, with $w = (\rho_{\mathrm{a}} - \rho_{\mathrm{d}})gh_{\mathrm{TVD}}$,

$$A = \begin{bmatrix} 0 & 0 & -\frac{\beta_{\mathrm{d}}}{V_{\mathrm{d}}} \\ 0 & 0 & \frac{\beta_{\mathrm{a}}}{V_{\mathrm{a}}} \\ \frac{1}{M} & -\frac{1}{M} & 0 \end{bmatrix}, \tag{4.9}$$

$$B(u,t) = \begin{bmatrix} \frac{\beta_{\mathrm{d}}}{V_{\mathrm{d}}} & 0 \\ 0 & -\frac{\beta_{\mathrm{a}}}{V_{\mathrm{a}}} \\ -\frac{F_{\mathrm{d}}(q_{\mathrm{p}})L_{\mathrm{d}}}{M} & -\frac{F_{\mathrm{a}}(q_{\mathrm{c}})L_{\mathrm{a}}}{M} \end{bmatrix}, \tag{4.10}$$

$$C = \begin{bmatrix} 1 & 0 & 0 \\ 0 & 1 & 0 \end{bmatrix} \tag{4.11}$$

and

$$\Psi(u,t) = \begin{bmatrix} 0 & 0 & 0 \\ \frac{\beta_{\mathrm{a}}}{V_{\mathrm{a}}} & 0 & 0 \\ 0 & -\frac{F_{\mathrm{a}}(q_{\mathrm{p}})}{M}q_{\mathrm{p}} + \frac{F_{\mathrm{a}}(q_{\mathrm{c}})}{M}q_{\mathrm{c}} & -\frac{1}{M} \end{bmatrix}. \tag{4.12}$$

In order to use results from Zhang (2002) we have to verify that the assumptions stated therein are fulfilled. The assumptions are recapitulated in Appendix 4.A. Assumption 1 is satisfied by the fact that the matrix pair (A, C) is observable, so that there exists a matrix K (which is constant in our case, since A and C are) such that $A - KC$ is Hurwitz. Such a K can be found by pole-placement or as the Kalman gain, for instance. Assumption 2 requires that $\Psi(u,t)$ be persistently exciting, which is the case when $q_{\mathrm{p}} - q_{\mathrm{c}}$ is persistently exciting. In other words, there must be a difference in flow rate in and flow rate out, which is the case when there is an in-/out-flux. In view of these considerations, the following result follows from Zhang (2002).

Theorem 4.1. *Consider the adaptive observer*

$$\dot{\Upsilon}(t) = [A - KC]\Upsilon(t) + \Psi(u,t), \tag{4.13a}$$

$$\begin{aligned}\dot{\hat{z}}(t) &= A\hat{z}(t) + B(u,t)u(t) + \Psi(u,t)\hat{\theta}(t) \\ &\quad + \left[K + \Upsilon(t)\Gamma\Upsilon^\top(t)C^\top\Sigma\right][y(t) - C\hat{z}(t)],\end{aligned} \tag{4.13b}$$

$$\dot{\hat{\theta}}(t) = \Gamma\Upsilon^\top(t)C\Sigma[y(t) - C\hat{z}(t)], \tag{4.13c}$$

where Γ and Σ are symmetric, positive definite matrices and K is selected such that $A - KC$ is Hurwitz. If $q_p - q_c$ is persistently exciting, then the errors $\hat{z}(t) - z(t)$ and $\hat{\theta}(t) - \theta(t)$ tend to zero exponentially fast when $t \to \infty$.

4.4 Controller design

In case of an in-/out-flux, we would like to use the choke to mitigate the loss or gain as quickly as possible. This can be achieved by implementing a flow controller manipulating the choke. Our controller design is motivated by the following analysis. Combining (4.2) and (4.4) gives

$$\dot{p}_\mathrm{c} = \frac{\beta_\mathrm{a}}{V_\mathrm{a}}(q_\mathrm{bit} - k_\mathrm{c}u_\mathrm{c}\mathrm{sign}(p_\mathrm{c} - p_0)\sqrt{|p_\mathrm{c} - p_0|} + q_\mathrm{x}) \tag{4.14}$$

which has a stable origin when $u_\mathrm{c} > 0$. The steady state-solution of (4.14) has to satisfy $q_\mathrm{c} = q_\mathrm{bit} + q_\mathrm{x}$. From Theorem 4.1 we have that $\hat{q}_\mathrm{bit} \to q_\mathrm{bit}$ and $\hat{q}_\mathrm{x} \to q_\mathrm{x}$. For asymptotic analysis, consider the control law

$$q_\mathrm{c} = q_\mathrm{bit} - k_1 q_\mathrm{x} \tag{4.15}$$

where the positive constant k_1 can be used to tune the responsiveness in case of an in-/out-flux. Inserting (4.15) into (4.14) yields

$$\dot{p}_\mathrm{c} = \frac{\beta_\mathrm{a}}{V_\mathrm{a}}(k_1 + 1)q_\mathrm{x}. \tag{4.16}$$

The steady-state solution would now require $q_\mathrm{x} = 0$, which proves that the control law will mitigate the in-/out-flux. We now analyze the dynamics of (4.5) with the implementable version of the control law

$$u_\mathrm{c} = \frac{\hat{q}_\mathrm{bit} - k_1\hat{q}_\mathrm{x}}{k_\mathrm{c}\mathrm{sign}(p_\mathrm{c} - p_0)\sqrt{|p_\mathrm{c} - p_0|}}, \tag{4.17}$$

which gives the desired flow-rate

$$q_\mathrm{c} = \hat{q}_\mathrm{bit} - k_1\hat{q}_\mathrm{x} \tag{4.18}$$

through the choke. Taking the time-derivative of (4.5) gives

$$\dot{q}_\mathrm{x} = -k_\mathrm{PI}(\dot{p}_\mathrm{res} - \dot{p}_\mathrm{x}) = -k_\mathrm{PI}\frac{\beta_\mathrm{a}}{V_\mathrm{a}}(q_\mathrm{bit} - q_\mathrm{c} + q_\mathrm{x}) \tag{4.19}$$

where we have used $\dot{p}_{\mathrm{x}} \approx \dot{p}_{\mathrm{c}}$, neglecting any dynamics of the gravitational and frictional pressure losses. Substituting (4.18) into (4.19), yields

$$\dot{q}_{\mathrm{x}} = -k_{\mathrm{PI}} \frac{\beta_{\mathrm{a}}}{V_{\mathrm{a}}} (q_{\mathrm{bit}} - \hat{q}_{\mathrm{bit}} + k_1 \hat{q}_{\mathrm{x}} + q_{\mathrm{x}}). \tag{4.20}$$

Inserting $\hat{q}_{\mathrm{x}} = q_{\mathrm{x}} - \tilde{q}_{\mathrm{x}}$ and using $\tilde{q}_{\mathrm{bit}} = q_{\mathrm{bit}} - \hat{q}_{\mathrm{bit}}$ gives

$$\dot{q}_{\mathrm{x}} = -k_{\mathrm{PI}} \frac{\beta_{\mathrm{a}}}{V_{\mathrm{a}}} (k_1 + 1) q_{\mathrm{x}} - k_{\mathrm{PI}} \frac{\beta_{\mathrm{a}}}{V_{\mathrm{a}}} (\tilde{q}_{\mathrm{bit}} - k_1 \tilde{q}_{\mathrm{x}}). \tag{4.21}$$

The unforced system $\dot{q}_{\mathrm{x}} = -k_{\mathrm{PI}} \frac{\beta_{\mathrm{a}}}{V_{\mathrm{a}}} (k_1 + 1) q_{\mathrm{x}}$ has a globally exponentially stable origin. Since the exogenous signals $\tilde{q}_{\mathrm{bit}}$ and $\tilde{q}_{\mathrm{x}}$ decay exponentially to zero, we can conclude that the origin of (4.21) is globally exponentially stable (GES). Note that (4.21) has similar structure as the error dynamics of the pressure tracking controller in Godhavn et al. (2011) which is thoroughly tested for industrial use. However, our controller is different since it is a pure flow controller and does not rely on estimates of the down-hole pressure.

4.5 System Identification

There are many parameters that must be identified for the observer and control law to work correctly. In this section we treat how these parameters can be identified prior to use of the observer and controller.

The localization algorithm is highly sensitive to the friction parameters in the drillstring and annulus because it is the frictional pressure drop that gives away the position of the loss. There are many formulas available for computation of the friction factor, and they often include terms such as viscosity, roughness and fluid velocity, which can be hard to quantify. The vast amount of research carried out within the field of friction flow modeling is reflected in Brkic (2011), and references therein, which compares 21 explicit expressions for the Colebrook relation for flow friction.

Instead of introducing an expression for the friction factor, we assume that it is possible to measure the frictional pressure drop in the drillstring and annulus at different flow rates. This is possible when the bottomhole pressure is measured. Some drilling rigs are equipped with a wired drill pipe, where measurements from the bit are sent electronically through a wire in the drillstring, but mud pulse telemetry is more commonly used. When adding stands to the drillstring, the flow rate from the main pump is ramped down and then up again, and the frictional pressure drop can be recorded in this period. The measured frictional pressure losses can be used to compute the friction functions $F_{\mathrm{d}}(q)$ and $F_{\mathrm{a}}(q)$. Note that we do not assume that the bottomhole pressure is available when detecting, locating or stopping an in-/out-flux.

In the following sub-sections, we clarify how unknown parameters are determined prior to an in-/out-flux for the experiments and simulations.

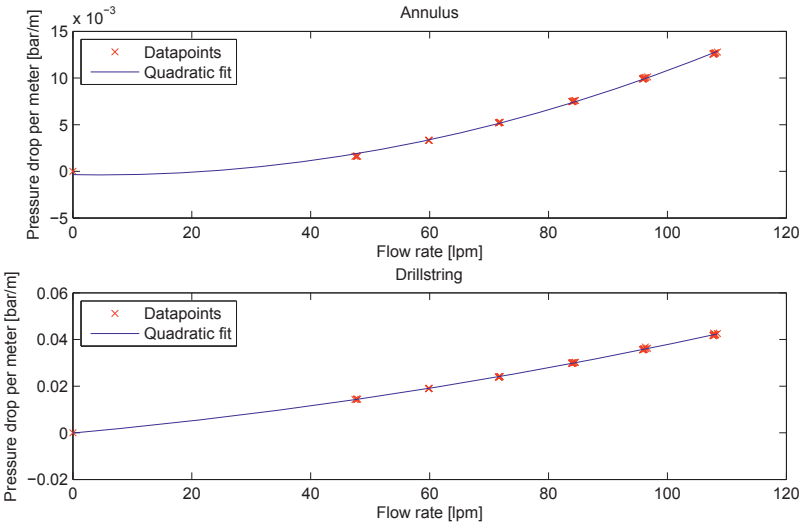

Figure 4.2: Quadratic fit of the pressure drop.

4.5.1 Experiment – Friction

From the experimental data we have a set of time-averaged steady state measurements of the frictional pressure loss for increasing flow-rate which we fit to a quadratic function. The resulting functions, after dividing by q, are

$$F_{\mathrm{a}}^{\mathrm{e}}(q) = \begin{cases} a_{\mathrm{a}}|q| + b_{\mathrm{a}} + \frac{c_{\mathrm{a}}}{q} & \text{if } q \neq 0 \\ 0 & \text{else} \end{cases} \tag{4.22}$$

$$F_{\mathrm{d}}^{\mathrm{e}}(q) = \begin{cases} a_{\mathrm{d}}|q| + b_{\mathrm{d}} + \frac{c_{\mathrm{d}}}{q} & \text{if } q \neq 0 \\ 0 & \text{else} \end{cases} \tag{4.23}$$

where the superscript e is used to denote experiment. Plots of data points for the frictional pressure drop per meter, which corresponds to $F_{\mathrm{a}}^{\mathrm{e}}(q)q$ and $F_{\mathrm{d}}^{\mathrm{e}}(q)q$, and the quadratic fits can be seen in Figure 4.2.

4.5.2 Experiment – Bulk-moduli

The bulk-moduli β_{d} and β_{a} are pressure dependent and vary for each experiment. There is not enough persistency of excitation in the experimental data set to use recursive least-square methods to find the bulk-moduli. We determine them by trying a range of values with the available data set and choosing the ones which makes the observer reproduce the dynamics of the rig. We assume that they are linear functions of the reference pressure upstream the choke, $p_{\mathrm{c,ref}}$. They are computed in the following way.

$$\beta_{\mathrm{a}}(p_{\mathrm{c,ref}}) = 12.5 p_{\mathrm{c,ref}} + 7.5 \tag{4.24}$$

$$\beta_{\mathrm{d}}(p_{\mathrm{c,ref}}) = 2\beta_{\mathrm{a}}. \tag{4.25}$$

where $p_{\mathrm{c,ref}}$ is given in barg. The unusually low bulk-moduli are a result of the flexibility of the PVC pipes and possibly trapped gas. Note that we fix the bulk-moduli to these values before starting the observer, i.e. they are not time-varying during a particular experiment.

4.5.3 Experiment – Difference in hydrostatic head

The estimate of the difference in hydrostatic head in the drillstring and annulus, w, is only active prior to starting quantification of the loss. This is because it would interfere with the estimate of the position of the in-/out-flux if left active for the remaining period. The estimate of the hydrostatic pressure, $\hat{w}$, is set to the mean of $\hat{w}$ during the 10 seconds before being deactivated. When deactivating, we assume that the magnitude of the influx to the wellbore is such that the effect on the density in the annulus is negligible. This assumption is justified when there is a loss.

4.5.4 Simulation – Friction

From the simulation data we have a time-series of the frictional pressure drop when slowly ramping up the flow-rate from the main pump. We use this data to make the look-up tables $F_{\mathrm{a}}^{\mathrm{l}}(q)$ and $F_{\mathrm{d}}^{\mathrm{l}}(q)$ and the following friction functions

$$F_{\mathrm{a}}^{\mathrm{s}}(q) = F_{\mathrm{a}}^{\mathrm{l}}(q)|q| \tag{4.26}$$

$$F_{\mathrm{d}}^{\mathrm{s}}(q) = F_{\mathrm{d}}^{\mathrm{l}}(q)|q| \tag{4.27}$$

where the superscript s is used to denote simulation. The value for k_{c} is also found during this process.

4.5.5 Simulation – Bulk-moduli

Since the simulation is carried out with water and there are no compressibility effects due to flexible piping, the bulk-moduli are simply set to the nominal value for water.

4.5.6 Simulation – Difference in hydrostatic head

As for the experiments, the estimate of the difference in hydrostatic head in the drillstring and annulus, w, is only active prior to starting the quantification of the loss. Due to noise, $\hat{w}$ is set to the mean of $\hat{w}$ during the 40 seconds before being deactivated. When deactivating, we assume that the magnitude of the in-flux to the wellbore is such that the effect on the density in the annulus is negligible. This assumption is justified when the proposed controller is active.

4.6 Experimental setup

The rig is located at the University of Stavanger and is a small scale replica of the hydraulics of a well drilled using MPD. A schematic of the rig is depicted in

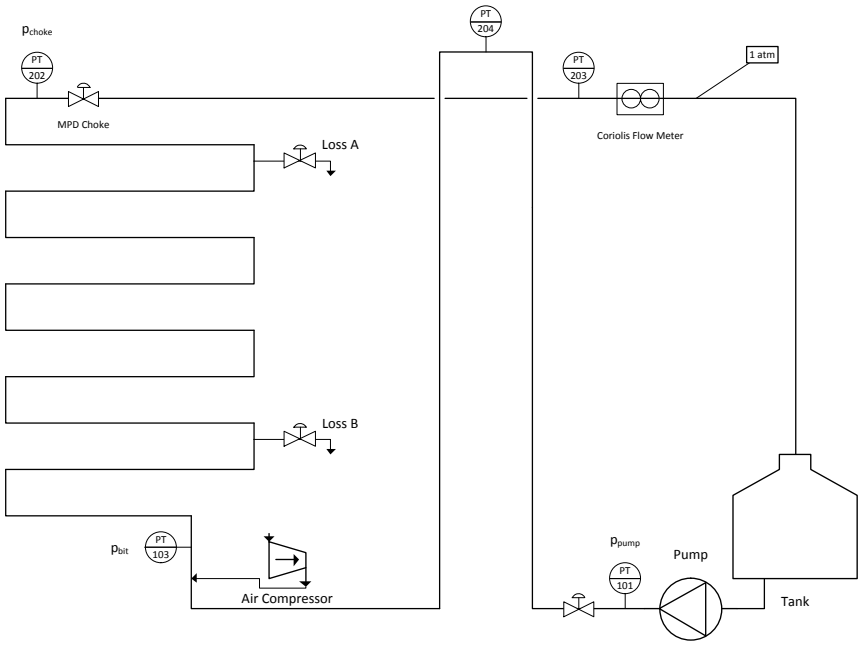

Figure 4.3: Schematic of the experimental rig.

Figure 4.3. Details on the rig are documented in Norwegian in Torsvik (2011), but we provide a short recapitulation for sake of the reader. The rig is made up by transparent PVC pipe sections with an inner diameter of 36 mm which are fitted and glued together with joints. A scaffold serves as framework for the pipes, instruments, chokes and valves, and the annulus part[3] of the rig encircles the scaffold in a helix-like fashion. The pump is seated on the floor, while the chokes are sitting on top of the scaffold. To elongate the drillstring-part of the rig, the piping going from the pump is directed over the top of the scaffold and down to the floor before it is joined with the annuls. There is a choke at the top of the scaffold, and after passing through the choke the flow is directed back to a tank through a return line. The tank, in turn, feeds the pump with water. The length of the piping that makes up the annulus is approximately 58.0 m, while the drillstring is about 13.2 m. The height difference from the start of the annulus to the choke is about 4.0 meters which results in an effective inclination of about 4 degrees. There are multiple 90 degrees bends along the drillstring, and especially many in the annulus (30). The reduction of the momentum of the fluid due to these bends, accounts for an unknown portion of the pressure drop. They also impose a spatially varying pressure drop. This spatially dependency is not captured by the function $F_{\mathrm{a}}(q)$. However, the pressure drop is accounted for. The rig is equipped with pressure transmitters and a flow meter as shown in Figure 4.3. Table 4.1 presents the distances and height differences between the pressure sensors. The rig has two loss-modules. Loss A is

[3] To ease the notation, we will denote this part of the piping annulus, even though it actually is a pipe.

Table 4.1: Distance/elevation between pressure sensors [m]. Approximate values.

	PT204	PT103	PT202	PT203
PT101	6.0/4.5	13.2/0.5	71.2/4.5	72.2/4.5
PT204	-	7.2/4.0	65.2/0.0	66.2/0.0
PT103	-	-	58.0/4.0	59.0/4.0
PT202	-	-	-	1.0/0.0

Table 4.2: Values of parameters used in the experiments.

Parameter	Value	Unit
ρ_{a}	$1.0000{\cdot}10^{3}$	kg/m^3
ρ_{d}	$1.0000{\cdot}10^{3}$	kg/m^3
L_{d}	$1.3200{\cdot}10^{1}$	m
L_{a}	$5.8000{\cdot}10^{1}$	m
h_{TVD}	$4.0000{\cdot}10^{0}$	m
D	$3.6000{\cdot}10^{-2}$	m
p_0	1.0325	bara
M	$6.9950{\cdot}10^{2}$	kg/m^4

located at the upper part of the annulus, 46.5 m from PT103; Loss B is located at the lower part of the annulus, 14.5 m from PT103. A controlled on/off valve and a manual valve make up a loss module which taps into the pipe. The on/off valves require 10 seconds to fully open or close. The loss rate depends on the pressure difference over the manual valve and its opening. No measurements of the loss rates are available so we use the difference $q_{\mathrm{c}} - q_{\mathrm{p}}$ as a replacement for q_{x}. The values for the rig parameters used in the simulations are presented in Table 4.2 where D is the inner diameter of the pipe.

The control law cannot be tested with the rig since the loss is not possible to stop by manipulating the choke opening. This is due to the "reservoir" pressure at the rig being atmospheric, which means that the differential pressure at the leak location only can be driven to zero by draining the pipe. Instead, the control law is tested with a state-of-the-art simulator in Section 4.9.

4.7 Experimental Results

A range of 29 loss experiments have been conducted with the rig. 15 of type Loss A and 14 of type Loss B. In the following section the results from using the observer with these data-sets are presented. The majority of the losses are of a magnitude between one and two percent of the flow rate from the pump. The flow rates from the pump vary from 48–107 lpm, and the pressure at the bit from 0.7–2.8 barg.

After 38 s, the estimation of in-/out-flux rate is activated, and the position estimate is not activated before the magnitude of the estimated in-/out-flux is greater than 0.2 lpm. The on/off valve starts to open at 40 seconds and starts to close at 100 seconds. Opening/closing duration is 10 seconds. Tuning parameters for the observer are found in the Appendix.

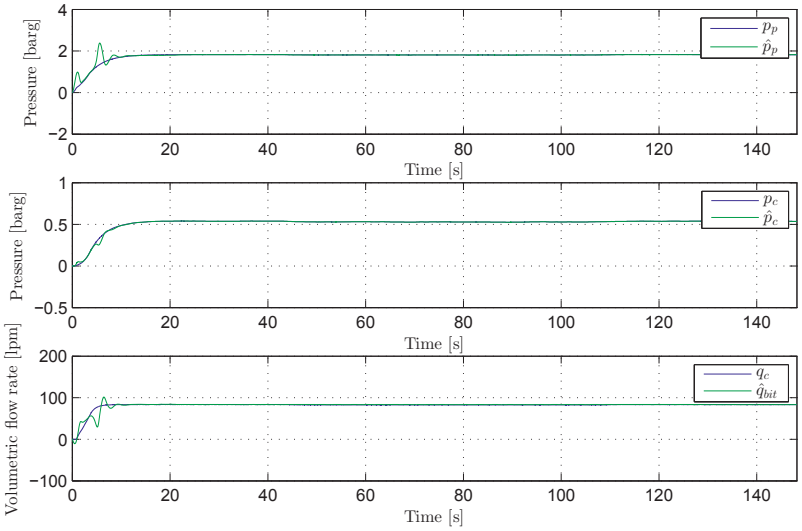

Figure 4.4: Experimental results. State estimates.

The mean values plotted in Figure 4.8 through Figure 4.10, are computed in the time interval 60–99 s.

Figure 4.4 through Figure 4.6 illustrate the typical behavior of the observer in case of a loss. The observer states quickly converge to the actual pressures and flow rate during the ramping-up phase. $\hat{q}_{\text{bit}}$ is compared to q_{c}, since q_{bit} is not measured. The loss rate is correctly estimated, while the position estimate indicates that the loss is in the lower part of the annulus. The variation of the convergence rates of the position estimates over the series of experiments are depicted in Figure 4.7. The convergence rate depends on the magnitude of the loss. The greater the loss rate, the quicker the observer locates it. In Figure 4.8 the loss rate is plotted against the pressure at the bit. The opening of the manual valve in the loss-module, has been kept constant through some of the experiments. From Figure 4.8 a vague trend is seen for some of the uppermost data points, which indicate that the loss rate is increasing with increasing bottomhole pressure. It can also be seen that the observer is able to correctly estimate the loss rate, even for small magnitude losses. In Figure 4.9 the loss position is plotted on the y-axis and flow rate through the choke on the x-axis. For Loss A, all, except two, estimated positions are in the upper part of the annulus. From Figure 4.10 we see that the two losses which are estimated to be at approximately 10 and 3 m are of small magnitude, actually less than one percent of the pump flow rate. For the Loss B losses, the estimated positions are all below 16 m.

4.8 Simulation setup

To test the control law we simulate the well hydraulics using OLGA. OLGA captures pressure pulses and compressibility of the liquid due to the pressure (and

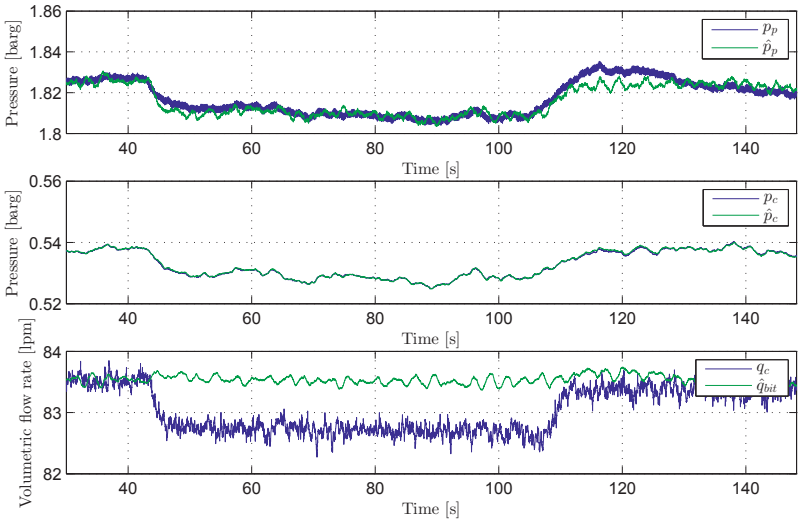

Figure 4.5: Experimental results. State estimates. Magnified.

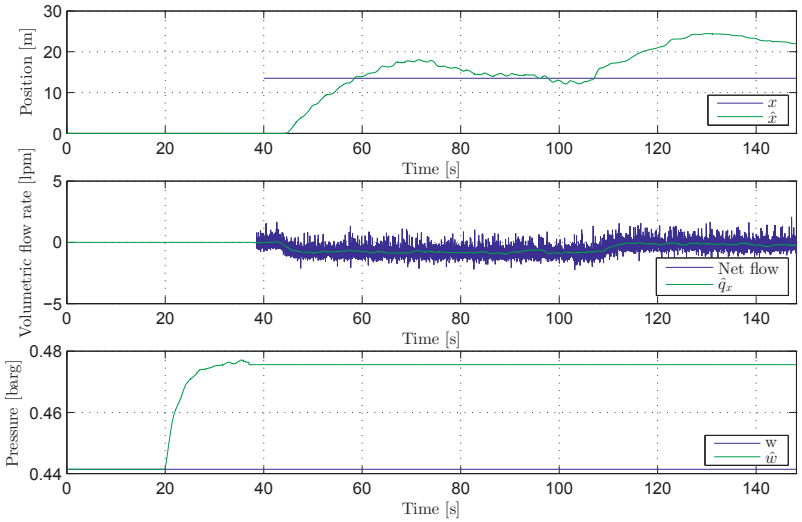

Figure 4.6: Experimental results. Parameter estimates.

temperature[4]) dependent density. These effects are significant for the well we are simulating. The (true) vertical depth of the well is 1500 m (TVD). The length (measured depth) of the wellbore is 2800 m (MD). The profile of the well is presented in Figure 4.11. The values for the parameters used in the simulation are presented in Table 4.3 where D_{di} is the inner diameter of the drillstring, D_{do} is the

[4]We carry out isothermal simulations with a fluid temperature of 15°C.

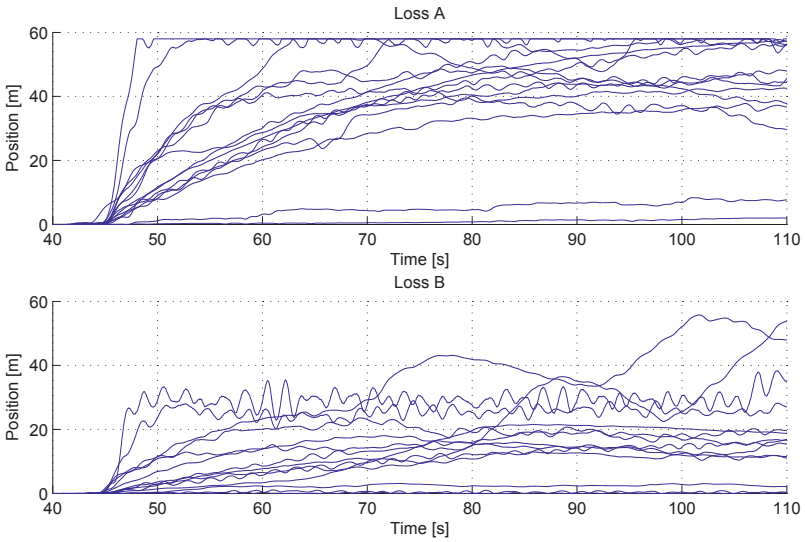

Figure 4.7: Experimental results. Position estimates.

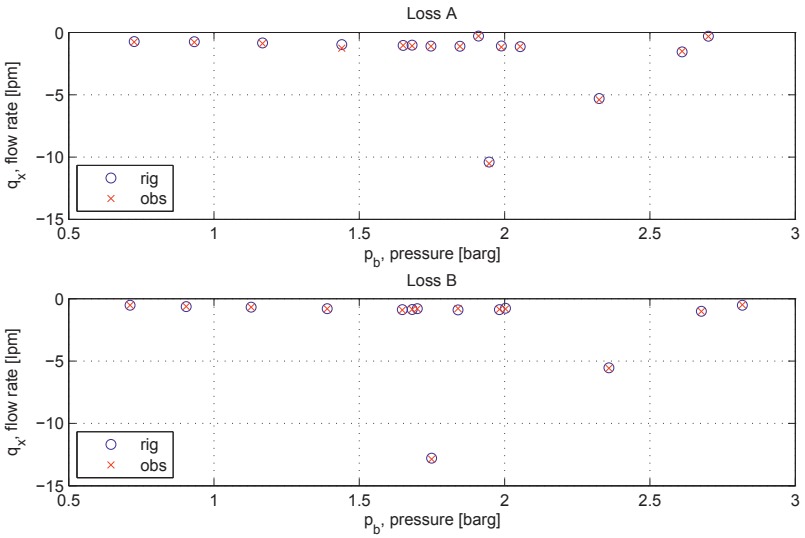

Figure 4.8: Experimental results. Loss rate versus pressure at the bit.

outer diameter of the drillstring, which is also the inner diameter of the annulus, and D_a is the outer diameter of the annulus. Note that we have added 25 m to the length of the annulus and drillstring to compensate for the additional length of the hose from the pump to the inlet of the drillstring and the outlet of the annulus to the choke. The volumetric flow rate from the main pump is 2000 lpm, which is a commonly used flow rate during managed pressure drilling. OLGA uses the same

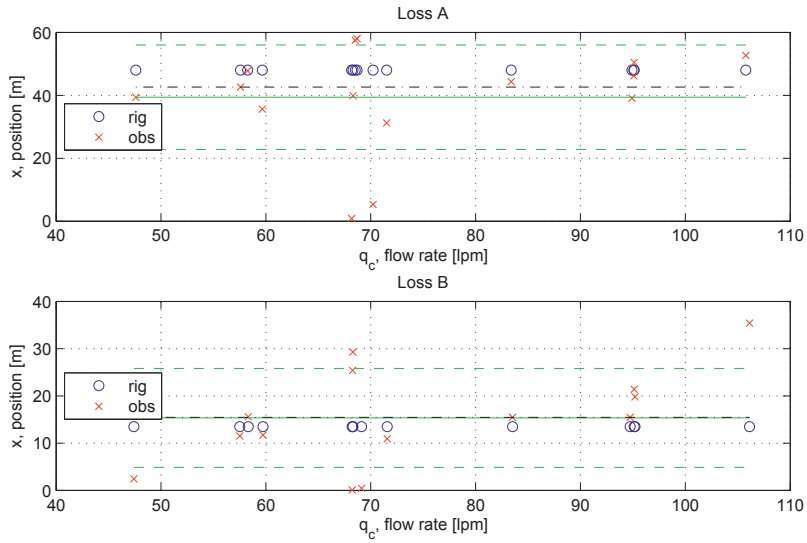

Figure 4.9: Experimental results. Loss position versus flow rate through the choke. The green lines are the mean ± standard deviation, and the black stippled line is the median.

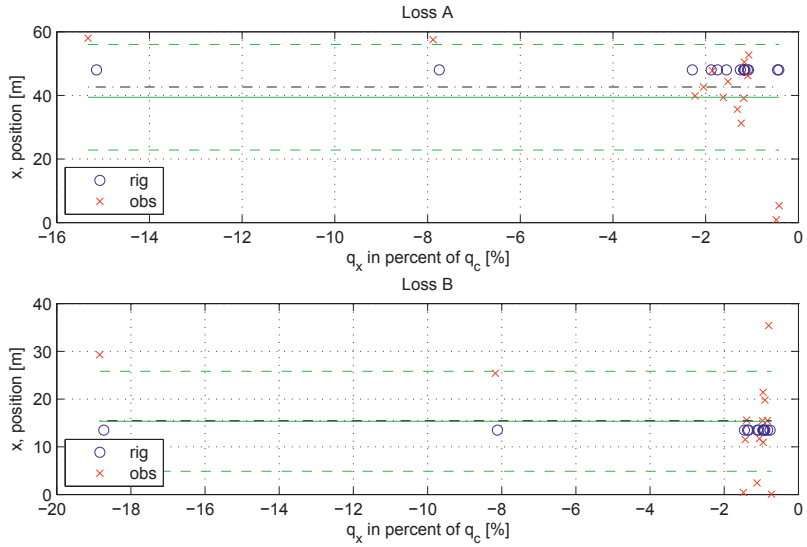

Figure 4.10: Experimental results. Loss position versus percentage of the loss rate compared to pump flow rate. The green lines are the mean ± standard deviation, and the black stippled line is the median.

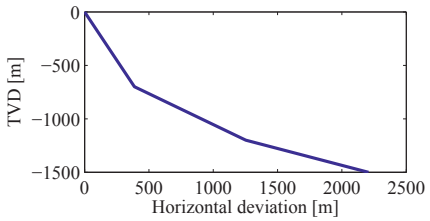

Figure 4.11: Profile of the well geometry.

Table 4.3: Values of parameters used in the simulation.

Parameter	Value	Unit
ρ_{a}	$1.0073{\cdot}10^{3}$	kg/m^3
ρ_{d}	$1.0046{\cdot}10^{3}$	kg/m^3
L_{d}	$2.8250{\cdot}10^{3}$	m
L_{a}	$2.8250{\cdot}10^{3}$	m
h_{TVD}	$1.5000{\cdot}10^{3}$	m
x	$1.5000{\cdot}10^{2}$	m
D_{di}	$8.8000{\cdot}10^{-2}$	m
D_{do}	$1.0000{\cdot}10^{-1}$	m
D_{a}	$2.0000{\cdot}10^{-1}$	m
β_{d}	$2.0000{\cdot}10^{4}$	bara
β_{a}	$2.0000{\cdot}10^{4}$	bara
p_0	3.0397	bara
M	$5.8437{\cdot}10^{3}$	kg/m^4
k_1	$1.0000{\cdot}10^{-1}$	-
k_{PI}	$5.0000{\cdot}10^{-2}$	m^3/(s bar)
p_{res}	$1.9600{\cdot}10^{2}$	bara

model for the flow rate from the reservoir as in (4.5).

4.9 Simulation results

After 120 s, the estimation of in-/out-flux rate is activated, and the position estimate is not activated before the magnitude of the estimated in-/out-flux is greater than 5 lpm. When an in-/out-flux is detected by the observer, the driller has to verify whether this is correct. To emulate this effect, the controller is activated 60 seconds after detection of the in-/out-flux. In the simulation, a fluid kick enters the wellbore 150 meters downstream the bit after 180 seconds. A measurement noise with a standard deviation of 0.1 bar is added to the measured pressures p_{p} and p_{c}. The flow rate from the main pump is varied with a standard deviation of 6.9 lpm to emulate the effect of an unsteady pump rate. The tuning parameters for the observer are found in Appendix 4.B.

In Figure 4.13, note that the mean of the position estimate is about 50 m upstream of the actual kick. This is due to a model error which most likely is

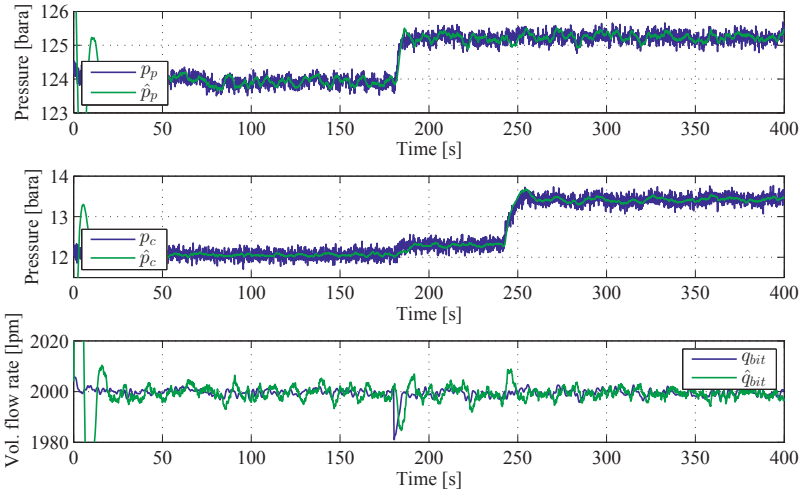

Figure 4.12: Simulation results. State estimates. Single kick.

caused by the simplifications of the frictional pressure drop functions, $F_{\mathrm{d}}^{\mathrm{s}}$ and $F_{\mathrm{a}}^{\mathrm{s}}$. We assume that the frictional pressure drop per unit length, at a given flow rate, is the same throughout the well. This is not the case since the density in the well is pressure dependent, and the real friction function depends upon density (and other spatially varying parameters). Subsequently, the actual frictional pressure drop per unit length, at a given flow rate, varies along the well.

Figure 4.12, Figure 4.13 and Figure 4.14 present the state estimates, parameter estimates, and the choke opening in the case where the kick is stopped, respectively. During the 60 seconds before the controller is activated, the location of the kick is pointed out by the observer, with an error which is about 1.7 percent of the total length of the well. The slightly oscillating choke opening causes some in-/outflow to/from the well. However, the kick is effectively stopped.

Figure 4.15 through Figure 4.17 show the results from a simulation where we drill into a reservoir with higher pressure than anticipated. The parameter estimates are active for the entire simulation period and the controller is first turned on after the parameter estimates have settled. After 180 s a kick is encountered, after 280 s the reservoir pressure gradually increases until 400 s, and at 401 s the reservoir pressure gradually drops with 3 bar until 410 s. This simulation demonstrates how the controller quickly mitigates the initial in-/out-flux and balances the flow in and out of the well without any interference from the driller.

4.10 Discussion

Localization of an in-/out-flux in a well based on pressure and flow rate measurements is inherently difficult due to the sensitivities of the frictional pressure drop to the flow rates and location of the in-/out-flux. The frictional pressure drop is highly

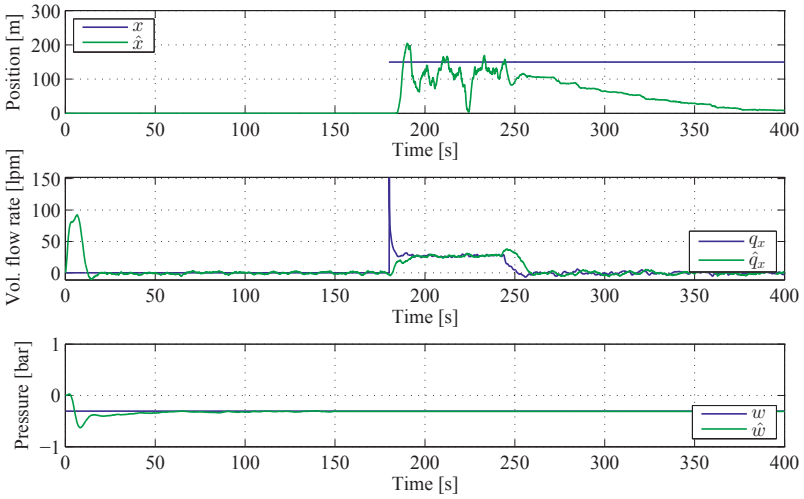

Figure 4.13: Simulation results. Parameter estimates. Single kick.

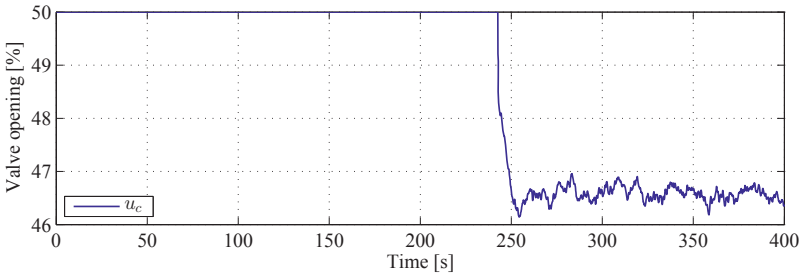

Figure 4.14: Simulation results. Choke opening. Single kick.

sensitive to the flow rate and insensitive to the location, which is the opposite of what we want. Accurate measurements are consequently crucial.

Correct modeling of the frictional pressure drop is difficult, especially for non-Newtonian fluids such as drilling mud. Although experiments and simulations have been carried out with water, which is Newtonian, the method of recording the pressure drop for a range of flow rates can still be carried out for drilling mud. However, one must be aware of gelling, sagging and thixotropic effects during transients which will corrupt the estimates from the observer.

Due to noise and imperfect friction models, there is a slight error margin related to the position estimates. However, with the OLGA simulation the error is about 1.7 percent of the total length of the well. If the in-/out-flux is not too close to the transition between casing and open-hole, it should be possible to distinguish between a perforated casing and an in-/out-flux from/to the formation. From the experimental results, no exact threshold for the magnitude of the loss rate which produces trustworthy position estimates can be seen. But when the loss rate exceeds

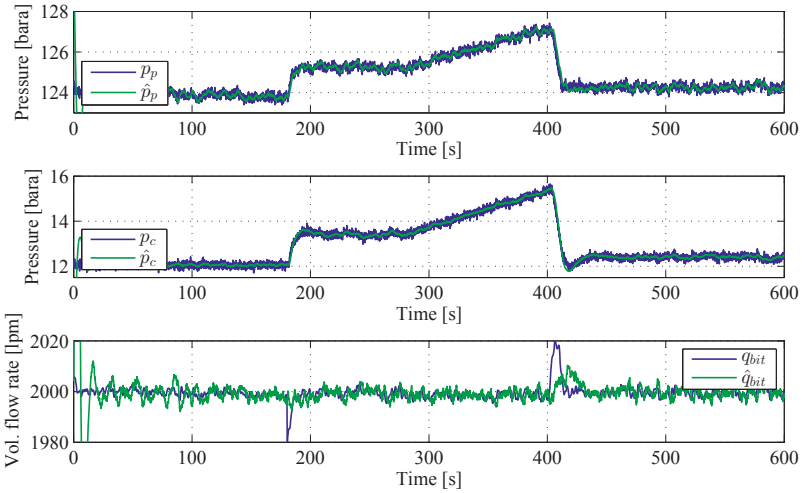

Figure 4.15: Simulation results. State estimates. Multiple kicks.

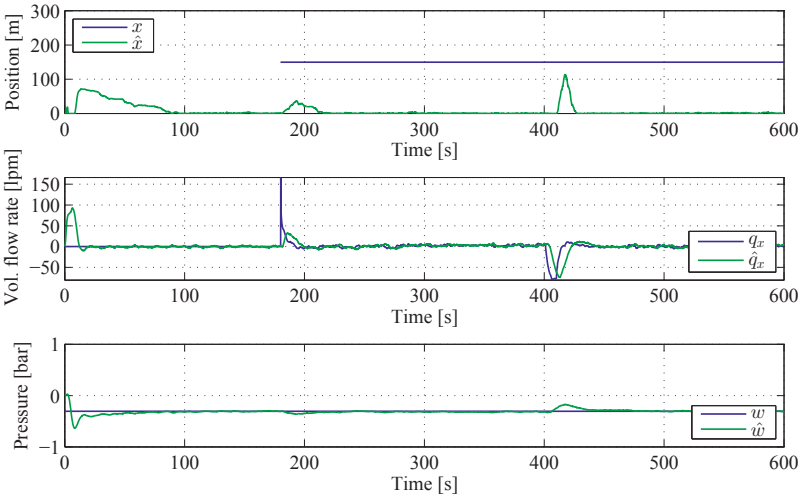

Figure 4.16: Simulation results. Parameter estimates. Multiple kicks.

one percent of the flow rate from the pump, 24 of the 27 position estimates are reasonably close to the correct value.

With the proposed observer we are able to prove exponential convergence of the state and parameter estimates. Convergence of the parameter estimates is ensured under a reasonable PE requirement, namely that there must be an in-/out-flux. The proposed controller is proven to render the origin of the reservoir-flow dynamics GES.

The decision to trade-off localization for mitigation, and vice versa, is a decision

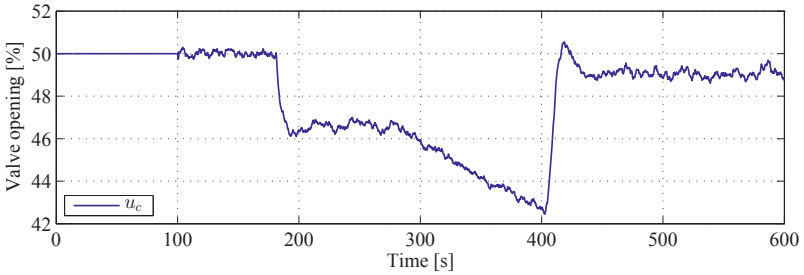

Figure 4.17: Simulation results. Choke opening. Multiple kicks.

for the crew at the drill-rig as it depends on factors such as magnitude of the in-/out-flux, anticipated formation pressure, length of the open-hole, among others.

Before drilling into a reservoir, the controller can be activated. And if an in-/out-flux is encountered the controller manages to mitigate it and balance the flow in and out of the well. If there is no contact with the reservoir while drilling and the controller is active, the choke opening, and subsequently the pressure in the well, will drift. This is because the control law considers only flow rates and not any pressures. However, an in-/out-flux connects the pressure in the wellbore to the reservoir, and stopping the in-/out-flux implies equalizing the reservoir pressure and the pressure in the wellbore at that point. This effectively keeps the pressure in the wellbore steady.

We test the control law with an external simulator with dynamics and effects which are not considered in the control design. Time-delay of the pressure propagation, pressure dependent density, and inaccurate flow-rate from the choke with respect to the flow-rate determined by the controller, are examples of this. Yet, the controller is able to mitigate the in-/out-flux, demonstrating robustness with respect to the aforementioned model uncertainties.

In Zhang (2002), it is shown that the expected values of the estimates from the observer will converge exponentially to the actual values assuming additive and bounded noise. The proof is valid only if the noise is independent of the matrices A, C, K, Σ, Υ and Ψ, and have zero mean. In our simulation case we add independent noise with zero mean to the measurements, thus we can still guarantee exponential convergence of the expected values of our estimates. For the experimental data, the measurement noise is in fact negligible. Seemingly random variations of the pump pressure are caused by the cyclic flow rate from the piston pump.

If the pressure in the loss zone, p_{res}, is such that the out-flux cannot be stopped by fully opening the choke, the flow rate from the pump must be decreased to alleviate the pressure in the wellbore. Similarly, if there is an in-flux that cannot be stopped by closing the choke, the flow rate from the pump must be increased. Our work has not covered these eventualities, but GES of (4.21) provides a useful result. Since we have an estimate of q_{bit}, and noting that $q_{\text{bit}} \approx q_{\text{p}}$ after transients, manually changing the flow rate from the pump when the choke saturates will not lead to an unstable controller.

4.11 Conclusions and further work

Due to the lack of instrumentation down-hole, a model-based in-/out-flux detection scheme is necessary for the hydraulic MPD system. The proposed globally exponentially stable adaptive observer is capable of quantifying and locating an in-/out-flux greater than one percent of the flow rate from the pump with reasonable precision. This is verified with both experimental and simulation results. To locate the in-/out-flux, the persistency of excitation requirement is that there is a difference in flow rate in and out of the well.

We design a control law for the choke which is proved to give a globally exponentially stable origin of the in-/out-flux dynamics when the system is not noise corrupted. When adding noise, we can guarantee that the expected values of the estimated states and parameters will converge exponentially to the actual values.

Further work will include estimation of the reservoir pressure and the production index while noting that increasing the number of estimated parameters calls for a more persistently exciting regressor. It would be interesting to discuss the controller's ability to deal with uncertainties. Another issue to address is the possibility for the choke to saturate. Coordinated control of the main pump is needed to avoid this. Unwanted fluctuation of the choke opening with the proposed control law could possibly be dampened by filtering. However, this would call for a new stability analysis. Modification of the rig which would allow for testing of the control law would also be of great interest.

4.12 Acknowledgements

The authors would like to thank Henning Stave for conducting the experiments and the University of Stavanger for providing the rig.

4.A Assumptions from Zhang (2002)

In the following the notation n, m and p are the number of states, measurements and parameters, respectively.

Assumption 1. Assume that the matrix pair $(A(t), C(t))$ in system (4.8) is such that there exists a bounded matrix $K(t) \in \mathbb{R}^n \times \mathbb{R}^m$ so that the system

$$\dot{\eta}(t) = [A(t) - K(t)C(t)]\eta(t) \tag{4.28}$$

is exponentially stable.

Assumption 2. Let $\Upsilon(t) \in \mathbb{R}^n \times \mathbb{R}^m$ be a matrix of signals generated by the ordinary differential equation (ODE) system

$$\dot{\Upsilon}(t) = [A(t) - K(t)C(t)]\Upsilon(t) + \Psi(t). \tag{4.29}$$

Assume that $\Psi(t)$ is persistently exciting, so that there exist positive constants α, β, T and some bounded symmetric positive-definite matrix $\Sigma(t) \in \mathbb{R}^m \times \mathbb{R}^m$ such

that, for all t, the following inequalities hold

$$\alpha I \leq \int_t^{t+T} \Upsilon^\top(\tau) C^\top \Sigma(\tau) C \Upsilon(\tau)\, \mathrm{d}\tau \leq \beta I. \tag{4.30}$$

4.B Tuning

For the adaptive observer used with the experimental data, we use the gains $\Gamma = \mathrm{diag}(5{\cdot}10^{-6} 4{\cdot}10^{5} 8{\cdot}10^{-2})$, K is found as the Kalman gain using the covariance matrix for the measurements, and Σ is a scaled version of the inverse of the covariance matrix for the measurements. The covariance matrix for the measurements is computed for each experiment during a 19 second period prior to the loss when the pressures are steady.

For the adaptive observer used with the OLGA simulations, we use the gains

$$\Sigma = \begin{bmatrix} 5.2757 \cdot 10^{-4} & 1.5148 \cdot 10^{-5} \\ 1.5148 \cdot 10^{-5} & 9.5569 \cdot 10^{-4} \end{bmatrix},$$

$$\Gamma = \begin{bmatrix} 10^{-3} & 0 & 0 \\ 0 & 10^{9} & 0 \\ 0 & 0 & 10^{2} \end{bmatrix},$$

and K is found as the Kalman gain using the covariance matrix for the measurements, and Σ is a scaled version of the inverse of the covariance matrix for the measurements.

4.C Nomenclature

Table 4.4: Nomenclature.

Variable	Description	Unit
β_{a}	Bulk modulus for the annulus	bara
β_{d}	Bulk modulus for the drillstring	bara
F_{a}	Friction function for the annulus	(bar s)/m^4
F_{d}	Friction function for the drillstring	(bar s)/m^4
g	Acceleration due to gravity	m/s^2
h_{TVD}	Vertival distance from drill-bit to rig floor	m
k_{PI}	Production index from reservoir	m^3/(bar s)
L_{d}	Lenght of the drillstring	m
L_{a}	Lenght of the annulus	m
M	Mass-like constant	10^{-5}kg/m^4
p_{c}	Choke pressure	bara
p_0	Ambient pressure	bara
p_{p}	Pump pressure	bara
p_{res}	Reservoir pressure	bara
p_{x}	Pressure in wellbore at x	bara
q_{bit}	Flow-rate through the bit	m^3/s
q_{c}	Flow-rate through the choke	m^3/s
$q_{\mathrm{c,ref}}$	Reference flow-rate for the controller	m^3/s
q_{p}	Flow-rate from the pump	m^3/s
q_{x}	Rate of in-/out-flux	m^3/s
ρ_{a}	Density of the fluid in the annulus	10^{-5}kg/m^3
ρ_{d}	Density of the fluid in the drillstring	10^{-5}kg/m^3
θ	Parameter vector	-
u	Input	m^3/s
u_{c}	Choke opening	-
V_{a}	Volume of the annulus	bara
V_{d}	Volume of the drillstring	bara
w	Pressure difference	bar
x	Location of in-/out-flux	m
y	Measured signals	bara
z	State vector	-

Chapter 5

Application of an infinite-dimensional observer for drilling systems incorporating kick and loss detection

Summary

We apply a PDE observer to a hydraulic system of a managed pressure drilling rig. The observer can be used to detect and quantify an in- or outflux. We show that the PDE model of the hydraulic system can be expressed as a 2×2 linear hyperbolic system of PDEs with spatially varying coefficients coupled with an ODE at the inlet boundary that models the in- or outflux. Using the method of backstepping, we design an observer which is exponentially stable at the origin in the $\mathcal{L}^2$-norm while relying on measurements taken at the outlet boundary, only. Simulation results verify the validity of the observer.

5.1 Introduction

Detection and quantification of leaks in pipelines have been a subject of research for many years. We look at an analog problem concerning detection and quantification of in-/out-flux during drilling of oil and gas wells. In the drilling community, an outflux to the formation from the wellbore is called a loss or "lost returns", while an influx is called a kick or "gaining fluid". These two unwanted events are a result of the pressure in the wellbore being either too high or too low compared to the surrounding formation. Even with proper pressure control and seismic surveys, loss and gain are bound to happen during the development of new fields. Drilling of exploration wells is a dangerous task where the crew runs the risk of drilling into a high-pressure gas-pocket or possibly losing/gaining fluid to/from the formation. This can lead to loss of control of the well, which again can result in damage to the well, or in worst case, a catastrophic blowout. The consequences are not only monetary and environmental, but also concern the safety of the rig personnel.

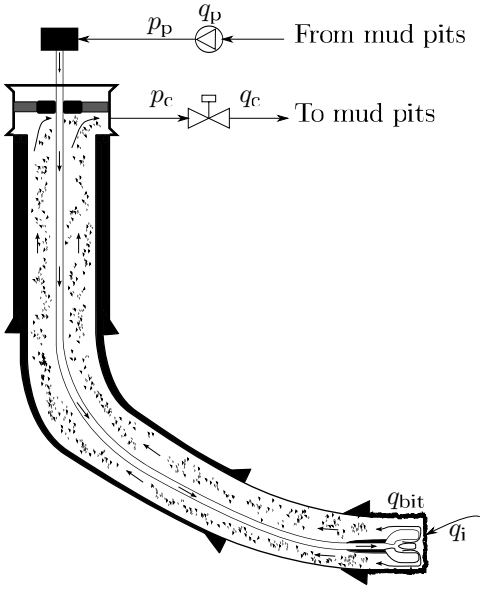

Figure 5.1: Schematic of a managed pressured drilling system.

Managed Pressure Drilling (MPD) Kaasa et al. (2011) is a new technology gaining more and more interest. MPD is an enabling technology to drill challenging wells into depleted reservoirs with narrow pressure margins. Also, MPD has the economical benefit of reduced rig time and health, safety and environmental benefits of improved well control. The concept includes a rig pump pumping drilling mud into the drillstring, through the bit at the bottom of the well, and up through the annulus. The annulus is sealed and the pressure in the closed volume is controlled by a choke. This is illustrated in Figure 5.1. By controlling the flow rate from the pump and the choke opening, it is possible to regulate the pressure at a point in the well to a predetermined value within a few seconds.

Due to the harsh conditions in the wellbore, the most reliable measurements of pressure and flow rate are the ones located at the rig. And subsequently, a monitoring system for in-/out-flux has to be model based. The ODE model in Kaasa et al. (2011) is applied to gas kick detection and mitigation in Zhou et al. (2011), where the concept of switched control of the bottomhole pressure is presented. An MPD system is considered where a controller manipulating the choke and backpressure pump switches between a combination of pressure and flow control when there is no in-flux and pure flow control when a kick is detected. In Hauge et al. (2012a) another model based in-/out-flux detection and mitigation scheme is presented. The adaptive observer is shown to be globally exponentially stable and is capable of quantifying and locating an in-/out-flux. The choke controller does not rely upon switching for stopping the in-/out-flux. An early example of model-based leak detection can be found in Billmann and Isermann (1987) where a correlation technique is used to detect, quantify and locate the leak. Using the water hammer equations based on a collocation method, a model based leak detection scheme

using an extended Kalman filter observer is implemented in Torres et al. (2008). In Torres et al. (2009), it is shown that multiple leaks in a pipeline can be detected if the system is sufficiently excited through the boundary conditions. The work of Aamo et al. (2006) covers a PDE-observer which is able to adapt to the friction of a horizontal pipeline before quantifying and locating a leak. The observer uses non-reflective boundaries for robustness to initial conditions. The boundary conditions are found by linearization of the nonlinear PDEs. The observer for the linearized system is proven to be exponentially stable at the origin in the $\mathcal{L}^2$-norm.

In this paper we consider a PDE observer for the well hydraulics. The model of the hydraulics is a system of linear 2×2 first-order hyperbolic PDEs which can be transformed into the system

$$u_t = -\epsilon_1(x)u_x + c_1(x)v, \tag{5.1}$$

$$v_t = \epsilon_2(x)v_x + c_2(x)u, \tag{5.2}$$

$$u(0,t) = qv(0,t) + v_{\mathrm{i}}(t) + CX(t), \tag{5.3}$$

$$v(1,t) = U(t), \tag{5.4}$$

$$\dot{X} = AX, \tag{5.5}$$

where $(x,t) \in [0,1] \times [0,\infty)$, $\epsilon_1(x) > 0$, $\epsilon_2(x) > 0$, $q \neq 0$, $v_{\mathrm{i}}(t)$ is a known injection at the boundary, $X(t)$ is a n-dimensional vector, A is a $n \times n$ matrix and C is a $1 \times n$ matrix. $U(t)$ is the control input, while $u(1,t)$ is the measurement. The subscripts t and x denote the time- and spatial-derivative, respectively. The objective is to demonstrate an application of an exponentially stable observer for (5.1)–(5.5) with measurements only at the boundary $x = 1$. Similar efforts have previously been made for heat exchangers, Xu and Sallet (2002); and irrigation canals, Coron et al. (2007), de Halleux et al. (2003). The observer is designed by combining results from Krstić and Smyshlyaev (2008a) and Vazquez et al. (2011b) which both use the method of backstepping. In Krstić and Smyshlyaev (2008a), backstepping boundary control is applied to first-order hyperbolic PDEs by using invertible Volterra integral transformations together with boundary feedback. The joint papers Vazquez et al. (2011b) and Vazquez et al. (2011a) consider boundary backstepping stabilization for a linear hyperbolic system, and a quasilinear hyperbolic system, respectively. Both of the systems considered are non-uniform. We use a similar observer structure and transformation as in Vazquez et al. (2011b) for (5.1)–(5.4) and an observer similar to the observer for ODE systems with sensor delays in Krstić and Smyshlyaev (2008a) for (5.5).

This article is structured as follows. Section 5.2 shows how the model of the well hydraulics can be transformed into (5.1)–(5.5). In Section 5.3 we briefly present the observer design. An application of the observer with the well hydraulics is illustrated with simulation results in Section 5.4. Conclusions are given in Section 5.5 which is followed by Section 5.6 concerning further work.

5.2 Well hydraulics

Consider a drilling rig, illustrated in Figure 5.1. We model the fluid dynamics of the return side (from the bit, up the annulus to the choke) in the standard way of

a hydraulic pipe flow White (1999) as

$$p_t(z,t) = -\frac{\beta}{A_\mathrm{a}} q_z(z,t), \tag{5.6}$$

$$q_t(z,t) = -\frac{A_\mathrm{a}}{\rho} p_z(z,t) - \frac{F}{\rho} q(z,t) - A_\mathrm{a} g, \tag{5.7}$$

$$q(0,t) = q_\mathrm{bit}(t), \tag{5.8}$$

$$p(l,t) = p_\mathrm{c}(t), \tag{5.9}$$

where $(z,t) \in [0,l] \times [0,\infty)$, p is the pressure along the annulus, q is the volumetric flow rate through the annulus, l denotes the total length of the annulus, β is the isothermal bulk modulus, A_a the area of the annulus, F a friction coefficient, g the gravitational constant, and ρ the density of the drilling mud. $p_\mathrm{c}(t)$ is the pressure upstream the choke and the controlled input, and $q_\mathrm{c}(t) = q(l,t)$ is the volumetric flow rate through the choke, which is measured. We can remove the contribution of the hydrostatic head from the momentum equation by defining

$$\bar{p}(z,t) = p(z,t) - \rho g (l - z), \tag{5.10}$$

which gives

$$\bar{p}_t(z,t) = p_t(z,t) = -\frac{\beta}{A_\mathrm{a}} q_z(z,t), \tag{5.11}$$

$$\begin{aligned} q_t(z,t) &= -\frac{A_\mathrm{a}}{\rho} \left(\bar{p}(z,t) + \rho g (l-z)\right)_z - \frac{F}{\rho} q(z,t) - A_\mathrm{a} g \\ &= -\frac{A_\mathrm{a}}{\rho} \bar{p}_z(z,t) + A_\mathrm{a} g - \frac{F}{\rho} q(z,t) - A_\mathrm{a} g \\ &= -\frac{A_\mathrm{a}}{\rho} \bar{p}_z(z,t) - \frac{F}{\rho} q(z,t), \end{aligned} \tag{5.12}$$

and

$$\bar{p}(l,t) = p(l,t) = p_\mathrm{c}(t). \tag{5.13}$$

We denote the volumetric flow rate and pressure at the bit with, q_bit and p_bit, respectively, and get

$$q_\mathrm{bit}(t) = q_\mathrm{p}(t) + q_\mathrm{i}(t), \tag{5.14}$$

$$p_\mathrm{bit}(t) = p(0,t), \tag{5.15}$$

where $q_\mathrm{p}(t)$ is the volumetric flow rate from the rig pump, which is measured, and q_i is the volumetric in-/out-flux. This gives

$$\bar{p}_t = -\frac{\beta}{A_\mathrm{a}} q_z, \tag{5.16}$$

$$q_t = -\frac{A_\mathrm{a}}{\rho} \bar{p}_z - \frac{F}{\rho} q, \tag{5.17}$$

$$q(0,t) = q_\mathrm{p}(t) + q_\mathrm{i}(t), \tag{5.18}$$

$$\bar{p}(l,t) = p_\mathrm{c}(t). \tag{5.19}$$

We now want to transform (5.16)–(5.19) into the form (5.1)–(5.5), which is needed for the observer design. A similar method of transformation was carried out in Bastin and Coron (2010), but we highlight the steps for sake of the reader. Consider the change of variables

$$\bar{u}(z,t) = \frac{1}{2}\left(q(z,t) + \frac{A_\mathrm{a}}{\sqrt{\beta\rho}}\bar{p}(z,t)\right), \tag{5.20}$$

$$\bar{v}(z,t) = \frac{1}{2}\left(q(z,t) - \frac{A_\mathrm{a}}{\sqrt{\beta\rho}}\bar{p}(z,t)\right). \tag{5.21}$$

Taking the time-derivative of (5.20) and (5.21) gives

$$\begin{aligned}\bar{u}_t =& \frac{1}{2}\left(q_t(z,t) + \frac{A_\mathrm{a}}{\sqrt{\beta\rho}}\bar{p}_t\right)\\ =& -\sqrt{\frac{\beta}{\rho}}\bar{u}_z - \frac{F}{2\rho}(\bar{u}+\bar{v}).\end{aligned} \tag{5.22}$$

and

$$\begin{aligned}\bar{v}_t =& \frac{1}{2}\left(q_t(z,t) - \frac{A_\mathrm{a}}{\sqrt{\beta\rho}}\bar{p}_t(z,t)\right)\\ =& \sqrt{\frac{\beta}{\rho}}\bar{v}_z - \frac{F}{2\rho}(\bar{u}+\bar{v}).\end{aligned} \tag{5.23}$$

The boundary conditions are

$$\bar{u}(0,t) = \frac{1}{2}\left(q_\mathrm{p}(t) + q_\mathrm{i}(t) + \bar{u}(0,t) - \bar{v}(0,t)\right), \tag{5.24}$$

$$\bar{v}(l,t) = \frac{1}{2}\left((\bar{u}(l,t) + \bar{v}(l,t)) - \frac{A_\mathrm{a}}{\sqrt{\beta\rho}}p_\mathrm{c}(t)\right), \tag{5.25}$$

so we get

$$\bar{u}(0,t) = -\bar{v}(0,t) + q_\mathrm{p}(t) + q_\mathrm{i}(t), \tag{5.26}$$

$$\bar{v}(l,t) = \bar{u}(l,t) - \frac{A_\mathrm{a}}{\sqrt{\beta\rho}}p_\mathrm{c}(t). \tag{5.27}$$

Next, consider the transformation $x = z/l$, and define

$$u(x,t) = \bar{u}(xl,t)\, e^{ax}, \tag{5.28}$$

$$v(x,t) = \bar{v}(xl,t)\, e^{-ax}, \tag{5.29}$$

where a is to be defined. Taking the time-derivative of (5.28) gives

$$u_t = -\sqrt{\frac{\beta}{\rho}}\bar{u}_z e^{ax} - \frac{F}{2\rho}\left(u(x,t) + v(x,t)\, e^{2ax}\right). \tag{5.30}$$

The spatial-derivative of (5.28) is

$$u_x(x,t) = l\bar{u}_z(xl,t)\,e^{ax} + a\bar{u}(xl,t)\,e^{ax}, \tag{5.31}$$

so

$$\bar{u}_z(xl,t) = \frac{1}{l}u_x(x,t)\,e^{-ax} - \frac{a}{l}u(x,t)\,e^{-ax}. \tag{5.32}$$

Inserting (5.32) into (5.30) yields

$$u_t = -\frac{1}{l}\sqrt{\frac{\beta}{\rho}}u_x(x,t) + \left(\frac{a}{l}\sqrt{\frac{\beta}{\rho}} - \frac{F}{2\rho}\right)u - \frac{F}{2\rho}e^{2ax}v(x,t). \tag{5.33}$$

Choosing

$$a = \frac{Fl}{2\sqrt{\beta\rho}} \tag{5.34}$$

gives

$$u_t = -\frac{1}{l}\sqrt{\frac{\beta}{\rho}}u_x(x,t) - \frac{F}{2\rho}e^{2ax}v(x,t). \tag{5.35}$$

Similar steps for (5.29) gives

$$v_t(x,t) = \frac{1}{l}\sqrt{\frac{\beta}{\rho}}v_x(x,t) - \frac{F}{2\rho}e^{-2ax}u(x,t). \tag{5.36}$$

We can now write the boundary conditions as

$$u(0,t) = -v(0,t) + q_{\mathrm{p}}(t) + q_{\mathrm{i}}(t), \tag{5.37}$$

and

$$v(1,t) = u(1,t)\,e^{-2a} - \frac{A_{\mathrm{a}}e^{-a}}{\sqrt{\beta\rho}}p_{\mathrm{c}}(t). \tag{5.38}$$

In summary, the model is

$$u_t = -\frac{1}{l}\sqrt{\frac{\beta}{\rho}}u_x - \frac{F}{2\rho}e^{2ax}v, \tag{5.39}$$

$$v_t = \frac{1}{l}\sqrt{\frac{\beta}{\rho}}v_x - \frac{F}{2\rho}e^{-2ax}u, \tag{5.40}$$

$$u(0,t) = -v(0,t) + q_{\mathrm{p}}(t) + q_{\mathrm{i}}(t), \tag{5.41}$$

$$v(1,t) = u(1,t)\,e^{-2a} - \frac{A_{\mathrm{a}}e^{-a}}{\sqrt{\beta\rho}}p_{\mathrm{c}}(t), \tag{5.42}$$

which corresponds to (5.1)–(5.5) with

$$\epsilon_1(x) = \epsilon_2(x) = \frac{1}{l}\sqrt{\frac{\beta}{\rho}}, \tag{5.43}$$

$$c_1(x) = -\frac{F}{2\rho}e^{2ax}, \tag{5.44}$$

$$c_2(x) = -\frac{F}{2\rho}e^{-2ax}, \tag{5.45}$$

$$q = -1, \tag{5.46}$$

$$v_{\mathrm{i}}(t) = q_{\mathrm{p}}(t) \tag{5.47}$$

$$U(t) = u(1,t)\,e^{-2a} - \frac{A_{\mathrm{a}}e^{-a}}{\sqrt{\beta\rho}}p_{\mathrm{c}}(t), \tag{5.48}$$

where a is given by (5.34), and (A, C) such that

$$\dot{X} = AX, \tag{5.49}$$

$$q_{\mathrm{i}}(t) = CX(t). \tag{5.50}$$

The original variables are obtained as

$$q(z,t) = u\left(\frac{z}{l},t\right)e^{-\frac{a}{l}z} + v\left(\frac{z}{l},t\right)e^{\frac{a}{l}z}, \tag{5.51}$$

$$p(z,t) = \frac{\sqrt{\beta\rho}}{A_{\mathrm{a}}}\left(u\left(\frac{z}{l},t\right)e^{-\frac{a}{l}z} - v\left(\frac{z}{l},t\right)e^{\frac{a}{l}z}\right) + \rho g(l-z). \tag{5.52}$$

In the presence of a constant in-/out-flux, we can simply set $A = 0$ and $C = 1$.

5.3 Observer design

In this section we present an exponentially stable observer for (5.1)–(5.5). The observer is based on Vazquez et al. (2011a,b), where an observer without the disturbance at x=1 was designed using backstepping. While a detailed derivation of the observer augmented with the disturbance was carried out in Aamo (2012), here we repeat some of the steps for clarity. Consider the observer

$$\hat{u}_t = -\epsilon_1(x)\hat{u}_x + c_1(x)\hat{v} + p_1(x)\tilde{u}(1,t), \tag{5.53}$$

$$\hat{v}_t = \epsilon_2(x)\hat{v}_x + c_2(x)\hat{u} + p_2(x)\tilde{u}(1,t), \tag{5.54}$$

$$\hat{u}(0,t) = q\hat{v}(0,t) + v_{\mathrm{i}}(t) + C\hat{X}(t), \tag{5.55}$$

$$\hat{v}(1,t) = U(t), \tag{5.56}$$

$$\dot{\hat{X}} = A\hat{X} + e^{A\phi(0)}L\tilde{u}(1,t), \tag{5.57}$$

where

$$\phi(x) = \int_x^1 \frac{1}{\epsilon_1(\gamma)}d\gamma, \tag{5.58}$$

and

$$\tilde{u}(1,t) = u(1,t) - \hat{u}(1,t). \tag{5.59}$$

The functions $p_1(x)$ and $p_2(x)$, and the matrix L are output injection gains to be designed. Forming error equations by subtracting (5.53)–(5.57) from (5.1)–(5.5), denoted by a tilde, we have

$$\tilde{u}_t = -\epsilon_1(x)\,\tilde{u}_x + c_1(x)\,\tilde{v} - p_1(x)\,\tilde{u}(1,t), \tag{5.60}$$
$$\tilde{v}_t = \epsilon_2(x)\,\tilde{v}_x + c_2(x)\,\tilde{u} - p_2(x)\,\tilde{u}(1,t), \tag{5.61}$$
$$\tilde{u}(0,t) = q\tilde{v}(0,t) + C\tilde{X}(t), \tag{5.62}$$
$$\tilde{v}(1,t) = 0, \tag{5.63}$$
$$\dot{\tilde{X}} = A\tilde{X} - e^{A\phi(0)}L\tilde{u}(1,t). \tag{5.64}$$

In Vazquez et al. (2011b), the following backstepping transformation

$$\tilde{u}(x,t) = \tilde{\alpha}(x,t) - \int_x^1 P^{uu}(x,\xi)\,\tilde{\alpha}(\xi,t)\,d\xi - \int_x^1 P^{uv}(x,\xi)\,\tilde{\beta}(\xi,t)\,d\xi, \tag{5.65}$$
$$\tilde{v}(x,t) = \tilde{\beta}(x,t) - \int_x^1 P^{vu}(x,\xi)\,\tilde{\alpha}(\xi,t)\,d\xi - \int_x^1 P^{vv}(x,\xi)\,\tilde{\beta}(\xi,t)\,d\xi. \tag{5.66}$$

was used for observer design in the case without disturbance, where the kernels are given by the system of equations[1]

$$\epsilon_1(x)\,P^{uu}_x(x,\xi) + \epsilon_1(\xi)\,P^{uu}_\xi(x,\xi) = -\epsilon_1'(\xi)\,P^{uu}(x,\xi) + c_1(x)\,P^{vu}(x,\xi), \tag{5.67}$$
$$\epsilon_1(x)\,P^{uv}_x(x,\xi) - \epsilon_2(\xi)\,P^{uv}_\xi(x,\xi) = \epsilon_2'(\xi)\,P^{uv}(x,\xi) + c_1(x)\,P^{vv}(x,\xi), \tag{5.68}$$
$$\epsilon_2(x)\,P^{vu}_x(x,\xi) - \epsilon_1(\xi)\,P^{vu}_\xi(x,\xi) = \epsilon_1'(\xi)\,P^{vu}(x,\xi) - c_2(x)\,P^{uu}(x,\xi), \tag{5.69}$$
$$\epsilon_2(x)\,P^{vv}_x(x,\xi) + \epsilon_2(\xi)\,P^{vv}_\xi(x,\xi) = -\epsilon_2'(\xi)\,P^{vv}(x,\xi) - c_2(x)\,P^{uv}(x,\xi), \tag{5.70}$$

on $\mathcal{T} = \{(x,\xi) : 0 \le \xi \le x \le 1\}$ with boundary conditions

$$P^{uu}(0,\xi) = qP^{vu}(0,\xi), \tag{5.71}$$
$$P^{uv}(x,x) = \frac{c_1(x)}{\epsilon_1(x) + \epsilon_2(x)}, \tag{5.72}$$
$$P^{vu}(x,x) = -\frac{c_2(x)}{\epsilon_1(x) + \epsilon_2(x)}, \tag{5.73}$$
$$P^{vv}(0,\xi) = \frac{1}{q}P^{uv}(0,\xi). \tag{5.74}$$

It was shown in Vazquez et al. (2011b) that there exists a unique solution to (5.67)–(5.74) which is $C(\mathcal{T})$. We have the following result for our error system (5.60)–(5.64) (the proof is similar to that in Krstić and Smyshlyaev (2008b) but omitted due to page limitation).

[1] Note that there are typos in equations (24)–(25) in Vazquez et al. (2011b).

Lemma 5.1. *Let $(P^{uu}, P^{uv}, P^{vu}, P^{vv})$ be the solution to (5.67)–(5.74). If*

$$p_1(x) = Ce^{A\phi(x)}L - P^{uu}(x,1)\epsilon_1(1) - \int_x^1 P^{uu}(x,\xi)Ce^{A\phi(\xi)}Ld\xi, \tag{5.75}$$

$$p_2(x) = -P^{vu}(x,1)\epsilon_1(1) - \int_x^1 P^{vu}(x,\xi)Ce^{A\phi(\xi)}Ld\xi, \tag{5.76}$$

then the transformation (5.65)–(5.66) maps (5.60)–(5.64) into the system

$$\tilde{\alpha}_t(x,t) = -\epsilon_1(x)\tilde{\alpha}_x(x,t) - Ce^{A\phi(x)}L\tilde{\alpha}(1,t), \tag{5.77}$$

$$\tilde{\beta}_t = \epsilon_2(x)\tilde{\beta}_x(x,t), \tag{5.78}$$

with boundary conditions

$$\tilde{\alpha}(0,t) = q\tilde{\beta}(0,t) + C\tilde{X}, \tag{5.79}$$

$$\tilde{\beta}(1,t) = 0, \tag{5.80}$$

and

$$\dot{\tilde{X}} = A\tilde{X} - e^{A\phi(0)}L\tilde{\alpha}(1,t). \tag{5.81}$$

It was shown in Vazquez et al. (2011b) that the transformation (5.65)–(5.66) is invertible, so that stability properties of (5.60)–(5.64) and (5.77)–(5.81) are equivalent. We therefore analyze stability of the origin of (5.77)–(5.81). The system (5.77)–(5.81) can be viewed as a cascade consisting of the parts

$$\tilde{\beta}_t = \epsilon_2(x)\tilde{\beta}_x(x,t), \tag{5.82}$$

$$\tilde{\beta}(1,t) = 0, \tag{5.83}$$

and

$$\tilde{\alpha}_t(x,t) = -\epsilon_1(x)\tilde{\alpha}_x(x,t) - Ce^{A\phi(x)}L\tilde{\alpha}(1,t), \tag{5.84}$$

$$\tilde{\alpha}(0,t) = q\tilde{\beta}(0,t) + C\tilde{X}, \tag{5.85}$$

$$\dot{\tilde{X}} = A\tilde{X} - e^{A\phi(0)}L\tilde{\alpha}(1,t), \tag{5.86}$$

where the former affects the latter only through the boundary condition (5.85). It is clear from (5.82)–(5.83) that $\tilde{\beta}(x,t)$ converges to 0 in finite time, so it suffices to consider stability of the origin of

$$\tilde{\alpha}_t(x,t) = -\epsilon_1(x)\tilde{\alpha}_x(x,t) - Ce^{A\phi(x)}L\tilde{\alpha}(1,t), \tag{5.87}$$

$$\tilde{\alpha}(0,t) = C\tilde{X}, \tag{5.88}$$

$$\dot{\tilde{X}} = A\tilde{X} - e^{A\phi(0)}L\tilde{\alpha}(1,t). \tag{5.89}$$

Based on Krstić and Smyshlyaev (2008a), we obtain the following result (see Aamo (2012) for proof).

Table 5.1: Values of parameters used in the simulation.

Parameter	Value	Unit
ρ	$1.250{\cdot}10^3$	$\mathrm{kg/m^3}$
l	$2.000{\cdot}10^3$	m
F	$1.500{\cdot}10^2$	$\mathrm{kg/sm^3}$
A_a	$2.530{\cdot}10^{-2}$	$\mathrm{m^2}$
β	$2.000{\cdot}10^{-9}$	Pa

Lemma 5.2. *Let L be chosen such that $A-LC$ is Hurwitz. The origin of (5.87)–(5.89) is exponentially stable in the norm*

$$\left(\left|\tilde{X}\left(t\right)\right|^2+\int_0^1\tilde{\alpha}^2\left(x,t\right)dx\right)^{1/2}. \tag{5.90}$$

The following theorem summarizes the observer design.

Theorem 5.3. *Consider the observer (5.53)–(5.57) with initial conditions $\hat{u}_0$ and $\hat{v}_0$, with output injection kernels given by (5.75)–(5.76), where P^{uu} and P^{vu} are found from (5.67)–(5.74), and where L is chosen such that $A-LC$ is Hurwitz. Under the assumptions*

$$\epsilon_1,\epsilon_2\in\mathcal{C}^1([0,1]),\ c_1,c_2\in\mathcal{C}([0,1]),\ u_0,\ v_0\in\mathcal{L}^2([0,1]), \tag{5.91}$$

and $\epsilon_1(x),\epsilon_2(x)>0$, it is guaranteed that $\hat{X}$, $\hat{u}$, $\hat{v}$ exponentially converge to X, u, v, i.e., more specifically, that the observer error system is exponentially stable in the sense of the norm (5.90).

Proof. This follows from Lemma 5.1 and Lemma 5.2 and the fact that the transformation (5.65)–(5.66) is invertible. □

5.4 Simulations

We demonstrate the use of the observer with simulations of the model of the well hydraulics. The well is vertical and 2000 m deep, and the flow rate from the rig pump is 1000 lpm. At 100 seconds a loss of 20 lpm occurs, i.e. X is changed from 0 to -20 lpm. We consider the particularly simple case when there is no dynamics associated with X, i.e., $A=0$ and $C=1$. We choose $L=5$. The well parameters are listed in Table 5.1. In Figure 5.2 we see that the loss rate is accurately estimated 10 seconds after the loss has occurred. The initial discrepancy is due to the observer being initialized with values different from the plant. Figure 5.3 and Figure 5.4 illustrate that the observer converges to the value of the plant throughout the well. Note that the plotted errors are in the transformed coordinates. However, the invertibility of the transformation ensures that the system also converges in

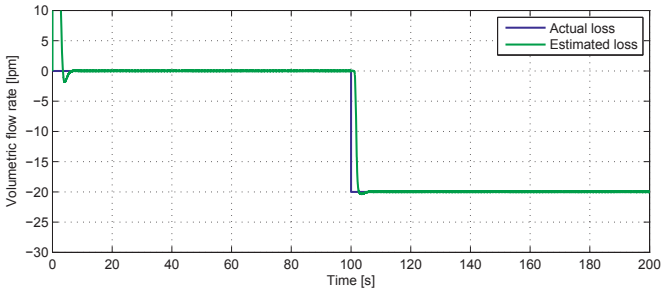

Figure 5.2: The actual and estimated loss rate.

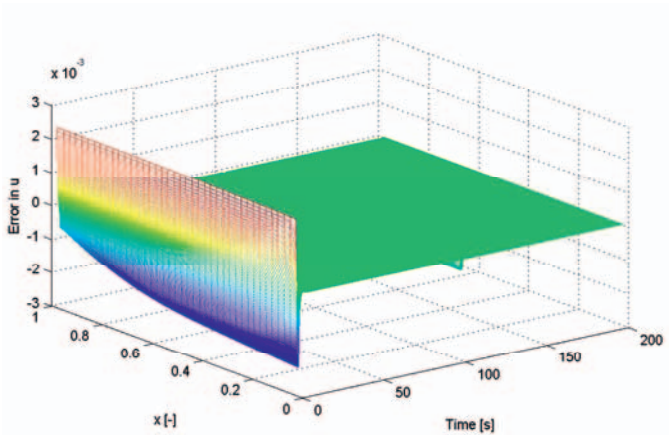

Figure 5.3: The error $\tilde{u}(x,t)$.

its original coordinates. The output injection gains $p_1(x)$ and $p_2(x)$ are shown in Figure 5.5. The flow rates and pressures at the inlet and outlet of the plant and observer are plotted in Figure 5.6 through Figure 5.9. The slight oscillations seen at the observer boundaries in these figures are due to the numerical scheme. The results can be improved by refining the spatial discretization grid.

5.5 Conclusions

The main result in this paper is the application of a PDE observer for a hydraulic system of an MPD rig. The hydraulics can be expressed as a 2×2 linear hyperbolic system of PDEs coupled with an ODE at the inlet boundary. By using the method of backstepping, we are able to design an observer which is exponentially stable at the origin in the $\mathcal{L}^2$-norm. A simulation of the mud circulation system at a drilling rig is used to demonstrate an application of the observer.

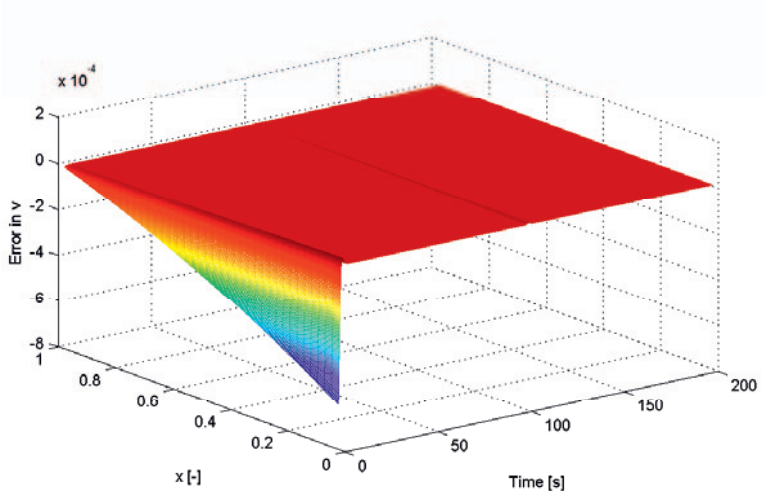

Figure 5.4: The error $\tilde{v}(x,t)$.

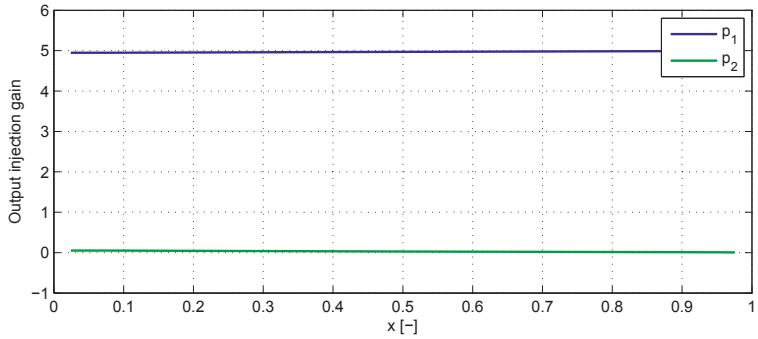

Figure 5.5: The output injection terms $p_1(x)$ and $p_2(x)$.

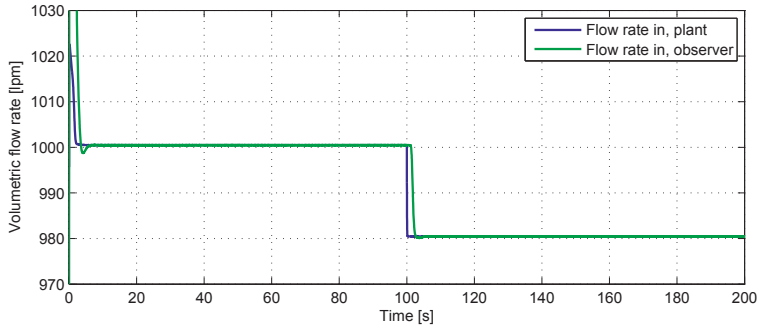

Figure 5.6: The flow rate at the inlet.

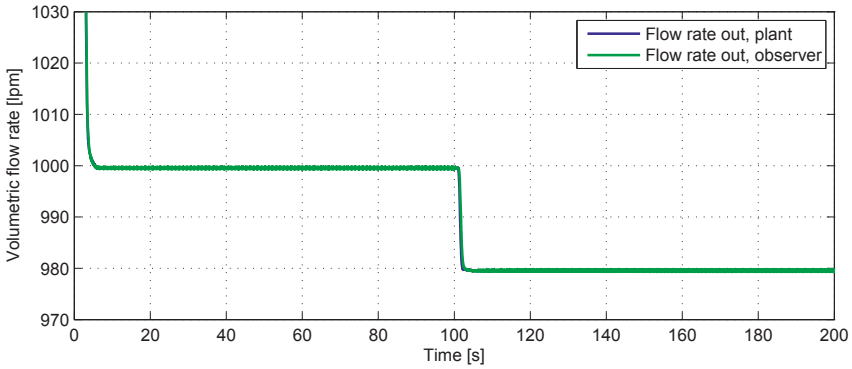

Figure 5.7: The flow rate at the outlet.

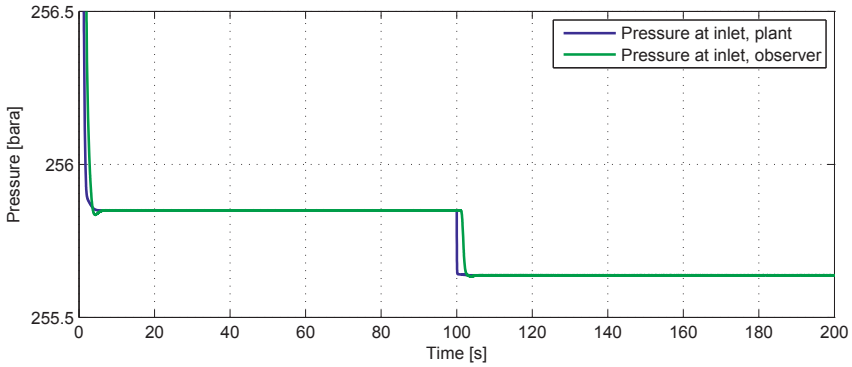

Figure 5.8: The pressure at the inlet.

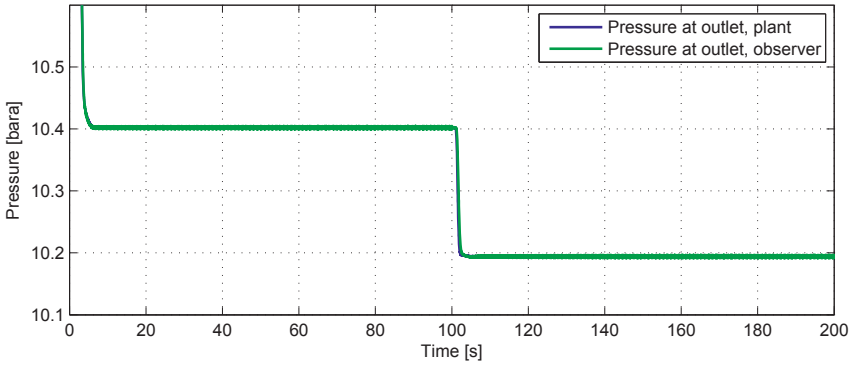

Figure 5.9: The pressure at the outlet.

5.6 Further work

When an in-/outflux occurs, it is of interest to attenuate it by automatic control. Towards that end, it would be beneficial to model the in-/out-flux as a pressure dependent disturbance by defining

$$\dot{X} = AX + Bw, \tag{5.92}$$

$$q_{\mathrm{i}}(t) = CX + Dw, \tag{5.93}$$

$$w(t) = u(0,t) + sv(0,t). \tag{5.94}$$

Extending the results in Aamo (2012) to incorporate disturbances of the form (5.92)–(5.94), and developing a controller for the attenuation of undesired in-/outfluxes, would be valuable contributions.

Part III

In-/out-flux prevention

Chapter 6

Tracking of choke pressure during managed pressure drilling

Summary

Two types of tracking controllers are designed for a hydraulic model of a managed pressure drilling system. Both controllers are designed using backstepping. The first controller is based on a simplified model of the drilling process and considers the disturbance as measured. For the second controller, we regard the disturbance as unmeasured and slowly varying. This allows us to introduce its estimate and design an adaptive controller. The first controller gives exponential stability and tunable convergence rate, while the latter gives asymptotic stability. The performance of the tracking controllers is compared.

6.1 Introduction

The narrow pressure margins at bottomhole when drilling through deeper and more difficult reservoirs, calls for accurate control of the pressure in the well. The current standard for drilling under such conditions is managed pressure drilling (MPD). When drilling with MPD, the annulus is sealed with a rotary control device so that the annulus can be pressurized by using the control choke, the rig pump and a back-pressure pump. The schematic of an MPD rig is presented in Figure 6.1. A thorough description of the model used in this paper, as well as an introduction to MPD, can be found in Kaasa et al. (2011). In the aforementioned reference, the model is used to design an adaptive observer which is applied to field data for verification. The model has served as a fundament for many applications, such as in Stamnes et al. (2008) where the authors design a reduced order observer which adapts to unknown friction and density, and estimates the bottomhole pressure. Another adaptive observer is designed in Stamnes et al. (2011) where multiple delayed observers enhance the convergence rate of the parameters. In Godhavn et al. (2011) the model is used in designing a tracking controller manipulating the choke opening. The reference signal for the choke pressure is based on an estimate of bottomhole pressure. The controller has been thoroughly tested on a drilling

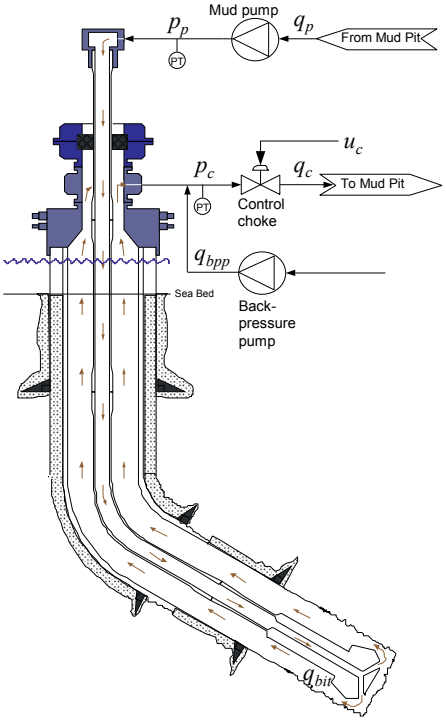

Figure 6.1: Schematic of a managed pressured drilling system.

rig. The paper does not consider actuator dynamics. The model is also applied to gas kick detection and mitigation in Zhou et al. (2011), where the concept of switched control of the bottomhole pressure is presented. An MPD system is considered where a controller manipulating the choke and back-pressure pump switches between a combination of pressure and flow control when there is no in-flux and pure flow control when a kick is detected.

Our objective is to design a tracking controller for the pressure upstream the choke. The controller governs the opening of the choke which has first order dynamics. Due to this choke dynamics, we apply backstepping to find a suitable control law. Two cases are considered: one with a simplified model of the hydraulics, and one with the full model. For the simplified model we consider the disturbance as known and use regular backstepping. While for the full model the disturbance is unknown and we have to use adaptive backstepping.

The structure of the paper is as follows. The model for the hydraulics of the MPD system is presented in Section 6.2, and the two tracking controllers are presented in Sections 6.3 and 6.4. Simulation results for both methods are presented and compared in Section 6.5. Conclusions are given in Section 6.6.

6.2 Mathematical Model

Consider the model of the hydraulic system at a drilling rig equipped for MPD.

$$\dot{p}_{\mathrm{p}} = \frac{\beta_{\mathrm{d}}}{V_{\mathrm{d}}}(q_{\mathrm{p}} - q_{\mathrm{bit}}), \tag{6.1a}$$

$$\dot{p}_{\mathrm{c}} = \frac{\beta_{\mathrm{a}}}{V_{\mathrm{a}}}(q_{\mathrm{bit}} - q_{\mathrm{c}} + q_{\mathrm{bpp}}), \tag{6.1b}$$

$$\begin{aligned}\dot{q}_{\mathrm{bit}} = &\frac{1}{M_{\mathrm{d}} + M_{\mathrm{a}}}[p_{\mathrm{p}} - p_{\mathrm{c}} - F_{\mathrm{d}}|q_{\mathrm{bit}}|q_{\mathrm{bit}} - F_{\mathrm{a}}q_{\mathrm{bit}} \\ &+ (\rho_{\mathrm{d}} - \rho_{\mathrm{a}})gh_{\mathrm{bit}}],\end{aligned} \tag{6.1c}$$

$$\dot{z}_{\mathrm{c}} = -\frac{z_{\mathrm{c}}}{\tau_{\mathrm{c}}} + \frac{u_{\mathrm{c}}}{\tau_{\mathrm{c}}}, \tag{6.1d}$$

$$q_{\mathrm{c}} = g(p_{\mathrm{c}})z_{\mathrm{c}}. \tag{6.1e}$$

The model of the hydraulic system consists of two mass balances which give the dynamics of the pump pressure, p_{p}, and the choke pressure, p_{c}, respectively. The mass balances describe two separate control volumes; the drillpipe and the annulus. β denotes the bulk modulus and V the volume, while the subscripts a and d denote annulus and drillstring. q_{p} is the main pump volumetric flow rate, q_{bpp} is the back-pressure pump volumetric flow rate and q_{c} is the volumetric flow rate through the choke. A combined momentum equation for drillstring and annulus gives the dynamics of the volumetric flow rate through the bit, q_{bit}. M_{d} and M_{a} are mass-like constants, F_{d} and F_{a} are friction factors, ρ_{d} and ρ_{a} are densities, g is the gravitational constant and h_{bit} is the vertical depth of the well. z_{c} is the choke opening and $g(p_{\mathrm{c}})$ is a function of the choke pressure that characterizes the choke. The dynamics of the choke opening is governed by (6.1d) where τ_{c} is the time constant of the valve. The available inputs are u_{c}, q_{p} and q_{bpp}. The outputs are p_{p}, p_{c}, q_{c} and z_{c}. The following general assumption is made regarding the hydraulic system.

Assumption 3. $g(p_{\mathrm{c}})$ is continuously differentiable, $g(p_{\mathrm{c}}) \geq \delta > 0 \, \forall p_{\mathrm{c}}$, and $g'(p_{\mathrm{c}})$ is locally Lipschitz. The pressure reference, $p_{\mathrm{c,ref}}(t)$; the flow rate from the main pump, $q_{\mathrm{p}}(t)$; the flow rate from the back-pressure pump, $q_{\mathrm{bpp}}(t)$; and their time-derivatives, $\dot{p}_{\mathrm{c,ref}}(t)$, $\ddot{p}_{\mathrm{c,ref}}(t)$, $\dot{q}_{\mathrm{p}}$, $\dot{q}_{\mathrm{bpp}}$, are continuous and bounded functions of t.

6.3 Tracking with measured disturbance

The flow rate through the bit can be considered as a disturbance. In this section, we assume that the flow rate through the bit is equal to the flow rate from the main pump, so that we can consider it as a measured disturbance. The resulting model of the choke pressure is

$$\dot{p}_{\mathrm{c}} = \frac{\beta_{\mathrm{a}}}{V_{\mathrm{a}}}(q_{\mathrm{p}} - q_{\mathrm{c}} + q_{\mathrm{bpp}}). \tag{6.2}$$

The dynamics for the choke opening is given by (6.1d), and the flow rate through the choke by (6.1e). We now use this model to design a tracking controller for the

pressure upstream the choke, p_c, which manipulates the choke opening z_c through u_c. The desired choke pressure is given by $p_{c,ref}$ which is time-varying. $\dot{p}_{c,ref}$, $\ddot{p}_{c,ref}$ and $\dot{q}_{bpp}$ are assumed available. q_p is considered a known disturbance with known time-derivative $\dot{q}_p$.

Following a standard backstepping procedure, we define the error $z_1 = p_c - p_{c,ref}$ and write its time-derivative as

$$\dot{z}_1 = \frac{\beta_a}{V_a}\left(q_p - g(p_c)z_c + q_{bpp}\right) - \dot{p}_{c,ref} \tag{6.3}$$

by inserting (6.2). Adding and subtracting $\alpha\frac{\beta_a}{V_a}g(p_c)$ in (6.3), where α is the so-called virtual control, gives

$$\dot{z}_1 = \frac{\beta_a}{V_a}q_p - \dot{p}_{c,ref} - \frac{\beta_a}{V_a}g(p_c)\alpha + \frac{\beta_a}{V_a}q_{bpp} - \frac{\beta_a}{V_a}g(p_c)(z_c - \alpha). \tag{6.4}$$

We now choose α such that (6.4) with $z_c - \alpha = 0$ is stabilized, which results in

$$\alpha = \frac{1}{g(p_c)}(q_p + q_{bpp} - \frac{V_a}{\beta_a}\dot{p}_{c,ref} + \frac{V_a}{\beta_a}k_1 z_1), \tag{6.5}$$

where $k_1 > 0$ is a design constant. By inserting (6.5) into (6.4) we find that

$$\dot{z}_1 = -k_1 z_1 - \frac{\beta_a}{V_a}g(p_c)(z_c - \alpha), \tag{6.6}$$

and the time-derivative of the Lyapunov function

$$V_1(z_1) = \tfrac{1}{2}z_1^2, \tag{6.7}$$

is

$$\dot{V}_1 = -k_1 z_1^2 - z_2\frac{\beta_a}{V_a}g(p_c)z_1, \tag{6.8}$$

where we have defined $z_2 = z_c - \alpha$. Having backstepped through the integrator, we can design the control law from the composite Lyapunov function

$$V_2(z_1,\, z_2) = V_1(z_1) + \tfrac{1}{2}z_2^2. \tag{6.9}$$

The time-derivative of V_2 is

$$\dot{V}_2 = -k_1 z_1^2 + z_2\big(-\frac{z_c}{\tau_c} + \frac{u_c}{\tau_c} - \dot{\alpha} - \frac{\beta_a}{V_a}g(p_c)z_1\big). \tag{6.10}$$

Selecting the control law

$$\frac{u_c}{\tau_c} = \frac{z_c}{\tau_c} + \dot{\alpha} - k_2 z_2 + \frac{\beta_a}{V_a}g(p_c)z_1, \tag{6.11}$$

where k_2 is a positive design constant, and substituting into (6.10), we get

$$\dot{V}_2 = -k_1 z_1^2 - k_2 z_2^2 \leq 0. \tag{6.12}$$

This gives us uniform local exponential stability of the origin of the error coordinates according to Theorem 4.10 in Khalil (2002). We also get tunable convergence rate since the constants k_1 and k_2 do not appear in V_2. This means that we can increase the tuning constants to improve the performance of the tracking controller. However, in practice the unmodeled dynamics will constrain the values of these constants.

The control law can be summarized as

$$\begin{aligned} u_{\mathrm{c}} = {} & z_{\mathrm{c}} - k_2\tau_{\mathrm{c}}z_2 + z_1\frac{\beta_{\mathrm{a}}\tau_{\mathrm{c}}}{V_{\mathrm{a}}}g(p_{\mathrm{c}}) \\ & - \tau_{\mathrm{c}}\left(\frac{g'(p_{\mathrm{c}})\beta_{\mathrm{a}}}{g^2(p_{\mathrm{c}})V_{\mathrm{a}}}(q_{\mathrm{p}} - g(p_{\mathrm{c}})z_{\mathrm{c}} + q_{\mathrm{bpp}})\right)\left(q_{\mathrm{p}} + q_{\mathrm{bpp}} - \frac{V_{\mathrm{a}}}{\beta_{\mathrm{a}}}\dot{p}_{\mathrm{c,ref}} + \frac{V_{\mathrm{a}}}{\beta_{\mathrm{a}}}k_1z_1\right) \\ & + \frac{\tau_{\mathrm{c}}}{g(p_{\mathrm{c}})}\left(\dot{q}_{\mathrm{p}} + \dot{q}_{\mathrm{bpp}} - \frac{V_{\mathrm{a}}}{\beta_{\mathrm{a}}}\ddot{p}_{\mathrm{c,ref}} + k_1\tau_{\mathrm{c}}\big(q_{\mathrm{p}} - g(p_{\mathrm{c}})z_{\mathrm{c}} + q_{\mathrm{bpp}} - \frac{V_{\mathrm{a}}}{\beta_{\mathrm{a}}}\dot{p}_{\mathrm{c,ref}}\big)\right). \end{aligned} \tag{6.13}$$

6.4 Tracking with unmeasured disturbance

In this section we design a tracking controller for the choke pressure based on (6.1b), but as opposed to the previous section, we distinguish between q_{p} and q_{bit}. Thus, we consider q_{bit} as a constant disturbance which cannot be measured. The resulting controller governing the choke opening is an adaptive controller where q_{bit} is estimated by the parameter estimate ξ. As before, the signals $\dot{p}_{\mathrm{c,ref}}$, $\ddot{p}_{\mathrm{c,ref}}$ and $\dot{q}_{\mathrm{bpp}}$ are considered known.

Proceeding as in the previous section, we start by defining $z_1 = p_{\mathrm{c}} - p_{\mathrm{c,ref}}$ and write its time-derivative as

$$\dot{z}_1 = \frac{\beta_{\mathrm{a}}}{V_{\mathrm{a}}}\left(q_{\mathrm{bit}} - g(p_{\mathrm{c}})z_{\mathrm{c}} + q_{\mathrm{bpp}}\right) - \dot{p}_{\mathrm{c,ref}}, \tag{6.14}$$

using (6.1b). Next, we add and subtract the so-called virtual control term $\frac{\beta_{\mathrm{a}}}{V_{\mathrm{a}}}g(p_{\mathrm{c}})\alpha$ to obtain

$$\dot{z}_1 = \frac{\beta_{\mathrm{a}}}{V_{\mathrm{a}}}\big(q_{\mathrm{bit}} + q_{\mathrm{bpp}}\big) - \dot{p}_{\mathrm{c,ref}} - \frac{\beta_{\mathrm{a}}}{V_{\mathrm{a}}}g(p_{\mathrm{c}})\alpha - \frac{\beta_{\mathrm{a}}}{V_{\mathrm{a}}}g(p_{\mathrm{c}})(z_{\mathrm{c}} - \alpha). \tag{6.15}$$

Defining a second error coordinate, $z_2 = z_{\mathrm{c}} - \alpha$, we want to choose α such that it stabilizes (6.15) with $z_2 = 0$. We cannot use (6.5) with q_{p} replaced by q_{bit}, since q_{bit} is not measured. Instead we introduce the estimate ξ for q_{bit} and get

$$\alpha = \frac{1}{g(p_{\mathrm{c}})}\left(\xi + q_{\mathrm{bpp}} - \frac{V_{\mathrm{a}}}{\beta_{\mathrm{a}}}p_{\mathrm{c,ref}} + \frac{V_{\mathrm{a}}}{\beta_{\mathrm{a}}}k_{\mathrm{p}}z_1\right) \tag{6.16}$$

where $k_{\mathrm{p}} > 0$. By substituting (6.16) into (6.15) we get

$$\dot{z}_1 = \frac{\beta_{\mathrm{a}}}{V_{\mathrm{a}}}(q_{\mathrm{bit}} - \xi) - k_{\mathrm{p}}z_1 - \frac{\beta_{\mathrm{a}}}{V_{\mathrm{a}}}g(p_{\mathrm{c}})z_2. \tag{6.17}$$

We now define the Lyapunov function

$$V_3(z_1,\, z_2,\, \tilde{\theta}) = \frac{1}{2}z_1^2 + \frac{1}{2}z_2^2 + \frac{1}{2k_{\mathrm{i}}}\tilde{\theta}^2 \tag{6.18}$$

with the parameter error $\tilde{\theta} = q_{\text{bit}} - \xi$. The time-derivative of (6.18) is

$$\dot{V}_3 = -k_{\text{p}} z_1^2 + \tilde{\theta}\frac{\beta_{\text{a}}}{V_{\text{a}}} z_1 - z_2 \frac{\beta_{\text{a}}}{V_{\text{a}}} g(p_{\text{c}}) z_1 + z_2 \dot{z}_2 + \frac{1}{k_{\text{i}}}\tilde{\theta}\dot{\tilde{\theta}} \tag{6.19}$$

where we have inserted (6.17). Inserting

$$\dot{z}_2 = -\frac{z_{\text{c}}}{\tau_{\text{c}}} + \frac{u_{\text{c}}}{\tau_{\text{c}}} - \dot{\alpha} \tag{6.20}$$

and rearranging yields

$$\dot{V}_3 = -k_{\text{p}} z_1^2 + \tilde{\theta}\Big[\frac{\beta_{\text{a}}}{V_{\text{a}}} z_1 + \frac{1}{k_{\text{i}}}\dot{\tilde{\theta}}\Big] - z_2 \frac{\beta_{\text{a}}}{V_{\text{a}}} g(p_{\text{c}}) z_1 + z_2\big(-\frac{z_{\text{c}}}{\tau_{\text{c}}} + \frac{u_{\text{c}}}{\tau_{\text{c}}} - \dot{\alpha}\big) \tag{6.21}$$

where

$$\dot{\alpha} = \frac{1}{g(p_{\text{c}})}\Big[\dot{\xi} + \dot{q}_{\text{bpp}} - \frac{V_{\text{a}}}{\beta_{\text{a}}}\ddot{p}_{\text{c,ref}} + \frac{V_{\text{a}}}{\beta_{\text{a}}} k_{\text{p}}\Big(\frac{\beta_{\text{a}}}{V_{\text{a}}}(q_{\text{bit}} - q_{\text{c}} + q_{\text{bpp}}) - \dot{p}_{\text{c,ref}}\Big)\Big] \\ - \frac{g'(p_{\text{c}})}{g^2(p_{\text{c}})}\Big[\frac{\beta_{\text{a}}}{V_{\text{a}}}(q_{\text{bit}} - q_{\text{c}} + q_{\text{bpp}})\Big]. \tag{6.22}$$

Inserting $q_{\text{bit}} = \tilde{\theta} + \xi$ gives

$$\dot{\alpha} = \frac{1}{g(p_{\text{c}})}\Big[\dot{\xi} + \dot{q}_{\text{bpp}} - \frac{V_{\text{a}}}{\beta_{\text{a}}}\ddot{p}_{\text{c,ref}} + k_{\text{p}}\Big(\tilde{\theta} + \xi - q_{\text{c}} + q_{\text{bpp}} - \frac{V_{\text{a}}}{\beta_{\text{a}}}\dot{p}_{\text{c,ref}}\Big)\Big] \\ - \frac{g'(p_{\text{c}})}{g^2(p_{\text{c}})}\Big[\frac{\beta_{\text{a}}}{V_{\text{a}}}(\tilde{\theta} + \xi - q_{\text{c}} + q_{\text{bpp}})\Big]. \tag{6.23}$$

Inserting (6.23) into (6.21) and rearranging result in

$$\dot{V}_3 = -k_{\text{p}} z_1^2 + \tilde{\theta}\Big[\frac{\beta_{\text{a}}}{V_{\text{a}}} z_1 + \frac{1}{k_{\text{i}}}\dot{\tilde{\theta}} - z_2\Big(\frac{k_{\text{p}}}{g(p_{\text{c}})} - \frac{g'(p_{\text{c}})\beta_{\text{a}}}{g^2(p_{\text{c}})V_{\text{a}}}\Big)\Big] \\ - z_2\Big[\frac{\beta_{\text{a}}}{V_{\text{a}}} g(p_{\text{c}}) z_1 + \frac{z_{\text{c}}}{\tau_{\text{c}}} - \frac{u_{\text{c}}}{\tau_{\text{c}}} + \frac{1}{g(p_{\text{c}})}\Big(\dot{\xi} + \dot{q}_{\text{bpp}} - \frac{V_{\text{a}}}{\beta_{\text{a}}}\ddot{p}_{\text{c,ref}} + k_{\text{p}}\big(\xi - q_{\text{c}} + q_{\text{bpp}} - \frac{V_{\text{a}}}{\beta_{\text{a}}}\dot{p}_{\text{c,ref}}\big)\Big) \\ - \frac{g'(p_{\text{c}})\beta_{\text{a}}}{g^2(p_{\text{c}})V_{\text{a}}}(\xi - q_{\text{c}} + q_{\text{bpp}})\Big]. \tag{6.24}$$

We now select

$$\dot{\tilde{\theta}} = -\dot{\xi} = -k_{\text{i}}\Big[\frac{\beta_{\text{a}}}{V_{\text{a}}} z_1 - \Big(\frac{k_{\text{p}}}{g(p_{\text{c}})} - \frac{g'(p_{\text{c}})\beta_{\text{a}}}{g^2(p_{\text{c}})V_{\text{a}}}\Big) z_2\Big] \tag{6.25}$$

and

$$u_{\text{c}} = z_{\text{c}} - k_3\tau_{\text{c}} z_2 + \tau_{\text{c}}\frac{\beta_{\text{a}}}{V_{\text{a}}} g(p_{\text{c}}) z_1 + \frac{\tau_{\text{c}}}{g(p_{\text{c}})}\Big[k_{\text{i}}\frac{\beta_{\text{a}}}{V_{\text{a}}} z_1 - \Big(\frac{k_{\text{i}}k_{\text{p}}}{g(p_{\text{c}})} - \frac{k_{\text{i}}g'(p_{\text{c}})\beta_{\text{a}}}{g^2(p_{\text{c}})V_{\text{a}}}\Big) z_2 + \dot{q}_{\text{bpp}} \\ - \frac{V_{\text{a}}}{\beta_{\text{a}}}\ddot{p}_{\text{c,ref}} + k_{\text{p}}(\xi - g(p_{\text{c}})z_{\text{c}} + q_{\text{bpp}} - \frac{V_{\text{a}}}{\beta_{\text{a}}}\dot{p}_{\text{c,ref}})\Big] \\ - \tau_{\text{c}}\frac{g'(p_{\text{c}})\beta_{\text{a}}}{g^2(p_{\text{c}})V_{\text{a}}}(\xi - g(p_{\text{c}})z_{\text{c}} + q_{\text{bpp}}). \tag{6.26}$$

Inserting (6.25) and (6.26) into (6.24) gives

$$\dot{V}_3 = -k_\mathrm{p} z_1^2 - k_3 z_2^2 \leq 0. \tag{6.27}$$

The choice of $\dot{\xi}$ and u_c renders $\dot{V}_3$ negative semidefinite. We invoke Theorem 1 from Appendix 6.A to prove uniform asymptotic stability of the origin of (6.15), (6.20) and (6.25) in closed loop with (6.26). Consider the auxiliary function

$$W = z_1 \tilde{\theta} \tag{6.28}$$

with the time-derivative

$$\dot{W} = -k_\mathrm{i}\Big[\frac{\beta_\mathrm{a}}{V_\mathrm{a}} z_1^2 - \Big(\frac{k_\mathrm{p}}{g(p_\mathrm{c})} - \frac{g'(p_\mathrm{c})\beta_\mathrm{a}}{g^2(p_\mathrm{c})V_\mathrm{a}}\Big) z_1 z_2\Big] + \frac{\beta_\mathrm{a}}{V_\mathrm{a}}\tilde{\theta}^2 - k_\mathrm{p} z_1 \tilde{\theta} - \frac{\beta_\mathrm{a}}{V_\mathrm{a}} g(p_\mathrm{c}) z_2 \tilde{\theta}. \tag{6.29}$$

The assumptions of Theorem 1 are verified as follows.

1. Select $a = \min(\frac{1}{2}, \frac{1}{2k_\mathrm{i}})\|x\|$ and $b = \max(\frac{1}{2}, \frac{1}{2k_\mathrm{i}})\|x\|$.
2. $V^*(x) = \dot{V}_3 = -k_\mathrm{p} z_1^2 - k_3 z_2^2$, and the set $E \triangleq \{z_1 = z_2 = 0\}$.
3. Boundedness of $|W|$ follows from the boundedness of z_1, z_2 and $\tilde{\theta}$ which is inferred from (6.18) and (6.27).
4. a) Assured through Assumption 3.
   b) Fulfilled with the choice $k(\|x\|) = \frac{\beta_\mathrm{a}}{V_\mathrm{a}}(|z_1|^2 + |z_2|^2 + |\tilde{\theta}|^2)$ since $|\dot{W}| = \frac{\beta_\mathrm{a}}{V_\mathrm{a}}\tilde{\theta}^2 \; \forall x \in E$.
5. Satisfied since z_1, z_2 and $\tilde{\theta}$ are bounded and since the exogenous signals are bounded (Assumption 3).

6.5 Simulation results

We simulate drilling of a well specified in Table 6.1 with the choke flow rate given by (6.1e) with

$$g(p_\mathrm{c}) = k_\mathrm{c}\mathrm{sign}(p_\mathrm{c} - p_0)\sqrt{|p_\mathrm{c} - p_0|}, \tag{6.30}$$

where k_c is a lumped constant reflecting the valve characteristic, and p_0 the pressure downstream the choke. In this manner, we have assumed a linear valve characteristic. The form of (6.30) results in an equation for the flow rate through the choke similar to the valve equation given in Merritt (1967). We assume that the initial conditions, flow rate from the pumps, and reference signal are such that the flow rate through the choke does not saturate.

The goal of MPD is to control the pressure at a certain depth in the well, typically at the bottom. This pressure can be expressed as

$$p_\mathrm{bit} = p_\mathrm{c} + \rho_\mathrm{a} g h_\mathrm{bit} + F_\mathrm{a} q_\mathrm{bit}. \tag{6.31}$$

We simulate a so-called flow sweep where the flow rate from the main pump is ramped up from 100 lpm to 2000 lpm and back down to 100 lpm again. The flow sweep is carried out about ten times faster than usual to highlight the performance

Parameter	Value	Unit
h_{bit}	1000	m
V_{a}	11800	m^3
V_{d}	4600	m^3
β_{a}	$2.00 \cdot 10^9$	Pa
β_{d}	$2.00 \cdot 10^9$	Pa
$M_{\text{d}} + M_{\text{a}}$	$4.23 \cdot 10^{-2}$	kg/m^4
ρ_{a}	1400	kg/m^3
ρ_{d}	1400	kg/m^3
p_0	1.00	atm
g	9.81	m/s^2
F_{a}	$1.80 \cdot 10^{-3}$	$\text{kg/(sm}^2\text{)}$
F_{d}	1.80	kg/m^5
k_{c}	$4.54 \cdot 10^{-5}$	$\text{m}^2\sqrt{\text{m}^3/\text{kg}}$
τ_{c}	1.00	s

Table 6.1: Parameters for the hydraulic system.

Parameter	Value	Unit
k_1	$5.00 \cdot 10^1$	-
k_2	$1.00 \cdot 10^3$	-

Table 6.2: Tuning constants for the simulation with measured disturbance.

of the controllers. During this operation the choke opening is manipulated to keep p_{bit} constant. The pressure reference trajectory for the choke is computed solving (6.31) for p_{c} and using a previously recorded q_{bit} from a flow sweep. The same initial conditions and pressure reference are given for the simulations with and without measured disturbance. The flow rate from the back pressure pump is kept constant at 500 lpm. At five seconds, the controllers are turned on. Tuning parameters for the two controllers are presented in Table 6.2 and Table 6.3. Since we are simulating a faster flow sweep than usual, we have tuned the controllers to be fast. In practice slower tuning would suffice and give better robustness. Figure 6.2 shows the simulation results for the tracking controller with measured disturbance. The fluttering of the choke opening during the first seconds and after the change in pressure reference is due to the saturated input u_{c} from the choke controller. Figure 6.3 displays the volumetric flow rate from the main pump and through the bit when considering the disturbance as measured. Figure 6.4 through Figure 6.6 present simulation results for the tracking controller without measured disturbance. The choke pressure and choke opening are plotted in Figure 6.4. Figure 6.5 displays the volumetric flow rate from the main pump and through the bit. Figure 6.6 shows the error of the parameter estimate. In Figure 6.7, the resulting pressures at bottomhole produced by the two controllers are plotted.

Parameter	Value	Unit
k_p	$1.00 \cdot 10^{-1}$	-
k_3	$1.00 \cdot 10^{3}$	-
k_i	$1.00 \cdot 10^{-4}$	-

Table 6.3: Tuning constants for the simulation with unmeasured disturbance.

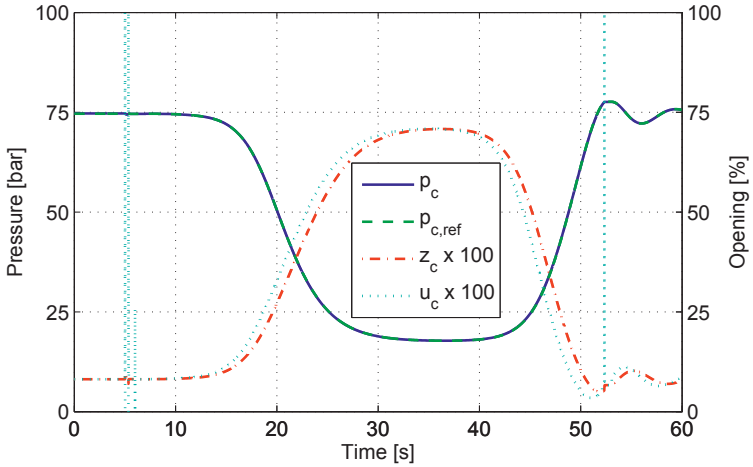

Figure 6.2: Tracking of a choke pressure reference in the case of measured disturbance. Reference pressure, choke pressure, choke opening and control input.

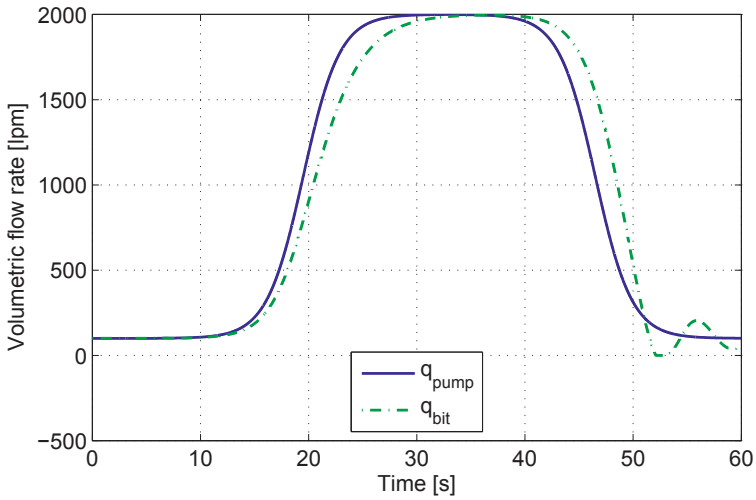

Figure 6.3: Tracking of a choke pressure reference in the case of measured disturbance. Volumetric flow rate from pump and through bit.

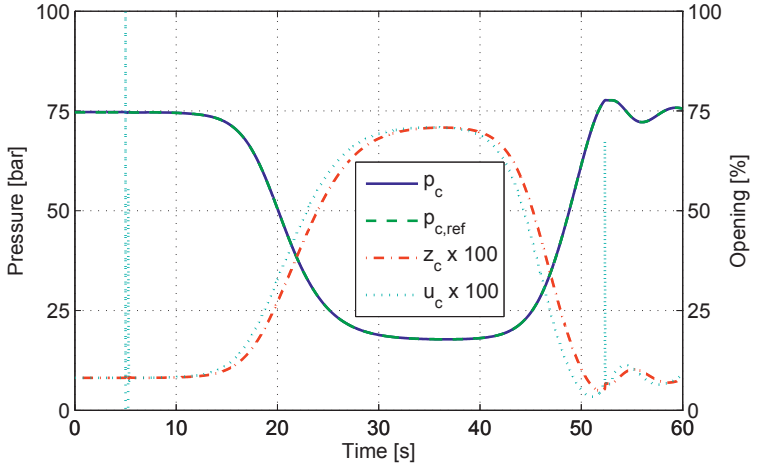

Figure 6.4: Controlling the choke pressure with unmeasured disturbance. Reference pressure, choke pressure, choke opening and control input.

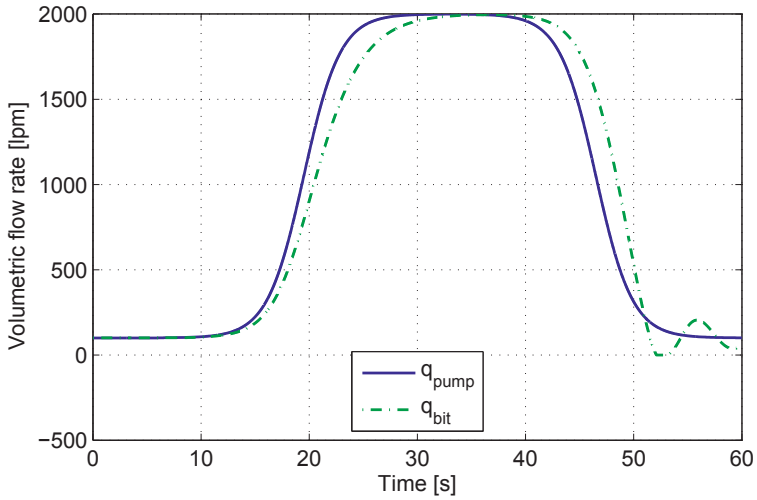

Figure 6.5: Controlling the choke pressure with unmeasured disturbance. Volumetric flow rate from pump and through bit.

6.6 Conclusions

The two controllers perform almost equally well comparing the tracking errors. The most notable difference is the response towards the end of the simulations, which can be attributed to both different tuning and design. The controller designed considering the disturbance as measured, is based on a simplified model of the hydraulics of the MPD process where the dynamics of the flow rate through

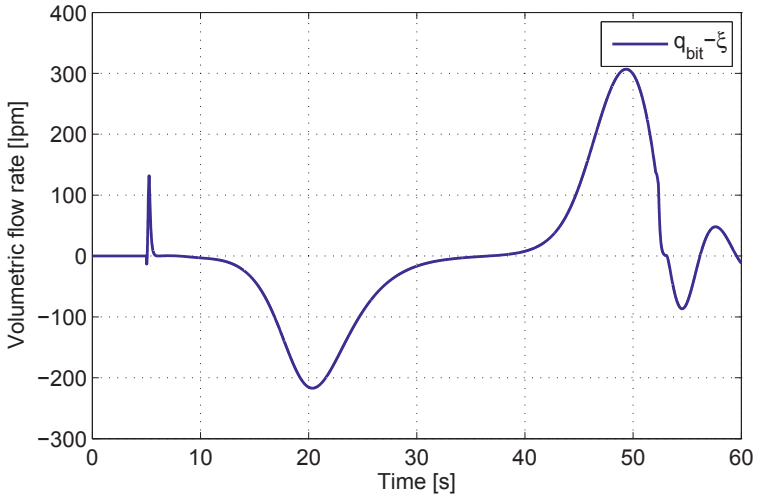

Figure 6.6: Controlling the choke pressure with unmeasured disturbance. Error in parameter estimate.

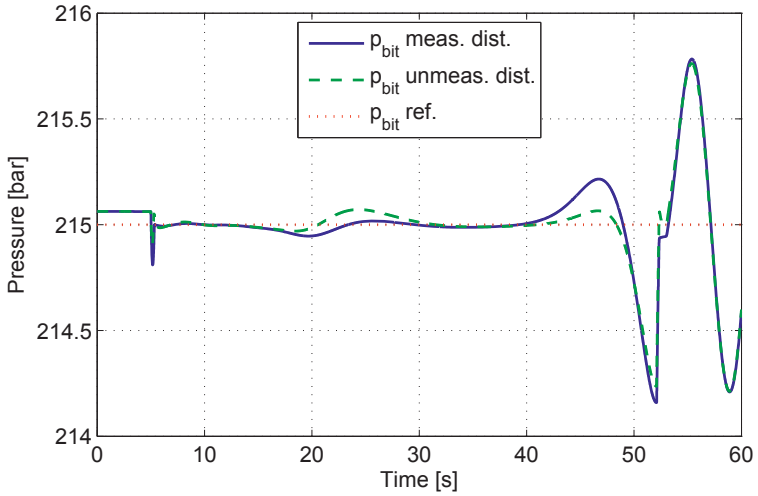

Figure 6.7: Pressure at bottomhole with and without measured disturbance.

the bit is neglected. Designing the controller for the case with unmeasured disturbance, we regard the flow rate through the bit as a slowly varying parameter and introduce its estimate. With this design we conclude uniform asymptotic stability. Considering complexity and performance, the first controller is the better. It also has the advantages of exponential stability and tunable convergence rate.

6.A Matrosov's Theorem

The following theorem can be found in Paden and Panja (1988). Consider the dynamics $\dot{x} = f(t, x)$ with an equilibrium point at 0 at time t_0.

Theorem 1 (Matrosov)**:** Let $\Omega \in \mathbb{R}^n$ be an open connected region in $\mathbb{R}^n$ containing the origin. If there exist two C^1 functions $V : [t_0, \infty) \times \Omega \to \mathbb{R}$, $W : [t_0, \infty) \times \Omega \to \mathbb{R}$; a C^0 function $V^* : \Omega \to \mathbb{R}$; three functions a, b, c of class $\mathcal{K}$ such that, for every $(t, x) \in [t_0, \infty) \times \Omega$,

1. $a(\|x\|) \leq V(t, x) \leq b(\|x\|)$
2. $\dot{V}(t, x) \leq V^*(x) \leq 0$. Define $E \triangleq \{x \in \Omega | V^*(x) = 0\}$.
3. $|W(t, x)|$ is bounded.
4. a) $\dot{W}(t, x)$ is continuous in both arguments and depends on time in the following way. $\dot{W}(t, x) = h(x, \gamma(t))$ where h is continuous in both of its arguments. $\gamma(t)$ is also continuous and its image lies in a bounded set K_1.(For simplicity, we simply say that $\dot{W}(t, x)$ *depends on time continuously through a bounded function.*)
   b) There exists a class K function, k, such that $|\dot{W}(t, x)| \geq k(\|x\|) \forall\, x \in E$ and $t \geq t_0$.
5. $\|f(t, x)\|$ is bounded.

Choosing $\delta > 0$ such that $\bar{B}_\delta \subset \Omega$, define for all $t \in [t_0, \infty)$

$$V^{-1}_{t_0, \delta} = x \in \Omega : V(t, x) \leq a(\delta)$$

Then

7. For all $x_0 \in V^{-1}_{t_0, \delta}$, $x(t)$ tends to zero uniformly in t_0, x_0 as t tends to infinity.
8. The origin is asymptotically stable.

Closing remarks

Chapter 7

Conclusions and further work

7.1 Conclusions

Drilling is dangerous and will continue to be so. The desire to drill into less accessible reservoirs in exposed areas under harsh conditions increases the consequences of possible failures. The best we can do to lessen the risk associated with drilling, is to reduce the probability of failure. Proper automatic control and contingency management are two contributions which will help lower this probability.

The thesis presents two models of percolating gas which facilitate state and parameter estimation. The first model is applicable to rigs with a sealed annulus, while the second model tailored for an evacuated riser. The latter also applies for conventional rigs. The gas is modeled as a triangular distribution which is meant to encapsulate a realistic distribution of the gas. Through simulations it is shown that states and parameters related to the distribution of the gas can be estimated with an UKF using distributed measurements from a WDP as the gas is percolating. Since it is of utmost importance to keep the pressure at the in-flux zone steady while circulating out a kick, there is little persistency of excitation to reveal unknown states and parameters. Using only topside measurements for the purpose of estimation, it is not possible to extract state and parameter information. Successful estimation of the gas distribution provides the driller with valuable information when circulating out the gas, such as position of the gas front.

Detection of an in-/out-flux is possible with both ODE and PDE models. The presented ODE model has the capability of representing the position of the in-/out-flux, which can be anywhere along the annular part of the wellbore, while the position is restricted to the inlet of the PDE model. Experiments with a small-scale rig of the hydraulics of an MPD system show that detection, quantification and localization is possible for losses with a magnitude which is greater than one percent of the total flow rate. A pure flow controller using estimated flow rates is shown to stabilize the reservoir dynamics and is tested through simulations.

If the pressure upstream the choke, and thus the downhole pressure, is controlled properly during drilling activities, the chance of an in-flux event is reduced. The pressure upstream the choke can be controlled using a tracking controller based on backstepping and a simplified version of the MPD hydraulics.

7.2 Further work

Valuable extensions of the presented model for percolating gas would be including wells with varying inclination and casing diameter. Expanding the model to work with oil-based mud where the gas is dissolved in the drilling fluid at high temperatures and pressures is also important. Drilling fluids are in general non-Newtonian, which affects the frictional pressure drop, among other. It is desirable to model the friction in the annulus to correctly estimate the pressure at a given location in the well. As the distribution of percolating gas is depending on the flow-rate, relating the slip velocity and liquid holdup would improve the model. More advanced PDE models of gas kicks already exist, such as two-fluid and drift-flux models. A useful contribution is using an existing model, possibly simplified, for observer design with wired drillpipe measurements.

If there is sufficient persistency of excitation when an in-/out-flux occurs, it would be useful to estimate parameters related to the surrounding formation, such as the productivity index. The proposed method for quantification and localization of an in-/out-flux should be tested with data from a larger rig such as either the flow-loop at the International Research Senter of Stavanger (IRIS) or the test rig Ullrig. Field data is also possible to use. The proposed control law for mitigation of an in-/out-flux can be tested on the small-scale rig at the University of Stavanger when a pressure gauge has been installed at the point of gas injection. Since the control law only manipulates the choke opening, which can saturate, coordinated control of the flow-rate from the pumps and choke is necessary.

Prevention of in-/out-flux through pressure control is necessary during a range of events when drilling. Examples are connections, running liner or casing, and tripping. Control of the pressure under such circumstances requires coordinated control using both choke and pumps, which is a task well suited for model predictive control.

It is possible to combine the in-/out-flux detection method with the gas kick model, such that estimated in-flux volume, and possibly position, are used as initial guesses when estimating the distribution of the percolating gas. This approach should be tested.

References

O. M. Aamo. Rejecting disturbances by output feedback in linear hyperbolic systems. In *Australian Control Conference 2012, Proceedings*, Sydney, Australia, November 15–16 2012.

O. M. Aamo, G. Eikrem, H. Siahaan, and B. Foss. Observer design for multiphase flow in vertical pipes with gas-lift – theory and experiments. *Journal of Process Control*, 15(3):247–257, 2005. ISSN 0959-1524. doi: 10.1016/j.jprocont.2004.07.002.

O. M. Aamo, J. Salvesen, and B. A. Foss. Observer design using boundary injections for pipeline monitoring and leak detection. In *International Symposium on Advanced Control of Chemical Processes, Proceedings*, Gramado, Brazil, April 2–5 2006.

B. Anfinsen and R. Rommetveit. Sensitivity of early kick detection parameters in full-scale gas kick experiments with oil- and water-based drilling muds. In *Drilling Conference, Proceedings*, pages 775–782, New Orleans, Louisiana, USA, 18–21 February 1992. doi: 10.2118/23934-MS.

D. R. Babu. Effect of P-ρ-T behavior of muds on loss/gain during high-temperature deep-well drilling. *Journal of Petroleum Science and Engineering*, 20(1–2):46–62, 1998. ISSN 0920-4105. doi: 10.1016/S0920-4105(98)00003-5.

G. Bastin and J.-M. Coron. Further results on boundary feedback stabilisation of 2×2 hyperbolic systems over a bounded interval. In *8th IFAC Symposium on Nonlinear Control Systems, Proceedings*, Bologna, Italy, September 1–3 2010.

N. Bedjaoui and E. Weyer. Algorithms for leak detection, estimation, isolation and localization in open water channels. *Control Engineering Practice*, 19(6):564–573, 2011. ISSN 0967-0661. doi: 10.1016/j.conengprac.2010.06.008.

N. Bedjaoui, E. Weyer, and G. Bastin. Methods for the localization of leak in open water channels. *Networks and Hetrogeneous Media*, 4(2):189–210, 2009. doi: 10.3934/nhm.2009.4.189.

L. Billmann and R. Isermann. Leak detection methods for pipelines. *Automatica*, 23(3):381–385, 1987. ISSN 0005-1098. doi: 10.1016/0005-1098(87)90011-2.

K. Bjørkevoll, A. Vollen, I. Barr Aas, and S. Hovland. Successful use of real time dynamic flow modelling to control a very challenging managed pressure drilling operation in the north sea. In *SPE/IADC Managed Pressure Drilling and Underbalanced Operations Conference and Exhibition, Proceedings*, Kuala Lumpur, Malaysia, February 24–25 2010. doi: 10.2118/130311-MS.

D. Brkic. Review of explicit approximations to the Colebrook relation for flow friction. *Journal of Petroleum Science and Engineering*, 77(1):34–48, 2011. ISSN 0920-4105. doi: 10.1016/j.petrol.2011.02.006.

N. Chen. An explicit equation for friction factor in pipe. *Industrial & Engineering Chemistry Fundamentals*, 18(3):296–297, 1979. ISSN 0196-4313.

J. Chirinos, J. Smith, and D. Bourgoyne. A simplified method to estimate peak casing pressure during mpd well control. In *SPE Annual Technical Conference and Exhibition, Proceedings*, Denver, Colorado, USA, October 30 – November 2 2011. doi: 10.2118/147496-MS.

J.-M. Coron, B. d'Andréa Novel, and G. Bastin. A strict Lyapunov function for boundary control of hyperbolic systems of conservation laws. *IEEE Transactions on Automatic Control*, 52(1):2–11, 2007. ISSN 0018-9286.

A. K. Das, J. R. Smith, and P. J. Frink. Simulations comparing different initial responses to kicks taken during managed pressure drilling. In *IADC/SPE Drilling Conference, Proceedings*, 2008. doi: 10.2118/112761-MS.

M. Davoudi, J. R. Smith, B. M. Patel, and J. E. Chirinos. Evaluation of alternative initial responses to kicks taken during managed pressure drilling. In *IADC/SPE Drilling Conference and Exhibition, Proceedings*, New Orleans, Lousiana, USA, February 2–4 2010. doi: 10.2118/128424-MS.

J. de Halleux, C. Prieur, J. M. Coron, B. d'Andréa Novel, and G. Bastin. Boundary feedback control in networks of open channels. *Automatica*, 39(8):1365–1376, 2003. ISSN 0005-1098. doi: 10.1016/S0005-1098(03)00109-2.

F. Di Meglio, G.-O. Kaasa, and N. Petit. A first principle model for multiphase slugging flow in vertical risers. In *48th IEEE Conf. held jointly with the 28th Chinese Control Conf. Decision and Control (CDC/CCC), Proceedings*, pages 8244–8251, Shanghai, China, December 15–18 2009. doi: 10.1109/CDC.2009.5400680.

F. Di Meglio, G.-O. Kaasa, N. Petit, and V. Alstad. Slugging in multiphase flow as a mixed initial-boundary value problem for a quasilinear hyperbolic system. In *American Control Conference (ACC) 2011, Proceedings*, pages 3589–3596, San Francisco, California, USA, June 29 – July 1 2011.

F. Di Meglio, R. Vazquez, M. Krstic, and N. Petit. Backstepping stabilization of an underactuated 3×3 linear hyperbolic system of fluid flow equations. In *American Control Conference (ACC) 2012, Proceedings*, pages 3365–3370, Montreal, Canada, June 27–29 2012.

G. C. Downton. Challenges of modeling drilling systems for the purposes of automation and control. In *2012 IFAC Workshop on Automatic Control in Offshore Oil and Gas Production, Proceedings*, Trondheim, Norway, May 31 – June 1 2012. doi: 10.3182/20120531-2-NO-4020.00054.

Z. Duan, N. Møller, and J. H. Weare. An equation of state for the CH4-CO2-H2O system: I. Pure systems from 0 to 1000°C and 0 to 8000 bar. *Geochimica et Cosmochimica Acta*, 56(7):2605–2617, 1992. ISSN 0016-7037. doi: 10.1016/0016-7037(92)90347-L.

G. O. Eikrem. *Stabilization of Gas-Lift Wells by Feedback Control*. PhD thesis, Norwegian University of Science and Technology, May 4 2006.

G. O. Eikrem, O. M. Aamo, and B. Foss. On instability in gas lift wells and schemes for stabilization by automatic control. *SPE Production & Operations*, 23(2):268–279, 2008. doi: 10.2118/101502-PA.

S. Ekrann and R. Rommetveit. A simulator for gas kicks in oil-based drilling muds. In *SPE Annual Technical Conference and Exhibition*, Las Vegas, Nevada, USA, September 22–26 1985. doi: 10.2118/14182-MS.

K. Falk, B. Fossli, C. Lagerberg, A. Handal, and S. Sangesland. Well control when drilling with a partly-evacuated marine drilling riser. In *IADC/SPE Managed Pressure Drilling and Underbalanced Operations Conference & Exhibition, Proceedings*, Denver, Colorado, USA, April 5–6 2011. doi: 10.2118/143095-MS.

F. Florence and J. Burks. New surface and down-hole sensors needed for oil and gas drilling. In *2012 IEEE International Instrumentation and Measurement Technology Conference (I2MTC), Proceedings*, pages 670–675, Graz, Austria, May 13–16 2012. doi: 10.1109/I2MTC.2012.6229568.

B. Fossli and S. Sangesland. Managed pressure drilling for subsea applications; well control challenges in deep waters. In *SPE/IADC Underbalance Technology Conference and Exhibition, Proceedings*, Houston, Texas, USA, October 11–12 2004. doi: 10.2118/91633-MS.

G. Geiger and T. Werner. Leak detection and location. A survey. In *Proceedings on PSIG Annual Meeting*, pages 1–11, Bern, Switzerland, October 15–17 2003.

J.-M. Godhavn. Control requirements for high-end automatic MPD operations. In *SPE/IADC Drilling Conference, Proceedings*, pages 589–603, Amsterdam, Netherlands, 17-19 March 2009. doi: 10.2118/119442-MS.

J.-M. Godhavn, A. Pavlov, G.-O. Kaasa, and N. L. Rolland. Drilling seeking automatic control. In *18th IFAC World Congress, Proceedings*, Milan, Italy, August 28 – September 2 2011.

B. Graham, W. K. Reilly, F. Beinecke, D. F. Boesch, T. D. Garcia, C. A. Murray, and F. Ulmer. Deep water, the gulf oil disaster and the future of offshore drilling. Technical report, National Commision on the BP Deepwater Horizon Oil Spill and Offshore Drilling, 2011.

J. Gravdal, H. Lohne, G. Nygaard, E. Vefring, and R. Time. Automatic evaluation of near well formation flow during drilling operations. In *International Petroleum Technology Conference, Proceedings*, Kuala Lumpur, Malaysia, December 3–5 2008. doi: 10.2523/12395-MS.

J. Gravdal, R. Lorentzen, and R. Time. Wired Drill Pipe Telemetry Enables Real-Time Evaluation of Kick During Managed Pressure Drilling. In *SPE Asia Pacific Oil & Gas Conference and Exhibition, Proceedings*, Brisbane, Australia, October 18–20 2010. doi: 10.2118/132989-MS.

J. E. Gravdal. Real-time evaluation of kick during managed pressure drilling based on wired drill pipe telemetry. In *International Petroleum Technology Conference, Proceedings*, Doha, Qatar, December 7–9 2009.

J. E. Gravdal, M. Nikolaou, Ø. Breyholtz, and L. A. Carlsen. Improved kick management during MPD by real-time pore-pressure estimation. In *SPE Annual Technical Conference and Exhibition, Proceedings*, Louisiana, USA, October 4–7 2009.

B. Grayson and A. Gans. Closed loop circulating systems enhance well control and efficiency with precise wellbore monitoring and management capabilities. In *SPE/IADC Managed Pressure Drilling and Underbalanced Operations Conference and Exhibition, Proceedings*, Milan, Italy, March 20–21 2012. doi: 10.2118/156893-MS.

H. F. Grip, T. A. Johansen, L. Imsland, and G.-O. Kaasa. Parameter estimation and compensation in systems with nonlinearly parameterized perturbations. *Automatica*, 46(1):19–28, 2010. doi: 10.1016/j.automatica.2009.10.013.

J. Hage and D. ter Avest. Borehole acoustics applied to kick detection. *Journal of Petroleum Science and Engineering*, 12:157–166, 1994. doi: 10.1016/0920-4105(94)90015-9.

T. Harmathy. Velocity of large drops and bubbles in media of infinite or restricted extent. *AIChE Journal*, 6(2):281–288, 1960. ISSN 1547-5905.

E. Hauge, O. M. Aamo, and J.-M. Godhavn. Model based pipeline monitoring with leak detection. In *Seventh IFAC Symposium on Nonlinear Control Systems*, volume 7, Pretoria, South-Africa, August 22–24 2007.

E. Hauge, O. M. Aamo, and J.-M. Godhavn. Model-based monitoring and leak detection in oil and gas pipelines. *SPE Projects, Facilities & Construction*, 4(3):53–60, 2009. doi: 10.2118/114218-PA.

E. Hauge, O. M. Aamo, and J.-M. Godhavn. Model-based estimation and control of in/out-flux during drilling. In *American Control Conference (ACC) 2012, Proceedings*, pages 4909–4914, Montreal, Canada, June 27–29 2012a.

E. Hauge, O. M. Aamo, and J.-M. Godhavn. Tracking of choke pressure during managed pressure drilling. In *Modelling, Identification and Control / 770: Advances in Computer Science and Engineering, Proceedings*, Phuket, Thailand, April 2–4 2012b. doi: 10.2316/P.2012.769-021.

E. Hauge, J.-M. Godhavn, Ø. N. Stamnes, and O. M. Aamo. A dynamic model of percolating gas in an open well-bore. In *7th Vienna Conference on Mathematical Modelling (MATHMOD), Proceedings*, Vienna, Austria, February 15–17 2012c.

E. Hauge, J.-M. Godhavn, Ø. N. Stamnes, and O. M. Aamo. Dynamic modelling of gas rising in a wellbore. In *Modelling, Identification and Control / 770: Advances in Computer Science and Engineering, Proceedings*, Phuket, Thailand, April 2–4 2012d. doi: 10.2316/P.2012.769-045.

E. Hauge, Ø. N. Stamnes, J.-M. Godhavn, and O. M. Aamo. A dynamic model of percolating gas in a wellbore. *SPE Drilling & Completion*, 27(2):204–215, 2012e. doi: 10.2118/160481-PA.

E. Hauge, O. M. Aamo, and J.-M. Godhavn. Application of an infinite-dimensional observer for drilling systems incorporating kick and loss detection. In *European Control Conference (ECC2013), Proceedings*, Zürich, Switzerland, July 17–19 2013a. Accepted for publication.

E. Hauge, O. M. Aamo, J.-M. Godhavn, and G. Nygaard. A novel model-based scheme for kick and loss mitigation during drilling. *Journal of Process Control*, -:–, 2013b. Accepted for publication.

O. A. Helstrup, Z. Chen, and S. S. Rahman. Time-dependent wellbore instability and ballooning in naturally fractured formations. *Journal of Petroleum Science and Engineering*, 43(1–2):113–128, 2004. ISSN 0920-4105. doi: 10.1016/j.petrol.2004.01.001.

L. Hoberock and S. Stanbery. Pressure dynamics in wells during gas kicks: Part 2-component models and results. *Journal of Petroleum Technology*, 33(8):1367–1378, 1981a.

L. Hoberock and S. Stanbery. Pressure dynamics in wells during gas kicks: Part 1-component models and results. *Journal of Petroleum Technology*, 33(8):1357–1366, 1981b.

P. Holand. *Offshore Blowouts: Causes and Control*. Gulf Professional Publishing, 1997.

F. Hovland and R. Rommetveit. Analysis of gas-rise velocities from full-scale kick experiments. In *SPE Annual Technical Conference and Exhibition, Proceedings*, volume Delta, pages 331–340, Washington, DC, USA, October 4–7 1992.

C. Jablonowski and A. Podio. The impact of rotating control devices on the incidence of blowouts: A case study for onshore Texas, USA. *SPE Drilling & Completion*, 26(3):364–370, 2011. doi: 10.2118/133019-PA.

E. Jahanshahi, K. Salahshoor, and R. Kharrat. Modified distributed delay model for void wave dynamics in gas-lifted wells. *Journal of Petroleum Science and Engineering*, 69(3–4):203–213, 2009. ISSN 0920-4105. doi: 10.1016/j.petrol.2009.08.015.

S. Julier and J. Uhlmann. Unscented filtering and nonlinear estimation. *Proceedings of the IEEE*, 92(3):401–422, 2004. doi: 10.1109/JPROC.2003.823141.

G. Kaasa, Ø. Stamnes, O. Aamo, and L. Imsland. Simplified hydraulics model used for intelligent estimation of downhole pressure for a managed-pressure-drilling control system. *SPE Drilling & Completion*, 27(1):127–138, 2012.

G.-O. Kaasa, Ø. N. Stamnes, L. Imsland, and O. M. Aamo. Intelligent estimation of downhole pressure using simplified hydraulic model. In *IADC/SPE Managed Pressure Drilling and Underbalanced Operations Conference & Exhibition, Proceedings*, Denver, Colorado, USA, April 5–6 2011. doi: 10.2118/143097-MS.

W. Karnavas, P. Sanchez, and A. Bahill. Sensitivity analyses of continuous and discrete systems in the time and frequency domains. *IEEE Transactions on Systems, Man and Cybernetics*, 23(2):488–501, March/April 1993. ISSN 0018-9472. doi: 10.1109/21.229461.

H. Khalil. *Nonlinear systems*. Prentice-Hall, Upper Saddel River, NJ 07458, USA, 3 edition, 2002.

M. Krstić and A. Smyshlyaev. Backstepping boundary control for first-order hyperbolic PDEs and application to systems with actuator and sensor delays. *Systems & Control Letters*, 57(9):750–758, 2008a. ISSN 0167-6911. doi: 10.1016/j.sysconle.2008.02.005.

M. Krstić and A. Smyshlyaev. *Boundary control of PDEs: A course on backstepping designs*, volume 16. Society for Industrial Mathematics, 2008b.

I. Landet, H. Mahdianfar, A. Pavlov, and O. Aamo. Modeling for MPD operations with experimental validation. In *IADC/SPE Drilling Conference and Exhibition, Proceedings*, 2012.

A. Lavrov and J. Tronvoll. Modeling mud loss in fractured formations. In *11th ADIPEC: Abu Dhabi International Petroleum Exhibition and Conference, Proceedings*, pages 377–386, Abu Dhabi, United Arab Emirates, October 10–13 2004. doi: 10.2118/88700-MS.

J. LeBlanc and R. Lewis. A mathematical model of a gas kick. *Journal of Petroleum Technology*, 20(8):888–898, 1968.

H. Mahdianfar, O. Aamo, and A. Pavlov. Suppression of heave-induced pressure fluctuations in mpd. In *2012 IFAC Workshop on Automatic Control in Offshore Oil and Gas Production, Proceedings*, Trondheim, Norway, May 31 – June 1 2012. doi: 10.3182/20120531-2-NO-4020.00013.

M. Mehrabi, M. Zeyghami, and M. Shahri. Modeling of fracture ballooning in naturally fractured reservoirs: A sensitivity analysis. In *Nigeria Annual International Conference and Exhibition, Proceedings*, Lagos, Nigeria, August 6–8 2012. doi: 10.2118/163034-MS.

H. Merritt. *Hydraulic control systems*. John Wiley & Sons Inc, New York, USA, 1967.

G. Milner. Real-time well control advisor. In *SPE 67th Annual Technical Conference and Exhibition, Proceedings*, Washington DC, USA, October 4–7 1992. doi: 10.2118/24576-MS.

S. Nas. Kick detection and well control in a closed wellbore. In *IADC/SPE Managed Pressure Drilling and Underbalanced Operations Conference and Exhibition, Proceedings*, Denver, Colorado, USA, April 5–6 2011. doi: 10.2118/143099-MS.

H. Nickens. A dynamic computer model of a kicking well. *SPE Drilling Engineering*, 2(2):159–173, 1987.

M. Nikolaou. Computer-aided process engineering in oil and gas production. In press, 2012. URL `http://www.sciencedirect.com/science/article/pii/S0098135412002773?v=s5`.

S. Ohara, F. Flores-Avila, and J. R. Smith. Improved kick tolerance analysis. Technical report, Lousiana State University, 2004.

A. Orell and R. Rembrand. A model for gas-liquid slug flow in a vertical tube. *Industrial & Engineering Chemistry Fundamentals*, 25(2):196–206, 1986. doi: 10.1021/i100022a004.

B. Paden and R. Panja. Globally asymptotically stable "PD+" controller for robot manipulators. *International Journal of Control*, 47(6):1697–1712, 1988. ISSN 0020-7179.

A. Pink, H. Kverneland, A. Bruce, and J. Applewhite. Building an automated drilling system where the surface machines are controlled by downhole and surface data to optimize the well construction process. In *IADC/SPE Drilling Conference and Exhibition, Proceedings*, San Diego, California, USA, March 6–8 2012. doi: 10.2118/150973-MS.

PSA. Risikonivå i norsk petroleumsvirksomhet. Technical report, Petroleum Safety Authority Norway, 2012. URL `http://www.ptil.no/getfile.php/PDF/RNNP%202011/RNNP2011_Hovedrapport.pdf`. Rev. 2; in Norwegian.

D. Rader and R. Ward. Factors affecting bubble-rise velocity of gas kicks. *Journal of Petroleum Technology*, 27(5):571–584, 1975.

K. Redmann Jr. Understanding kick tolerance and its significance in drilling planning and execution. *SPE Drilling Engineering*, 6(4):245–249, 1991. doi: 10.2118/19991-PA.

D. Reitsma. A simplified and highly effective method to identify influx and losses during managed pressure drilling without the use of a Coriolis flow meter. In *SPE/IADC Managed Pressure Drilling and Underbalanced Operations Conference and Exhibition, Proceedings*, Kuala Lumpur, Malaysia, February 24–25 2010. doi: 10.2118/130312-MS.

L. A. S. Rocha, P. Junqueira, and J. Roque. Overcoming deep and ultra deepwater drilling challenges. In *Offshore Technology Conference, Proceedings*, Houston, Texas, May 5–8 2003. doi: 10.4043/15233-MS.

R. Rommetveit and T. Olsen. Gas kick experiments in oil-based drilling muds in a full-scale, inclined research well. In *SPE Annual Technical Conference and Exhibition, Proceedings*, San Antonio, Texas, USA, October 8–11 1989. doi: 10.2118/19561-MS.

R. Rommetveit and E. Vefring. Comparison of results from an advanced gas kick simulator with surface and downhole data from full scale gas kick experiments in an inclined well. In *SPE Annual Technical Conference and Exhibition, Proceedings*, Dallas, Texas, USA, October 6–9 1991. doi: 10.2118/22558-MS.

R. Rommetveit, K. S. Bjørkvoll, J. E. Gravdal, C. J. Goncalves, A. C. V. Lage, J. E. Campos, Átila F.L. Aragao, A. Arcelloni, and S. Ohara. Ultradeepwater hydraulics and well-control tests wth extensive instrumentation: Field tests and data analysis. In *SPE Annual Technical Conference and Exhibition, Proceedings*, number 84316-MS, Denver, Colorado, USA, October 5–8 2005. doi: 10.2118/84316-MS.

S. Saeed, R. Lovorn, and K. Knudsen. Automated drilling systems for MPD – The reality. In *IADC/SPE Drilling Conference and Exhibition, Proceedings*, San Diego, California, USA, March 6–8 2012. doi: 10.2118/151416-MS.

S. Sangesland. Riser lift pump for deep water drilling. In *IADC/SPE Asia Pacific Drilling Technology, Proceedings*, Jakarta, Indonesia, September 7–9 1998. doi: 10.2118/47821-MS.

H. Santos, E. Catak, J. Kinder, and P. Sonnemann. Kick detection and control in oil-based mud: Real well-test results using microflux control equipment. In *SPE/IADC Drilling Conference, Proceedings*, pages 429–438, Amsterdam, The Netherlands, February 20–22 2007. doi: 10.2118/105454-MS.

H. Santos, E. Catak, and S. Valluri. Kick tolerance misconceptions and consequences to well design. In *SPE/IADC Drilling Conference and Exhibition, Proceedings*, Amsterdam, The Netherlands, March 1–3 2011. doi: 10.2118/140113-MS.

J. J. Schubert, H. C. Juvkam-Wold, and J. Choe. Well control procedures for dual gradient drilling as compared to conventional riser drilling. *SPE Drilling & Completion*, 21(4):287–295, 2006. doi: 10.2118/99029-PA.

P. Skalle. Pressure control during oil well drilling. Lecture material in the TPG4250 course at NTNU, 2010.

J. Speers and G. Gehrig. Delta flow: An accurate, reliable system for detecting kicks and loss of circulation during drilling. *SPE Drilling Engineering*, 2(4): 359–363, 1987. doi: 10.2118/13496-PA.

Ø. N. Stamnes. *Nonlinear Estimation with Applications to Drilling*. PhD thesis, Norwegian University of Science and Technology, 2011.

Ø. N. Stamnes, J. Zhou, G.-O. Kaasa, and O. M. Aamo. Adaptive observer design for the bottomhole pressure of a managed pressure drilling system. In *47th IEEE Conference on Decision and Control 2008, Proceedings*, pages 2961–2966, Cancun, Mexico, December 9–11 2008.

Ø. N. Stamnes, G.-O. Kaasa, and O. M. Aamo. Adaptive estimation of downhole pressure for managed pressure drilling operations. In *2011 IEEE Multi-Conference on Systems and Control (MSC), Proceedings*, pages 989–995, Denver, Colorado, USA, September 28–30 2011.

E. Storkaas. *Stabilizing control and controllability. Control solutions to avoid slug flow in pipeline-riser systems*. PhD thesis, Norwegian University of Science and Technology, 2005. URL `http://urn.kb.se/resolve?urn=urn:nbn:no:ntnu:diva-2075`.

J. Tarvin, A. Hamilton, P. Gaynord, and G. Lindsay. Gas rises rapidly through drilling mud. In *Drilling Conference, Proceedings*, pages 637–649, Dallas, Texas, USA, February 15–18 1994. doi: 10.2118/27499-MS.

L. Torres, G. Besançon, and D. Georges. A collocation model for water-hammer dynamics with application to leak detection. In *47th IEEE Conference on Decision and Control 2008, Proceedings*, pages 3890–3894, Cancun, Mexico, December 9–11 2008.

L. Torres, G. Besançon, and D. Georges. Mulit-leak estimator for pipelines based on an orthogonal collocation model. In *Joint 48th conference on decision and control and 28th Chinese control conference, Proceedings*, pages 410–415, Shanghai, China, December 16–18 2009.

M. T. Torsvik. Laboratoriemodell av boreprosess. Bygging, instrumentering, igangkjøring og regulering. Master's thesis, University of Stavanger, 2011. In Norwegian.

G. E. Totten. A timeline of highlights from the histories of ASTM committee D02 and the petroleum industry, July 2004. URL `http://www.astm.org/COMMIT/D02/to1899_index.html`. Accessed 02.10.2012.

R. Vazquez, J. Coron, M. Krstić, and G. Bastin. Local exponential H^2 stabilization of 2×2 quasilinear hyperbolic system using backstepping. In *50th IEEE Conference on Decicion and Control and European Control Conference (CDC–ECC), Proceedings*, Orlando, FL, USA, December 12–15 2011a.

R. Vazquez, M. Krstić, and J. Coron. Backstepping boundary stabilization and state estimation of a 2×2 linear hyperbolic system. In *50th IEEE Conference on Decicion and Control and European Control Conference (CDC–ECC), Proceedings*, Orlando, FL, USA, December 12–15 2011b.

D. Veeningen. Identify safe drilling margin, detect kicks, analyze negative pressure tests and better well control independently from surface measurements, addressing recommendations for deepwater. In *International Conference on Health, Safety and Environment in Oil and Gas Exploration and Production, Proceedings*, Perth, Australia, September 11–13 2012. doi: 10.2118/157220-MS.

E. Vefring, R. Rommetveit, and E. Borge. An advanced kick simulator operating in a user-friendly X-Window system environment. In *Petroleum Computer Conference, Proceedings*, Dallas, Texas, USA, June 19–21 1991. doi: 10.2118/22314-MS.

D. White and I. Walton. A computer model for kicks in water- and oil-based muds. In *SPE/IADC Drilling Conference, Proceedings*, Houston, Texas, USA, February 27 – March 2 1990. doi: 10.2118/19975-MS.

F. White. *Fluid Mechanics*. McGraw-Hill, New York, 4th edition, 1999.

C.-Z. Xu and G. Sallet. Exponential stability and transfer functions of processes governed by symmetric hyperbolic systems. *ESAIM: Control, Optimisation and Calculus of Variations*, 7:421–442, 2002. doi: 10.1051/cocv:2002062.

Q. Zhang. Adaptive observer for multiple-input-multiple-output (MIMO) linear time-varying systems. *IEEE Transactions on Automatic Control*, 47(3):525–529, 2002. doi: 10.1109/9.989154.

J. Zhou and G. Nygaard. Automatic model-based control scheme for stabilizing pressure during dual-gradient drilling. *Journal of Process Control*, 21(8):1138–1147, 2011. ISSN 0959-1524. doi: 10.1016/j.jprocont.2011.06.022.

J. Zhou, Ø. N. Stamnes, O. M. Aamo, and G.-O. Kaasa. Switched control for pressure regulation and kick attenuation in a managed pressure drilling system. *IEEE Transactions on Control Systems Technology*, 19(2):337–350, March 2011. ISSN 1063-6536. doi: 10.1109/TCST.2010.2046517.